UNIVERSITÀ DEGLI STUDI DI PALERMO

Mechanical, Manufacturing, Management and Aerospace Innovation

Dipartimento di Ingegneria

A study on hydrogen storage systems for sustainable aviation

Conceptual design, computational modelling and multidisciplinary optimization of light-weight cryogenic hydrogen tanks for aircraft integration

Dottorando

Dott. Sergio Bagarello

Tutor

Prof. Ivano Benedetti

Coordinatrice

Prof.ssa Giada La Scalia

R-Tutor

Ing. Ignazio Dimino

M3AI — CICLO XXXVIII PNRR

Abstract

The decarbonization of commercial aviation has renewed interest in hydrogen as an alternative energy carrier, with onboard storage emerging as a critical enabling technology. This thesis presents a comprehensive framework for the conceptual design, high-fidelity modelling, and multidisciplinary optimization of liquid hydrogen pressure vessels for aircraft integration.

The proposed approach focuses on a passively insulated sandwich-composite architecture, aiming to simultaneously maximize gravimetric efficiency and minimize boil-off losses under realistic operational and integration constraints. A computational tool is developed that couples multiphysics finite-element thermo-mechanical modelling with nonlinear, constraint-based multidisciplinary optimization. The framework explicitly accounts for standardized safety factors, cryogenic thermal loads, internal pressurization, material failure criteria, and pragmatic design features, including non-spherical end domes, refuelling cutouts, anti-sloshing baffles, and fuselage integration constraints.

The exploration of the optimized design space demonstrates that all-metal tank configurations are intrinsically penalized by structural mass, yielding gravimetric efficiencies below 30%. In contrast, composite-based architectures with metallic liners achieve gravimetric efficiencies approaching 50%, with overall tank mass reductions of up to 57% relative to whole metallic counterparts, even when realistic integration features are included. Scaling effects are inves-

tigated, highlighting the influence of tank size and geometry on both thermal and structural performance.

Finally, the optimized storage systems are integrated into a sustainable aircraft concept to assess system-level implications and identify pathways to mitigate the performance gap with conventional kerosene-fuelled aviation. Beyond design optimization, the results provide quantitative insights relevant to future certification activities, supporting the development of physically grounded methodologies for the safe introduction of liquid hydrogen storage in commercial aircraft.

List of Publications

Journal articles

J1. Bagarello, S., Campagna, D., and Benedetti, I. "A survey on hydrogen tanks for sustainable aviation". *Green Energy and Intelligent Transportation*, 2024. doi: https://doi.org/10.1016/j.geits.2024.100224.

J2. Bagarello, S., Campagna, D., and Benedetti, I. "Computational thermomechanical modelling and design-space exploration of cryogenic hydrogen tanks for aviation". *Aerospace Science and Technology*, 2026. doi: https://doi.org/10.1016/j.ast.2025.110755.

J3. Bagarello, S., Elham, A., and Benedetti, I. "Design, optimization, and integration of passively-insulated liquid hydrogen tanks for sustainable aviation". *International Journal of Hydrogen Energy*, 2026. doi: https://doi.org/10.1016/j.ijhydene.2025.153042.

Conference proceedings

C1. Bagarello, S. and Benedetti, I. "Electric conversion of a general aviation aircraft: a case study". *AIDAA XXVII International Congress*, 2023. doi: https://doi.org/10.21741/9781644902813-95.

C2. Bagarello, S., Campagna, D., Milazzo, A., and Benedetti, I. "A short

overview of hydrogen storage for sustainable aviation". *IV Aerospace PhD-Days*, 2024. doi: https://doi.org/10.21741/9781644903193-17.

C3. Bagarello, S., Campagna, D., and Benedetti, I. "Conceptual Design and Thermo-Mechanical Modelling of Liquid Hydrogen Storage Vessels for Aircraft Integration". *28th AIDAA Conference – 10th CEAS Aerospace Europe Conference*, 2025.

C4. Bagarello, S., Campagna, D., Milazzo, A., and Benedetti, I. "An overview of hydrogen storage for airborne applications". *Research & Education in Aircraft Design*, 2026.

C5. Bagarello, S., Campagna, D., Elham, A., and Benedetti, I. "Multidisciplinary optimization of passively-insulated liquid hydrogen tanks for aircraft applications". *Fifth International Conference on Mechanics of Advanced Materials and Structures*, 2026.

Contents

List of Figures

List of Tables

Chapter 1

Introduction

In recent years, the pursuit of sustainability and zero-emission propulsion has become of primary importance, as global warming represents a critical challenge, with severe implications for economies, industries, and social well-being. Aviation plays an essential role in modern society, being the only transport mode capable of moving people and goods worldwide within a single day. In 2016, it generated $2.7 trillion in economic activity and supported 65.5 million jobs, corresponding to 3.6% of global gross domestic product [10]. At the same time, however, the sector has a notable environmental impact.

Although aviation contributes only for $2-3\%$ of global anthropogenic carbon dioxide (CO_2) emissions, it remains difficult to decarbonize due to long development cycles and strong reliance on fossil fuels. Alarmingly, its annual pollutant emissions share is expected to rise with increasing demand for air travel [11], as highlighted in Fig 1.1.

Apart from carbon dioxide, aviation also emits water vapor, nitrogen oxides (NOx), unburnt hydrocarbons, carbon monoxide (CO), particulate matter (PM), and sulphur dioxide (SO_2) [12]. Thus, to align with current global climate protection policies, low and ideally non-pollutant means of propulsion in

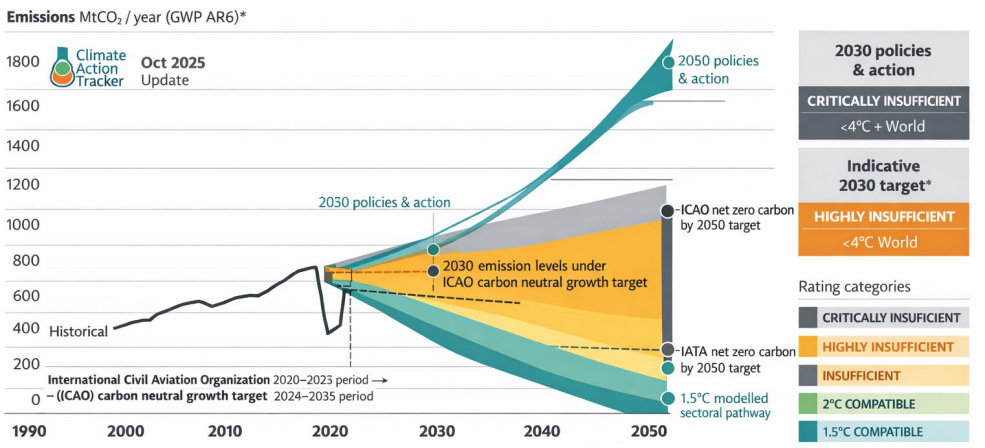

Figure 1.1: Historical and projected international aviation CO_2 emissions under current policies and Paris-aligned scenarios. Adapted from Ref.[1]

the aeronautical industry are being studied.

Among the proposed strategies, operational measures such as enhanced air traffic management and optimized flight trajectories and scheduling [13] provide short-term reductions in aviation emissions, but do not address the problem comprehensively. Likewise, the adoption of lightweight and sustainable materials, including advanced thermoplastic composites [14], can decrease fuel consumption in the near term and improve recyclability prospects in the long run. In this landscape, innovative aircraft configurations, such as the blended-wing-body (BWB) [15] and Flying-V [16], are being investigated for their aerodynamic efficiency and associated emission reductions, though their adoption would require significant changes in industrial expertise and regulatory standards.

Beyond these approaches, alternative energy carriers are gaining increasing attention as potential substitutes for petroleum-derived fuels. Electrochemical energy carriers, such as batteries, offer the prospect of clean and quiet propul-

sion, but their limited gravimetric energy density and life-cycle sustainability concerns currently restrict their applicability to short-range aircraft. Ammonia (NH_3), another carbon-free option, can be stored in liquid form at moderate conditions but its high toxicity raises severe handling and safety challenges that constrain its attractiveness [17]. Greater near-term feasibility is generally associated with sustainable aviation fuels (SAFs), derived mainly from biomass and organic waste and sharing many physical and chemical properties with kerosene [18]. While SAFs provide a transitional solution largely compatible with existing infrastructure, questions persist regarding their cost, production scalability and long-term environmental impact.

1.1 The case for hydrogen

Hydrogen (H_2) is driving interest as an energy carrier due to its virtually unlimited availability [19], its appealing *gravimetric energy density* [5], and clean combustion characteristics, resulting in zero carbon dioxide (CO_2) direct emissions [20]. Nonetheless, while being the most abundant element in the universe, hydrogen is not found in its gaseous or liquid forms on planet Earth, being mainly found in combined stable forms with water and hydrocarbons, from which it can be obtained upon energy absorbing processes [21].

Hydrogen is generally regarded as a safe and environmentally friendly fuel, although its overall impact strongly depends on the production methods, classified by colour according to the associated carbon emissions:

- Grey hydrogen is obtained through methane steam reforming, the most affordable but CO_2-intensive process;
- Blue hydrogen also relies on steam reforming, but incorporates carbon capture and storage;

- Green hydrogen is produced by water electrolysis powered by renewable energy, offering the lowest emissions but at the highest cost due to its energy intensity [22].

Since all processes are highly energy-demanding, large-scale adoption of hydrogen as fuel would require substantial electricity grid upgrades, estimated at about 1.6 times current capacity [23].

Nonetheless, the interest in H_2 adoption is not driven solely by environmental considerations. A complementary motivation is associated with energy security and the reduction of dependence on geographically concentrated fossil-fuel resources. Indeed, the first wave of studies on hydrogen aviation emerged in response to the petroleum crises of the 1970s, when the vulnerability of air transport to oil availability and price volatility became evident, and the prospect of a "Hydrogen Economy" was proposed as a possible pathway to reduce reliance on petroleum-based fuels [24]. Today, similar concerns are re-emerging in the context of geopolitical instability and disruptions to international energy supply chains. In this respect, hydrogen offers an additional strategic advantage, as it can be produced from water, hydrocarbons, biomass, or other hydrogen-containing feedstocks through different conversion pathways [19, 21]. Provided that adequate primary energy and infrastructure are available, such production routes could be deployed in a distributed manner, thereby contributing not only to the decarbonization of aviation, but also to improved fuel-supply resilience and reduced dependence on imported fossil resources.

1.2 Early attempts at hydrogen-powered aviation

The concept of using hydrogen in aviation is not new. As a matter of fact, H_2 has a rich history in aviation, beginning with its use in lighter-than-air vehicles such as balloons and rigid airships, and enabling the operation of large early 20^{th}-century Zeppelins [25].

A milestone was reached when the United States Air Force demonstrated the first liquid-hydrogen-powered flight using a modified B-57 bomber. Subsequent developments included the Lockheed CL-400 supersonic reconnaissance aircraft in the 1950s and, later, the Soviet TU-155 in the 1980s, a derivative of the TU-154 airliner equipped with a hydrogen-fuelled engine [26]. Schematics of the B-57 and Tu-155 are provided in Fig.(1.2). These test campaigns confirmed the technical feasibility and potential benefits of hydrogen propulsion, but also highlighted major technological and logistical barriers, notably the requirement to ensure liquid hydrogen availability at airports in parallel with conventional kerosene infrastructure [27].

In the early 2000s, the European Union launched the Cryoplane Project, which systematically assessed liquid hydrogen integration into various aircraft configurations. The study demonstrated the feasibility of hydrogen-fuelled aviation, while underscoring the penalty associated with fuel storage: the study, in fact, highlighted that H_2 tanks must be about four times larger than their kerosene counterparts, significantly influencing aircraft design and integration strategies [28].

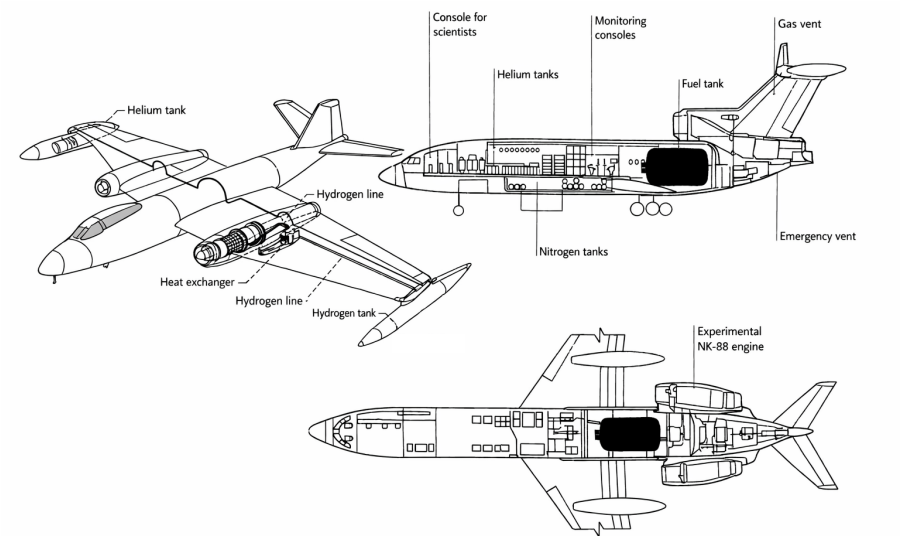

Figure 1.2: Examples of early attempts at hydrogen-powered aviation: the B-57 Canberra (left) and the Tupolev Tu-155 (right). Adapted from Ref.[2].

1.2.1 Onboard hydrogen storage

Both the appeal and challenges of H_2 in aviation stem from this fuel unique properties. Hydrogen has a gravimetric energy density about three times higher than conventional jet kerosene (120 MJ/kg vs. 43.2 MJ/kg) and its combustion produces no CO_2 [20], making it particularly attractive for meeting environmental targets. It is highly flammable, igniting faster than kerosene, and exhibits a wider flammability range. Its high thermal conductivity, heat capacity, and low viscosity provide excellent cooling capabilities at high speeds and combustor temperatures [29]. Moreover, it is the only energy carrier that can be produced on-site through carbon-free processes such as gasification, pyrolysis, or biomass-based steam gasification [30].

However, under standard conditions, its volumetric energy density is quite low (10.1 MJ/L vs. 33 MJ/L for kerosene), requiring about four times the volume and peculiar storage conditions, which complicates the *spatial integration*, i.e. accommodating passengers, payload, structures, and fuel within feasible

aircraft layouts [31]. Tab.(1.1) reports a comparison of the key properties between Jet A-1 and liquid hydrogen.

Table 1.1: Properties comparison between traditional aviation kerosene and liquid hydrogen at standard conditions.

Property	**Jet A-1**	**Liquid hydrogen**
Energy density [MJ/L]	33	10.1
Specific energy [MJ/kg]	43.2	120
Storage temperature [K]	ambient	20

1.2.2 Aircraft layout considerations

Given the low volumetric energy density of H_2, hydrogen-powered aircraft require substantial modifications compared to conventional designs [32], with one of the most significant differences being the integration of dedicated fuel tanks and systems. In fact, while engines can be adapted to operate on hydrogen with relative ease [5], the fuel storage and distribution systems must be entirely redesigned, including pipes, pumps, seals, and valves, to accommodate the unique physical properties of this energy carrier [22].

In kerosene-powered aircraft, fuel is commonly stored within the wings, a solution that offers several advantages: it maximizes fuselage space, simplifies the fuel system layout, and generates a favourable bending moment at the wing root that counteracts lift, thereby reducing wing-box structural requirements. Hydrogen tanks, by contrast, cannot efficiently be accommodated within the wing structure [31], necessitating the exploration of alternative configurations.

For this reason, hydrogen storage tanks are regarded by both industrial and academic stakeholders as one of the main *enabling technologies*, as these systems must minimize penalties in terms of aircraft safety, efficiency and

operating costs in order to make this fuel a viable solution to the environmental problem in aviation.

1.2.3 Gaseous hydrogen storage

As previously discussed, H_2 inherently low volumetric energy density necessitates dedicated storage strategies to achieve fuel densities compatible with aircraft applications. One such approach consists of compressing hydrogen gas to pressures on the order of 350–700 bar [33]. Increasing the storage pressure leads to higher gas density and, consequently, improves the volumetric fuel energy density, making gaseous hydrogen progressively more viable as an energy carrier.

Compared to liquid hydrogen systems, gaseous hydrogen tanks benefit from reduced system complexity. Indeed, since GH_2 is stored at ambient or near-ambient temperature, thermal management is not a critical design driver, which simplifies both the tank architecture and the associated subsystems. Nonetheless, the extremely high pressures required for GH_2 storage demand extremely robust pressure vessels. As a result, current aerospace-grade gaseous hydrogen tanks exhibit gravimetric indices that generally do not exceed 15%. As it will be clarified later in Sec. (3.1.3) where the gravimetric efficiency is defined, this means that more than 85% of the total system mass is associated with the storage vessel and its structural components rather than with usable fuel itself. Such poor gravimetric performance directly penalizes aircraft range relative to conventionally fuelled counterparts, thereby limiting the practical application of GH_2 primarily to small aircraft where range requirements are less stringent. Although increasing pressure improves volumetric energy density, identifying an optimal pressure level requires careful trade-off analyses between stored fuel mass and tank structural mass [34]. The relationship be-

tween fuel density and gravimetric efficiency is strongly pressure-dependent: while very high pressures enable high storage densities, they simultaneously induce a marked degradation in gravimetric efficiency, which decreases rapidly as pressure increases.

The high operating pressures of GH_2 tanks require structures designed not only to sustain nominal service loads, but also to provide an adequate safety margin against ultimate rupture. Burst pressure denotes the internal pressure at which the vessel loses its load-carrying capability and undergoes catastrophic structural failure [35]. For composite pressure vessels, this is generally not coincident with the onset of first-ply damage. Instead, it is the final outcome of a progressive degradation process involving interacting damage mechanisms such as matrix cracking, fibre fracture, delamination, and load redistribution among the laminate plies. In this context, damage-initiation criteria are indeed useful for detecting the occurrence of local failure mechanisms, but they do not constitute a complete assessment of the ultimate burst capacity of the vessel. A reliable prediction of burst pressure requires dedicated ultimate-load analyses, or experimental burst tests, in which the internal pressure is progressively increased until global collapse. In numerical simulations, this also requires progressive damage models capable of capturing the post-initiation response and residual load-carrying capability of the composite shell.

Regarding the classification of gaseous hydrogen tanks, these vessels are commonly categorized according to their construction materials, load-bearing architecture, and resulting gravimetric efficiency. *Composite overwrapped pressure vessels* (COPVs) denote pressure vessels in which a metallic or polymeric liner, primarily responsible for gas containment and permeation control, is externally reinforced by a fibre-reinforced composite overwrap that carries a significant portion of the pressure-induced structural load [36]. Accordingly, this definition applies mainly to *Type II–IV* architectures, whereas linerless *Type V*

tanks are more generally referred to as all-composite pressure vessels. These architectures range from relatively simple and low-cost *Type I* all-metal tanks, characterized by gravimetric efficiencies of approximately 2%, to state-of-the-art, liner-less composite *Type V* tanks, which achieve gravimetric efficiencies of up to 6% [37].

A graphical representation of common GH_2 storage solutions is provided in Fig. 1.3.

Table 1.2: Materials and features of different types of hydrogen storage tanks.

Tank Type	Material	Energy Density [MJ/kg]	Operating Pressure [bar]	Gravimetric Efficiency
Type I	All-metal	4–5	250–700	∼2%
Type II	Metal liner & Composite hoop wrap	4–5	700–875	∼2%
Type III	Metal liner & Composite full wrap	4–5	875–1100	∼4%
Type IV	Plastic liner & Composite full wrap	4–5	700–875	∼5%
Type V	No liner & All composite	5–8	875–1100	∼6%

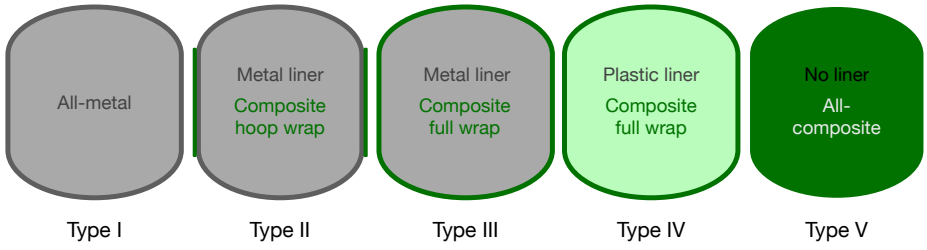

Figure 1.3: Graphical representation of gaseous hydrogen pressure vessels classification.

Concerning the feasibility of gaseous storage at the aircraft level, Brelje et al. [31] investigated the integration of GH_2 tanks using multidisciplinary design optimization (MDO) techniques, accounting for the mutual geometric con-

straints between the aircraft structure and the pressure vessels. Their results indicate that while compressed hydrogen storage may be feasible for regional-scale missions, the considerable mass of GH_2 tanks constitutes a critical drawback for longer-range applications. Accordingly, the weight penalty associated with compressed hydrogen storage likely precludes its use for transcontinental routes, for which cryogenic storage is indeed more suited [38]. For such mission profiles, the added complexity of insulation and thermal management systems necessary to maintain this fuel in its liquid phase may be justified. Also, according to NASA assessments, liquid hydrogen represents a more appropriate option for any aircraft carrying more than 100 passengers due to its superior energy density and range capability [39].

1.2.4 Liquid hydrogen storage

While GH_2 tanks may benefit from reduced complexity, the extremely high pressures necessary to store gaseous hydrogen require adequately robust pressure vessels whose gravimetric efficiency prevents their employment into efficient aircraft designs. In contrast, storing hydrogen at cryogenic temperatures greatly increases its volumetric energy density (from 2.9 MJ/L at 350 bar and ambient temperature for GH_2 to 8.5 MJ/L at 2 bar and 20 K for LH_2) thus allowing the use of much lower storage pressures and, in turn, reducing the structural burden imposed on the vessel. This translates into lower tank mass and can enable mass fractions up to 50% and beyond. The lower operating pressure of cryogenic tanks also modifies the role of burst-pressure assessment. Unlike high-pressure GH_2 vessels, which are nominally designed to sustain internal pressures of several hundred bar, the storage system considered in this work operates at much lower pressures. Although heat ingress inevitably induces partial evaporation of the liquid phase, the resulting boil-off gas is man-

aged by a dedicated venting system, which maintains the internal pressure within the prescribed operating range and prevents uncontrolled autogenous pressurization. For such reasons, this study, being addressed to highly-efficient future aircraft integration, investigates exclusively liquid hydrogen vessels.

For hydrogen to maintain its liquid phase demanding conditions are required. To achieve and sustain temperatures of $\approx 20\,\mathrm{K}$ diverse thermal insulation methods can be utilized.

The *multilayer insulation* (MLI) system, schematized in Fig. (1.4), reduces heat transfer by employing a sequence of thermal radiation shields oriented perpendicular to the direction of heat flow [40]. Such shields are typically composed of reflective foils that minimize radiative heat exchange, alternated with metallic layers such as aluminized or gold-coated Mylar, and low-conductivity spacer materials such as fibreglass, silk tissue, or polyester. In some instances, a vacuum jacket can be introduced between the warm and cold boundaries [41], thereby significantly enhancing insulation performance but at the cost of increased mass and system complexity. When combined with MLI, vacuum insulation exhibits densities in the range of $10 \div 100\,\mathrm{kg/m^3}$ and effective thermal conductivities between $3 \times 10^{-4} \div 3 \times 10^{-5}\,\mathrm{W/mK}$. The main limitation of this approach is indeed the additional weight and complexity associated with maintaining the insulating vacuum within the storage system architecture.

Similarly, although vacuum jackets provide effective insulation, as highlighted in Fig. (1.5), they require complex venting subsystems to maintain the evacuated region, thereby lowering their appeal in extremely mass- and reliability-sensitive applications. Another challenge lies in accommodating dimensional variations induced by thermal cycles during repeated filling and emptying with cryogenic hydrogen [42]: onboard hydrogen tanks may experience temperature differentials as large as $\approx 300\,\mathrm{K}$, so mismatches in the thermal expansion coefficients of tank components are a critical design factor

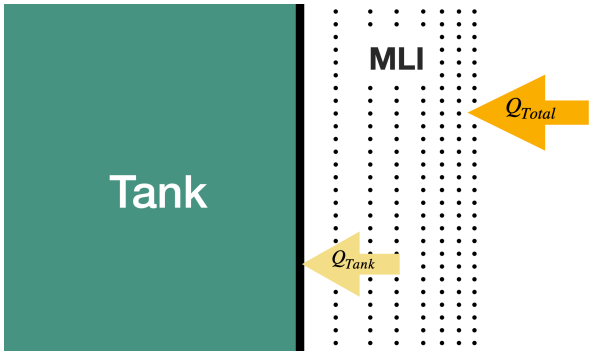

Figure 1.4: Schematic of multilayer insulation. It employs multiple thermal shields like reflective foil, metal radiation shields, and insulating materials like fiberglass, silk tissue, or polyester.

[43].

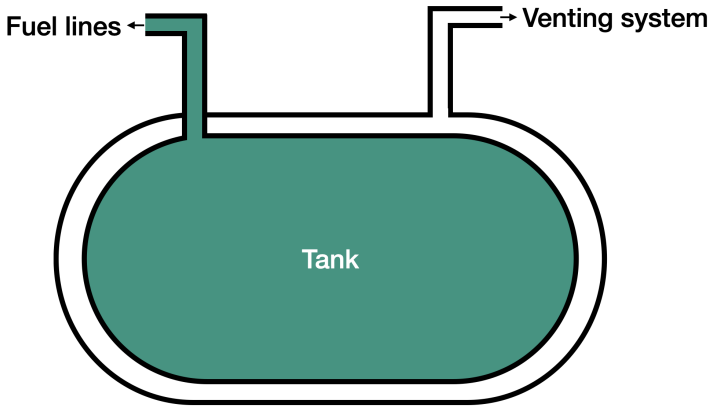

Figure 1.5: Vacuum insulation system schematic representation, where a vacuum jacket connected to a venting system insulates the cryogenic tank.

Therefore, an ideal insulation material is characterized by very low thermal conductivity, diffusivity, and density; consequently, *foams* are often employed, as exemplified by the external tank of the Space Shuttle, Fig. 1.6, or, more recently, by the cryogenic core stage of NASA Space Launch System [44].

Polyurethane foams offer a versatile material for *passive* insulation, with the possibility of selecting tailored densities ranging from 32 to 96 kg/m^3 for specific applications. The required insulation thickness depends on the material properties, tank geometry, allowable boil-off rate, and overall mass constraints. Foam insulation is relatively low cost, easy to implement and generally lightweight. This method of insulation, however, is not free of drawbacks: insulating spray-on foams (SOFIs) are known for a variety of risks such as environmental impact, fire hazard and structural considerations as testified by the events involving the Columbia Space Shuttle [45]. Hence, since foam cannot be used as a stand-alone solution for H_2 storage, careful integration with other materials is necessary: it is for example required that both sides of the foam layer are protected, on the inside from the corrosive fuel and on the outside from the external environment.

Figure 1.6: Detail of the Space Shuttle external cryogenic tank. Orange coated SOFI foam was used to insulate LH_2 and oxygen [3].

1.3 Hydrogen-induced embrittlement

Beyond the challenges associated with hydrogen storage conditions, an additional aspect that must be considered in the design of H_2 tanks is material degradation due to hydrogen embrittlement (HE). Hydrogen embrittlement is a degradation phenomenon whereby atomic hydrogen, due to its small size, diffuses into stressed materials, leading to a reduction in yield strength, ductility, and fracture toughness, and potentially promoting sudden crack initiation and growth [46, 47]. A schematic representation of the phenomenon is provided in Fig.(1.7).

The susceptibility to HE strongly depends on the material class. Steels and titanium alloys are generally the most affected, whereas aluminium alloys, copper, and stainless steels exhibit significantly lower sensitivity. In particular, several aluminium alloys, including Al–Mg systems, have been shown to retain ductile behaviour even under cryogenic hydrogen exposure [48].

Although the physical mechanisms behind hydrogen-induced embrittlement are still the subject of ongoing research, a range of effective mitigation strategies is known to be effective. These include appropriate alloy selection, the use of metallic liners, and the application of protective coatings or diffusion barriers [49]. Thus, while embrittlement represents an important design consideration for hydrogen storage systems, it does not constitute a fundamental bottleneck for tank development. Rather, it is a phenomenon that must be explicitly accounted for through informed material selection and structural design choices. Accordingly, the adoption of low-permeability metallic liners enables effective mitigation of HE, particularly in applications where composite materials, usually more prone to diffusion, are utilized.

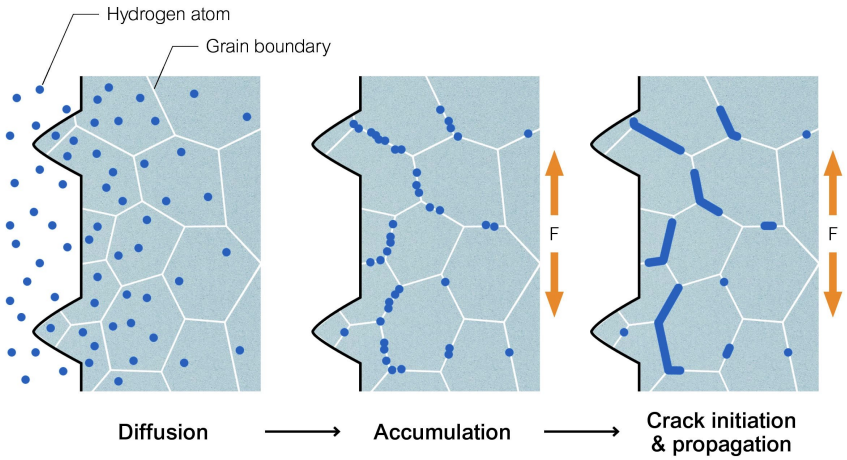

Figure 1.7: Representation of the embrittlement phases due to hydrogen diffusion in a metallic polycrystalline microstructure. Adapted from Ref. [4] (drawing not to scale).

1.4 Thesis outline

This thesis incorporates the author's prior work from various projects, including findings from previously published peer-reviewed journal and conference articles [7, 37, 50, 51, 52, 53, 54].

After the current *Introduction*, this document is structured as follows:

- *Chapter 2* provides an overview of the current state-of-the-art in the design and modelling of liquid hydrogen tanks for aircraft integration. In this chapter, the novelty of the present work is stated as it introduces an original framework for the optimization of LH_2 vessels.

- *Chapter 3* presents the specific tank architecture on which the study is based and defines key figures of merit in storage system design. The chapter then proceeds by justifying the methodological choices driving the computational modelling and describes the numerical implementation of the optimization framework.

- *Chapter 4* outlines the results obtained by the exploration of the optimized design space of sandwich-composite-based passively insulated vessels, including the assessment of pragmatic features and constraints. The optimized storage solution is thus integrated into a state-of-the-art sustainable aircraft concept and the high-fidelity analysis of each tank component is presented.

- *Chapter 5* discusses the main findings of this thesis through a comparative assessment of the analysed tank configurations, with emphasis on the remaining gap with conventional kerosene storage in the context of sustainable aviation. It also concludes the thesis by summarising the key results, acknowledging the main limitations of the present work, and outlining future developments in tank modelling and optimization, aircraft integration, risk assessment, and certification.

Chapter 2

State of the art

In order to clarify the context and motivation of the present work, this chapter provides a review of the current state of the art of hydrogen-powered aviation, with particular emphasis on onboard storage systems. The discussion focuses on previous contributions dealing with aircraft-level storage integration, liquid hydrogen tank sizing, thermal management strategies, composite pressure vessel technologies, and numerical modelling approaches, with the intent of identifying the technological and methodological background from which the present work originates.

2.1 Foundational contributions to hydrogen storage for aviation

Early contributions to the field of H_2-powered aviation come from Brewer [55], who systematically investigated the implications of using hydrogen as an aircraft fuel at both component and system level. Brewer identified many of the principal technological constraints that still characterize the field today, including the low volumetric energy density of this energy carrier, the influence

of tank placement on aircraft layout, the distinction between integral and non-integral storage, and the need to balance storage efficiency with structural and operational safety. Although several enabling technologies have advanced since this study, the main design challenge remains largely unchanged: hydrogen itself offers substantial appeal from its high gravimetric energy density, but its storage imposes non-negligible penalties in terms of volume, tank mass, thermal management, and integration complexity.

At the beginning of the century, Mital et al. [42] reviewed the state of the art and the practical design issues associated with aviation-specific cryogenic vessels. Their work was particularly relevant in identifying several of the recurring limitations of aeronautical LH_2 storage, including: *i)* the mass penalty introduced by conservative structural design; *ii)* the difficulty of achieving adequate insulation without excessive system complexity; *iii)* the consequences of thermal-expansion mismatch among tank-wall constituents; and *iv)* the limited maturity of advanced materials under direct exposure to cryogenic environments. The same study also emphasized that the design of liquid hydrogen tanks cannot be reduced to the independent selection of a structural material and an insulation layer, as the thermal, mechanical, and compatibility requirements are indeed coupled.

Subsequent studies further clarified the influence of tank geometry and insulation strategy on aircraft-level storage performance. Winnefeld et al. [56] focused on the conceptual design of cryogenic hydrogen tanks for fuel-cell aircraft propulsion. Their analysis focused on the interplay between tank geometry, thermal management, and storage performance, showing that boil-off control and volumetric efficiency must be jointly addressed in aircraft applications. Similarly, Verstraete et al. [57] investigated LH_2 fuel tanks for subsonic transport aircraft, with emphasis on the trade-off between active and passive insulation methods. They highlighted how the severe degradation of active

multilayer insulation following a vacuum-loss event may represent a critical safety concern for commercial operations, whereas passive foam-based insulation offers a simpler and more robust alternative, although generally at the cost of larger insulation thickness. Their work also clarified the relationship between tank size and storage performance, confirming that larger cryogenic tanks benefit from more favourable surface-to-volume ratios. Building upon these considerations, Huete and Pilidis [58] conducted a high-level parametric study on hydrogen tank integration for civil aviation propulsion, with particular attention to the role of insulation strategies in the feasibility of onboard storage. Consistently with the conclusions of Verstraete et al., they found that vacuum-insulated systems, despite their superior thermal performance, may not necessarily represent the most suitable option for aircraft applications once the associated mass, subsystem complexity, and energy requirements are taken into account. This finding highlights that insulation performance alone is not sufficient to determine the suitability of a storage concept: the overall tank architecture must also be assessed in terms of mass efficiency, reliability, maintainability, and compatibility with aircraft integration constraints. Thus, a parametric approach for the integration of LH_2 tanks in short- to medium-range aircraft was proposed by Cipolla et al. [59]. Their work focused on aircraft-level performance implications and highlighted how tank placement affects the internal layout, payload arrangement, centre-of-gravity management, and mission-level behaviour. Although the study did not address detailed component-level optimization of the tank structure, it provided evidence that, in order to be truly efficient, storage system integration must be considered from the early stages of conceptual aircraft design.

2.2 Computational modelling of liquid hydrogen aircraft tanks

As interest in hydrogen-powered aircraft has increased in recent years, the related scientific literature has expanded significantly in both scope and depth. Adler and Martins [5] provided a comprehensive review of hydrogen-powered aircraft, covering fundamental concepts, performance metrics, propulsion technologies, storage implications, and environmental impact. Their contribution is particularly relevant because it links tank-level storage performance to aircraft-level energy demand, showing that the feasibility of hydrogen aviation is governed not only by the intrinsic properties of the fuel, but also by the efficiency of the overall storage system. Later, Adler and Martins [60] addressed the modelling and optimization of the coupled physical phenomena governing LH_2 storage systems. Their work focused on the development of a reduced-order liquid hydrogen evaporation model tailored for vacuum-insulated tank architectures, capturing the interactions among heat ingress, phase change, fuel consumption, and time-dependent operating conditions. By explicitly accounting for fuel-environment interactions and mission dependent thermal loads, the study provided quantitative insight into boil-off behaviour and identified the dominant parameters influencing thermal performance. Moreover, the proposed model was embedded within a design and optimization framework, enabling systematic trade-off analyses between insulation effectiveness, tank mass, and operational losses.

The need for higher-fidelity simulations of onboard hydrogen storage systems motivated the work of Gomez and Smith [61], who investigated the structural sizing and stress behaviour of fully metallic integral cryogenic tanks located within the forward and aft fuselage sections of the MRT7-3 Meridian concept for conventional mid-range commercial aircraft. Their linear finite

element (FE) analysis considered the combined effects of internal pressure, hydrostatic loads, thermal loads at cryogenic temperature, and critical manoeuvre conditions. Although the study focused on metallic tank configurations, it provided important insight into the structural implications of integrating LH_2 tanks within the fuselage of transport aircraft. Tzoumakis et al. [62] performed a multiphysics parametric analysis of an all-metal cryogenic tank, considering Al 2219 for both the inner and outer layers. Their study contributed to the understanding of coupled thermal and structural behaviour in cryogenic metallic vessels. However, the investigated configuration did not include pragmatic aircraft-integration features or high-performance composite materials, thereby limiting its direct applicability to lightweight tank design. Mantzaroudis and Theotokoglou [6] carried out a computational analysis of LH_2 storage tanks for aircraft applications, focusing on the thermo-mechanical behaviour of simplified cryogenic vessels. Their work confirmed the sensitivity of thermal performance and storage efficiency to the main geometric parameters. Nevertheless, the analysis remained primarily based on idealized tank configurations, without extending to the systematic optimization of realistic tank architectures.

2.3 Pressure vessel technologies for gaseous hydrogen storage

Beyond studies focused specifically on liquid hydrogen aircraft tanks, substantial progress has been made in recent years in the field of pressure vessels for gaseous hydrogen storage. The transition from all-metal to composite-based architectures, progressing through the Type I to V classification recalled in Tab.(1.2), is driven by the need to reduce structural mass of such components.

For GH_2 storage, where high internal pressure represents the dominant load, composite overwrapped pressure vessels are becoming the reference technological direction because of the high specific strength of fibre-reinforced materials.

Filament winding is the most established manufacturing route for cylindrical composite pressure vessels [63]. The process enables controlled deposition of continuous fibres over a liner or mandrel, allowing the designer to tailor the winding angle, fibre tension, number of layers, and laminate thickness according to the stress distribution generated by internal pressure. Several studies have investigated the influence of fibre orientation, winding sequence, and ply thickness on burst pressure and structural efficiency. Among these, Cohen et al. [64, 65] conducted extensive experimental campaigns correlating fibre volume fraction with failure pressure, providing data for the general sizing of wound composite shells. More recently, Automated Fibre Placement has emerged as an evolution of filament winding, offering improved control of tow placement and enabling the manufacture of more complex geometries through multi-axis robotic deposition [66]. This technology may reduce material waste and increase manufacturing accuracy, while also enabling local stiffness tailoring in regions where classical winding patterns are geometrically constrained.

Given the high pressures involved, the shape of GH_2 tanks must usually be conservative, as classical cylindrical and spherical vessels result in more even stress distribution. Nonetheless, alternative geometries have also been investigated. Toroidal pressure vessels, for example, have been proposed as a means to improve volumetric packing efficiency in constrained spaces, although their stress distribution is more complex than that of conventional cylinders or spheres [67]. Similarly, super-ellipsoidal dome profiles have been explored to reduce bending-induced stress concentrations in composite shells under internal pressure, with variable-stiffness laminates used to tailor the local mechanical response [68]. Such approaches are attractive for aircraft integration, where

available volume may not coincide with structurally ideal tank shapes.

Progressive damage modelling of composite H_2 tanks has also received considerable attention, motivated by the need to predict burst pressure and failure modes under complex loading conditions. Finite element modelling based on continuum damage mechanics have demonstrated the capability to capture the sequential evolution of matrix cracking, fibre-matrix debonding, delamination, and fibre rupture in filament-wound vessels [69]. A condensed overview of representative numerical approaches is reported in Tab. (2.1). Multi-scale strategies, in which microscale material models are embedded within a macroscale finite element analysis, have been proposed to improve the predictive fidelity of burst simulations. Other works have introduced cohesive elements to represent delamination and material degradation laws to reproduce post-failure stiffness loss [70, 71].

More advanced formulations, including fully coupled mechanical-chemical-thermal phase-field frameworks [79], have been developed to address the simultaneous influence of diffusion, thermal gradients, and mechanical loading in multilayered composite vessels [80, 81]. Although these models are computationally demanding, they provide a more complete representation of degradation mechanisms relevant to hydrogen environments. The growing interest in composite cryogenic vessels has also stimulated the development of novel material strategies. Thermoplastic matrix composites, in particular, have attracted attention because of their potential resistance to microcracking, their weldability, and their recyclability advantages over conventional thermoset systems [82]. Nevertheless, their application to aircraft hydrogen tanks requires further validation in terms of permeability, damage tolerance, long-term durability, thermal cycling, and compatibility with cryogenic operating conditions.

Table 2.1: Condensed overview of representative numerical approaches for progressive damage analysis of composite pressure vessels.

Numerical approach	**Representative implementation**	**Main contribution**
Failure-pressure and degradation-based FE models	`ANSYS`-APDL and `ABAQUS`; instantaneous degradation, first-ply failure, and stiffness-degradation models	Prediction of nonlinear stress–strain response, manufacturing-imperfection effects, and burst pressure in filament-wound composite pressure vessels [35, 72, 73].
Continuum damage mechanics	`ANSYS`-APDL and `ABAQUS`; intralaminar damage and cohesive-interface modelling	Progressive simulation of matrix cracking, fibre-dominated failure, delamination, post-failure stiffness degradation, and ultimate strength of composite hydrogen vessels [74, 75, 76, 77].
Multiscale and micromechanics-based damage models	Coupled `ANSYS`-APDL/`ABAQUS` or `ABAQUS`-based implementations	Connection between microscale material degradation and macroscale vessel response, improving the prediction of burst pressure and thermo-mechanical failure mechanisms [69, 71, 78].
Phase-field formulations	In-house FE codes; coupled mechanical–chemical–thermal phase-field models	Representation of damage evolution in multilayered composite vessels under coupled mechanical loading, thermal gradients, material degradation, and hydrogen diffusion [79].

2.4 Material compatibility with hydrogen and degradation mechanisms

Material compatibility with the fuel properties is a central consideration in the design of both gaseous and liquid H_2 tanks. In gaseous storage, the issue is often associated with high pressure permeation and hydrogen-induced degradation of metallic liners or structural shells. In liquid storage, the problem becomes more complex because very low temperatures, thermal cycling, hydrogen diffusion, and thermal expansion mismatch may act simultaneously.

Moreover, hydrogen embrittlement has been widely studied for metals such as steels and titanium alloys, where hydrogen diffusion can reduce ductility, fracture toughness, and resistance to crack growth [46, 48, 83]. Aluminium alloys and copper-based materials are generally less susceptible, which explains their recurrent use as candidate liner materials in hydrogen storage applications. An overview of representative material candidates for hydrogen tank internal walls is reported in Tab. (2.2), with emphasis on their typical use, permeation behaviour, and main advantages and limitations.

Table 2.2: Material candidates for tank inner wall construction.

Material	**Use case**	**Density** [kg/m^3]	**Permeation susceptibility**	**Advantages**	**Disadvantages**
Al 2219-T8	Inner liner & tank wall	2840	Very low	Low cost, established	High mass, high conductivity
Al 8090-T8	Inner liner & tank wall	2540	Low	Low cost, established	High mass, high conductivity
Al 2090-T8	Inner liner & tank wall	2590	Very low	Low cost, established	High mass, high conductivity
CFRP	Outer structural layer	1600	High	Low mass, high mechanical properties	Higher cost, prone to microcracking and permeation

Therefore, mitigation strategies, such as the use of metallic liners, protective coatings, and zinc or nickel plating, are well documented and known to be effective. Nonetheless, the interaction among liner, composite overwrap, and insulation systems under mechanical and thermal loads combined with direct and prolonged hydrogen exposure remains not fully characterized.

For composite cryogenic tanks, material compatibility is not limited to hydrogen permeation. The mismatch between the coefficients of thermal expansion of carbon fibres and polymer matrices can generate residual stresses during cooldown and warm-up. These stresses may promote matrix microcracking, interfacial debonding, or delamination, creating possible permeation paths and reducing the durability of the laminate. The X-33 programme is often cited as an example of the risks associated with cryogenic composite tank design, where microcracking and trapped cryogenic fluid contributed to structural failure during testing [84]. Subsequent studies have shown that thin-ply laminates, toughened matrices, and more compliant interlayers can mitigate microcracking under cryogenic cycling [85, 86].

Thus, the main design implication from material compatibility challenges is that material selection cannot be separated from tank architecture. A material that is suitable for a liner may not be suitable for a load-bearing shell, and a composite laminate that performs well under ambient pressure vessel conditions may behave differently under cryogenic cycling.

2.5 Emerging strategies for improving storage efficiency

In parallel with conventional physical storage methods based on compressed or cryogenic hydrogen, several material-based storage strategies have been inves-

tigated to improve storage efficiency. These include metal-organic frameworks, carbon nanotubes, hollow glass microspheres, and graphene-based nanomaterials [37]. Unlike physical containment, these approaches rely on adsorption, encapsulation, or enhanced barrier behaviour. Their theoretical appeal lies in the possibility of improving volumetric or gravimetric storage density, reducing tank mass, or increasing resistance to permeation.

Accordingly, metal-organic frameworks are porous crystalline materials characterized by high specific surface area and tunable pore size [87]. They have been investigated for hydrogen adsorption because their internal structure can be tailored to increase storage capacity and regulate adsorption-desorption behaviour [88]. Carbon nanotubes and graphene-based materials have similarly attracted attention due to their low density, large surface area, and potential use as additives or barrier layers [89]. Indeed, graphene derivatives may improve polymer-matrix impermeability, whereas carbon nanotubes may contribute to hydrogen adsorption or multifunctional composite behaviour [90, 91]. Hollow glass microspheres have also been explored as encapsulation media, because hydrogen can diffuse into the microspheres at elevated temperature and pressure and then be retained after cooling [92].

Despite their scientific interest, these material-based strategies remain at comparatively low technology readiness for aviation. The principal barriers include scalable production, repeatable material quality, cost, charging and discharging time, system-level mass, and long-term durability concerns. Consequently, they should not be regarded as near-term replacements for compressed or liquid hydrogen tanks. Rather, they represent possible future pathways for improving storage efficiency, especially if integrated as multifunctional components within more conventional tank architectures.

In this context, as it will be further discussed in Chapter 5, structural health monitoring and non-destructive inspection represent another route to improved

storage efficiency. Hydrogen tanks are commonly designed with conservative safety margins because of uncertainty in material behaviour, manufacturing variability, damage tolerance, and the limited experimental database available under representative hydrogen conditions [42]. If damage, strain, temperature, pressure, and leakage could be monitored reliably throughout service, future designs may reduce excessive conservatism while preserving safety [93]. Optical fibres, fibre Bragg grating sensors, and piezoelectric transducers have been investigated for cryogenic applications and have shown potential for damage detection, strain monitoring, and leakage identification [94, 95, 96, 97]. However, their long-term reliability under repeated thermal cycles, their integration into composite or sandwich tank walls, and their acceptance within certification frameworks remain open research questions.

2.6 Hydrogen aviation projects and demonstrators

At the project and demonstrator level, a number of industrial and government-funded initiatives have provided tangible evidence of the progress being made toward H_2-powered flight. Early feasibility constraints were established by the European Cryoplane project [98] which assessed hydrogen integration within commercial aircraft. Later, the CHATT project investigated CFRP cryogenic vessels, including cylindrical tanks, dry-wing configurations, linerless concepts, and unconventional geometries [99]. The project showed that thin-ply laminates can considerably reduce or suppress microcracking in cryogenic environments, while also exploring advanced cryogenic insulation concepts. ENABLEH2 matured technologies for LH_2-based propulsion, developing conceptual-design tools for fuel-system components and investigating hydrogen-air com-

bustion [100]. THOR focused on thermoplastic composite pressure vessels, including aspects related to manufacturability, fire exposure, and optical-fibre monitoring [82].

The most recent project landscape is more dynamic. Some programmes have progressed toward component demonstration, whereas others have been delayed, re-scoped, or discontinued. Accordingly, Tables (2.3) and (2.4) provide the list of representative hydrogen aviation projects and companies, with emphasis on fuel storage technology and publicly available status as of 2026.

The updated project landscape indicates that hydrogen aviation is progressing, but at a more cautious pace than suggested by some early industrial roadmaps. Liquid hydrogen remains central to long-range and larger-aircraft concepts, where storage density is decisive, whereas gaseous hydrogen continues to fuel several near-term demonstrators because of its lower thermal complexity. The delay of some commercial aircraft timelines and the discontinuation of certain start-up activities do not reduce the technical relevance of hydrogen storage research. Rather, they reinforce the need for design methodologies capable of quantifying the mass, thermal, structural, and integration trade-offs of candidate tank architectures.

The same project landscape also highlights that technological demonstration and certification readiness do not necessarily progress at the same pace. For cryogenic hydrogen storage systems, the transition from demonstrator-scale hardware to certifiable aircraft components requires qualification evidence that extends beyond nominal performance metrics. In particular, future tank development must address pressure containment, venting and pressure-relief reliability, leak-tightness, material compatibility, damage tolerance, inspection capability, fire and impact resistance, and safe behaviour under abnormal thermal or pressure transients. In this respect, documents such as NASA-STD-6016 [101] provide useful guidance on materials and processes control, verifica-

tion logic, and qualification philosophy for aerospace hardware, although they are not directly applicable commercial aircraft certification rules. Similarly, EASA SC E-19 [102] is not a tank-specific hydrogen storage standard, but it illustrates the certification approach adopted for novel propulsion architectures.

2.7 Literature gap and positioning of the present work

The reviewed literature has substantially advanced the understanding of hydrogen storage for aviation. Foundational studies clarified the aircraft-level implications of hydrogen as a fuel; conceptual analyses quantified the influence of tank geometry and insulation strategy; finite element investigations provided insight into the thermo-mechanical response of selected cryogenic vessels; and composite pressure vessel research developed increasingly sophisticated manufacturing and damage modelling approaches. Nevertheless, a gap remains between high-level component sizing and detailed tank-level simulations.

In particular, studies such as those by Gomez and Smith [61], Tzoumakis et al. [62], and Mantzaroudis and Theotokoglou [6] provide valuable understanding of the behaviour of LH_2 storage vessels, but they do not address the systematic optimization of realistic tank layouts from a coupled thermo-mechanical perspective. Conversely, aircraft-level and reduced-order models are effective for system studies, but necessarily simplify the local structural and thermal behaviour of the storage component. Furthermore, the literature still contains limited examples in which composite-based cryogenic architectures, thermal insulation, material constraints, and integration-related design features are treated within a unified optimization framework.

Table 2.3: Summary of selected hydrogen-aviation projects and industrial initiatives relevant to onboard storage and propulsion, status as of 2026 (Part 1 of 2).

Project / Company	**Status (2026)**	**Main relevance to hydrogen aircraft storage and propulsion**
Airbus ZEROe	Active; delayed	Large-aircraft industrial benchmark for LH_2 integration, hydrogen combustion, and fuel-cell propulsion. The original mid-2030s entry target has been postponed due to slower maturation of enabling technologies and infrastructure [103, 104].
Universal Hydrogen	Discontinued (2024)	Regional-aircraft retrofit concept based on modular hydrogen capsules and hydrogen-electric propulsion. Its closure exposed the commercial and infrastructure challenges of hydrogen retrofit strategies [105].
H2FLY	Active	Hydrogen-electric propulsion demonstrator with cryogenic storage experience. The HY4 aircraft completed piloted flights powered by LH_2, providing evidence for small-aircraft cryogenic storage and fuel-cell integration [106].
ZeroAvia	Active; certification progressing	Hydrogen-electric powertrain developer for regional aircraft. Near-term demonstrators rely on gaseous hydrogen, making the programme relevant to early certification pathways and compressed-storage entry strategies [107].
THOR	Concluded	Developed thermoplastic composite pressure vessels with emphasis on manufacturability, safety under fire exposure, recyclability, and structural monitoring via embedded optical fibres [82].
ENABLEH2	Concluded	Matured technologies for LH_2-based civil aviation propulsion, including conceptual-design tools for fuel-system components and hydrogen combustion studies [100].
HYDEA	Active (2023–2026)	Clean Aviation project addressing hydrogen combustion, combustor design, engine fuel systems, low-NO_x emissions, and aircraft integration, targeting TRL 5 by the end of 2026 [108].

Table 2.4: Summary of selected hydrogen-aviation projects and industrial initiatives relevant to onboard storage and propulsion, status as of 2026 (Part 2 of 2).

Project / Company	**Status (2026)**	**Main relevance to hydrogen aircraft storage and propulsion**
CHATT	Concluded	Developed and tested CFRP cryogenic tank demonstrators including cylindrical, linerless, and dry-wing concepts. Key results concern thin-ply laminates, microcracking mitigation, and composite cryogenic feasibility [99, 86].
Project Fresson / Cranfield Aerospace Solutions	Active; reoriented	Small-aircraft hydrogen fuel-cell powertrain development with adaptable storage strategies, including gaseous hydrogen and possible future LH_2 solutions [109].
H2ELIOS	Active (2023–2026)	Directly focused on lightweight LH_2 storage for aircraft, including fuselage-integrated demonstrators and subsystem ground tests toward storage system TRL 5 [110].
CAVENDISH	Active	Develops LH_2 direct-combustion technologies for ground testing on a donor aeroengine, including dual-fuel combustion and cryo-compressed storage concepts [111].
COCOLIH2T	Active	Develops safe composite and vacuum-insulated conformal LH_2 tanks for aviation, relevant to non-cylindrical storage architectures and volumetric-efficiency improvement [112].
SHZ Advanced Technologies	Exploratory	Investigates LH_2 storage and distribution for blended-wing-body aircraft, relevant to unconventional layouts and future cryogenic tank integration [113].
Beyond Aero	Active; gaseous-H_2 route	Hydrogen-electric business-aircraft concept using externally mounted 700 bar gaseous-hydrogen tanks, illustrating the continued relevance of compressed storage for specific aircraft classes [114].

The present thesis is positioned within this gap. It develops a computational framework for the design and optimization of aviation-oriented cryogenic hydrogen tanks, combining finite element thermo-mechanical analysis with nonlinear constrained optimization. Although the underlying numerical modelling and optimization techniques are individually well established, their combined application to the exploration of realistic liquid hydrogen tank architectures remains limited in the open literature. The following chapter therefore introduces the tank architecture, modelling assumptions, and optimization strategy adopted in this work, providing the methodological basis for the subsequent design-space exploration and aircraft-integration assessment.

Chapter 3

Tank definition, modelling and optimization

This chapter discusses the methodological framework introduced by this thesis. In particular, the tank conceptual design is first presented with emphasis on geometric considerations and layered architecture followed by the definition of fundamental metrics necessary to compare and characterize the component performance. The chapter then proceeds with a comprehensive description of the numerical model utilized to simulate the thermo-mechanical response of the LH_2 vessel and its operating conditions followed by the definition of the optimization problem statement which, relying on safety-factor-adjusted constraints, is embedded into the framework to iteratively update the tank design until the optimum configuration is achieved.

3.1 Storage system design

Given the currently limited maturity and low standardization of liquid hydrogen tank integration strategies in aviation, the vessel examined in this study is conceived to maximize modularity and scalability across different airframe

architectures.

Figure 3.1: *a)* Non-integral tank architecture in which the pressure vessel is structurally independent from the aircraft fuselage. The tank experiences a pressure differential defined by the difference between the internal tank pressure and the internal fuselage pressure *vs b)* integral tank in which the walls are partially made by the aircraft fuselage structure. In this configuration, the tank is subjected to a pressure differential equal to the difference between the internal tank pressure and the external ambient pressure.

The tank model adopted in this study is therefore designed as a *non-integral* unit, which, as schematized in Fig.(3.1a), is a self-supporting vessel, structurally independent of the aircraft fuselage, and therefore does not participate in primary load transfer, simplifying its design. Unlike integral tanks, Fig.(3.1b), which are embedded within the airframe and must sustain global structural loads, the non-integral configuration allows greater flexibility in defining tank geometry, dimensions, and layout.

From a structural standpoint, the choice between integral and non-integral hydrogen tanks represents a major design trade-off. Integral tanks generally achieve higher volumetric efficiency due to a more effective use of available space; for example, Brewer [55] reports fuel volumetric efficiencies of 92.7% for integral tanks compared to 85.5% for non-integral solutions. However, integral designs require the tank structure to withstand airframe loads and tightly couple tank and fuselage design.

By contrast, non-integral tanks are primarily subjected to internal pressure,

fuel-induced loads, and dynamic effects associated with fluid motion, without reacting global airframe loads [56]. This decoupling allows the use of geometries that do not necessarily conform to the fuselage shape and enables modular design approaches that considerably facilitate inspections, maintenance, and adaptability to different aircraft layouts. For these reasons, the non-integral configuration is considered in the present work as a suitable baseline for the investigation of scalable liquid hydrogen storage solutions.

3.1.1 Geometric parameters

The geometry of cryogenic pressure vessels is another design consideration that strongly influences both thermal management and structural response.

From a thermal standpoint, heat leak is minimized by reducing the surface area-to-volume ratio, which favours shapes approaching a sphere as reported in Fig. (3.2). However, H_2 tanks, especially if spherical, are poorly suited for aircraft integration, particularly within the wing structure, and may therefore be located inside the fuselage, at the expense of payload volume or in a dedicated external fuel pod. If the aircraft internal volume is required to remain unchanged after the introduction of the hydrogen tanks, an increase in wetted area, for instance due to fuselage lengthening, is generally unavoidable, with a corresponding aerodynamic drag penalty. In addition, relocating fuel from the wing removes the structural load alleviation effect provided by the wet-wing storage solution, potentially increasing the structural weight of the wing/wingbox assembly. As a result, hydrogen storage is generally associated with both drag and mass penalties.

Beyond thermal and aerodynamic considerations, large spherical vessels also present substantial challenges in terms of *spatial integration* [31], defined as the effective arrangement of crew, payload, fuel, structural elements, and on-

board systems within a feasible aircraft layout. These constraints further limit the practical applicability of spherical or near-spherical tanks in conventional transport aircraft.

A pragmatic compromise is therefore required, favouring tank geometries that efficiently utilize the available volume while remaining compatible with aircraft layouts. Cylindrical-based vessels with hemi-spherical or hemi-ellipsoidal endcaps represent a commonly adopted solution [115], as they can be readily integrated within the conventional fuselages and adapt well to unconventional designs such as the BWBs. Such geometries are highly parametrizable and scalable, and offer advantages in terms of manufacturability and modularity.

An additional consideration arises from cryogenic tank scalability: larger tanks are indeed preferable, since surface area scales with the square of the characteristic dimension, whereas stored volume increases with its cube, resulting in improved thermal efficiency at larger scales.

Tank geometry is also considerably influenced by the necessity to comply with airworthiness regulations. For instance, the European certification specifications for large aeroplanes [116] require unobstructed crew access to the passenger cabin; consequently, when a forward H_2 tank is positioned behind the cockpit, the inclusion of a dedicated catwalk becomes necessary. On this subject, additional regulatory provisions may also be applicable to hydrogen pressure vessels, such as EASA CS§25.963, which addresses hydrostatic pressure increments under acceleration. Nevertheless, while portions of the current regulatory framework can be adapted to hydrogen-powered aircraft, several aspects specific to onboard H_2 storage require further assessment before commercial deployment becomes feasible as it will be outlined in Sec. (5.4.2).

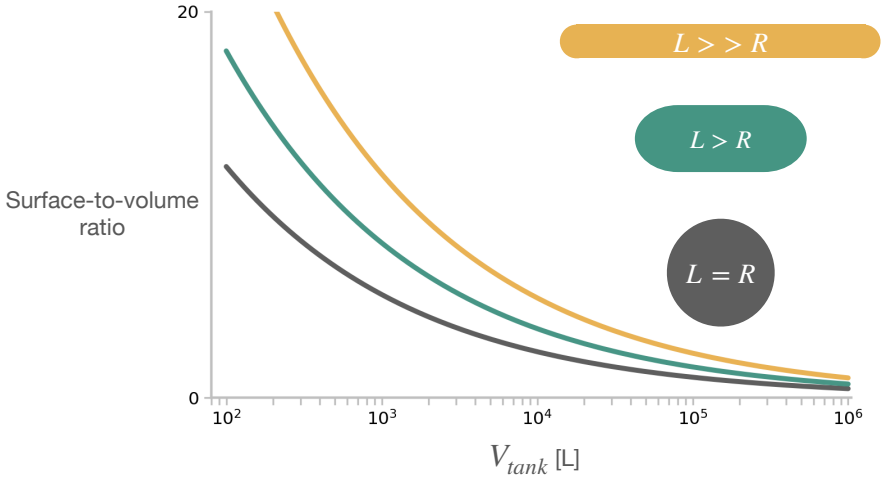

Figure 3.2: Effects of tank shape and scalability. Considering L the length of the vessel and R its radius, large, spherical tanks ($L = R$) are ideal from a thermal standpoint yet incompatible with most aircraft architectures. Cylindrical vessels ($L \neq R$) conform better to conventional fuselages but yield higher surface-to-volume ratios, degrading thermal performance. Adapted from Ref. [5].

3.1.2 The passively-insulated architecture

Under the combined demanding constraints imposed by mass minimization, integration compatibility, thermal management, and structural reliability, the *passively-insulated cryogenic sandwich-composite* tank architecture [37] is identified as a possible solution, which minimizes the number and mass of subsystems required for operation while reuniting in the same structure: *i*) a liner, required for H_2 containment; *ii*) a low density, low conductivity, low diffusivity insulation material that allows for dimensional variations; *iii*) an outer structural shell. A schematic representation of the passively-insulated layered layout is provided in Fig. (3.3),

A first layer, referred to as the internal liner, is necessary for fuel containment and in cryogenic H_2 tanks is commonly manufactured from lightweight

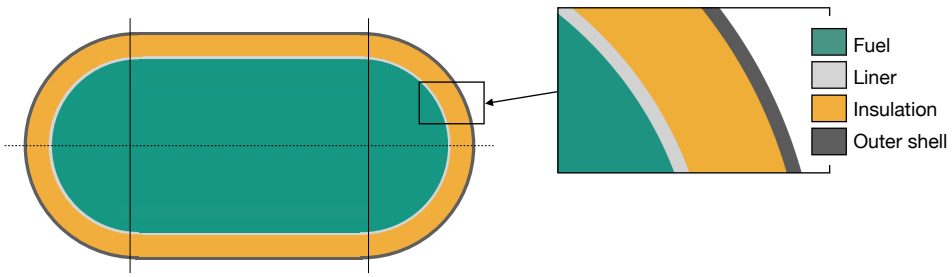

Figure 3.3: Schematic of the insulated cryogenic sandwich architecture featuring a thin inner liner and outer structural layers and thick intermediate foam insulation.

polymers or high-strength metallic alloys. In the present study, a specific aluminum–copper alloy, the Al 2219-T8, is selected due to its favourable combination of low density, excellent performance at cryogenic temperatures, corrosion resistance, and cost-effectiveness. This alloy undergoes a sequence of heat treatment, cold working, and artificial ageing processes to achieve the required mechanical properties [117, 118], which ultimately determine its negligible susceptibility to hydrogen-induced embrittlement [46].

Thermoset polyurethane (PUR) foam is employed as the core material of the sandwich architecture, with a thickness significantly greater than that of the surrounding structural layers. Its extensive use in aerospace cryogenic applications [119] demonstrates its effectiveness as a reliable and comparatively simple thermal barrier. In addition, PUR foam offers highly adaptable insulation characteristics, as spray-on deposition techniques enable precise control of thickness and uniformity [120]. Additionally, owing to its widespread adoption in aerospace systems, comprehensive thermo-mechanical characterization of PUR foam is available in the specialized literature [121, 122], allowing temperature-dependent material properties to be incorporated into the numerical tank model.

As discussed later in this thesis, Al 2219-T8 alone is not suitable for the construction of the outer structural layer of the tank, if no additional reinforce-

ment is considered, as done, for example, in the study by Gomez and Smith [61]. Consequently, materials possessing higher mechanical performance must be considered for this role. Hence, two mutually exclusive alternatives for the external layer are investigated: a titanium-based high-strength metallic outer shell and a fibre-reinforced composite laminate. Among metallic candidates, the titanium alloy Ti-6Al-4V is considered due to its high specific strength and well-established use in aerospace applications [123, 124, 125].

The thermo-mechanical material properties adopted in the present work for the modelling of the isotropic tank materials, namely the internal liner, the insulating foam, and the metallic outer shell are summarized in Tab. (3.1).

Table 3.1: Mechanical and thermal properties of aluminium 2219-T8 alloy, unreinforced polyurethane PUR-96 foam, and Ti-6Al-4V alloy.

Property	**Symbol**	**Aluminium**	**Polyurethane**	**Ti-6Al-4V**	**Unit**
Young's modulus	E	73.1	0.11	93.0	GPa
Poisson ratio	ν	0.33	0.30	0.34	—
Density	ρ	2840	96	4430	$\mathrm{kg/m^3}$
Conductivity	κ	121	0.0163	6.7	$\mathrm{W\,m^{-1}\,K}$
Specific heat capacity	C_p	864	1100	560	$\mathrm{J\,kg^{-1}\,K}$
Thermal expansion coefficient	α	2.2×10^{-5}	30.9×10^{-6}	8.6×10^{-6}	$\mathrm{K^{-1}}$
Yield strength	$\bar{\sigma}_y^{\mathrm{mat}}$	500	2.25	1273	MPa
Reference temperature	T_{ref}	20	95	288	K

The second material candidate for the manufacturing of the outer structural

shell is a carbon fibre–reinforced plastic (CFRP). Although the application of composite materials in cryogenic environments presents challenges due to the limited characterization of their behaviour at extremely low temperatures, several studies have demonstrated their feasibility when appropriately integrated within multilayer architectures.

Early investigations by Horiuchi and Ooi [126], for example, showed that CFRP laminates retain high tensile strength at cryogenic temperatures, while long-duration operation and vibration tests of cryogenic support structures reported no measurable degradation in structural performance. Subsequent experimental studies have provided insight into the dominant degradation mechanisms under cryogenic conditions. Accordingly, Gates et al. [127] observed that interfacial debonding in sandwich composites primarily occurs at the adhesive–core interface, with fracture toughness increasing by approximately 20% at 4 K compared to ambient temperature, indicating enhanced resistance to delamination rather than embrittlement at low temperatures. Conversely, Islam et al. [85] highlighted the effects of the pronounced mismatch in the coefficients of thermal expansion α, between carbon fibres ($\approx -1 \times 10^{-6}\,\mathrm{K}^{-1}$) and epoxy matrices ($\approx 50 \times 10^{-6}\,\mathrm{K}^{-1}$), which can induce thermally driven stresses during cyclic operation, promoting matrix microcracking and resin embrittlement. The same study also demonstrated that these effects can be effectively mitigated through matrix toughening strategies and the introduction of compliant or low-α interlayers, which suppress microcrack formation and improve interlaminar toughness at cryogenic temperatures.

In the present multilayer tank architecture, these risks are further reduced by positioning the composite shell on the exterior side of the insulation, away from the cryogenic and potentially aggressive fuel environment. As a result, the CFRP layer remains close to ambient temperature, limiting exposure to severe thermal gradients and associated thermal stresses, while physically sep-

arating the composite material from the stored H_2, both in its gaseous form, present in the ullage, and liquid phase. The presence of the metallic inner liner additionally acts as a barrier against hydrogen permeation, further enhancing operational safety and protecting the weaker foam inner surface. Based on these considerations, the use of a composite outer shell is adopted in the present study.

The CFRP material is modelled using individual ply properties which are summarized in Tab. (3.2) and extracted from Refs. [128, 6].

As the proposed tank configuration involves both a multilayer wall architecture and a laminated composite shell, a distinction in terminology is adopted throughout this work to avoid ambiguity. In particular, the term *layer* refers exclusively to the three main constituents of the tank wall, namely the liner, the foam insulation, and the outer shell, whereas the term *ply* denotes an individual lamina within the laminated composite stack. Additionally, the tank considered in this thesis may be classified as a cryogenic composite pressure vessel with COPV-like features, since it combines a metallic liner for hydrogen containment with an external composite structural shell. However, it differs from conventional composite overwrapped pressure vessels because the composite shell is separated from the liner by a thick insulation layer and the tank operates at low pressure rather than at the several-hundred-bars typical of compressed hydrogen COPVs.

Table 3.2: Mechanical and thermal properties of the carbon fibre-reinforced plastic, reported as individual ply properties.

Property	**Symbol**	**Value**	**Unit**
Young's modulus	E_{11}	133	GPa
	$E_{22} \equiv E_{33}$	9.13	GPa
Poisson's ratio	$\nu_{12} \equiv \nu_{13} \equiv \nu_{23}$	0.30	—
Shear modulus	$G_{12} \equiv G_{13} \equiv G_{23}$	5.2	GPa
Density	ρ	1600	$\mathrm{kg\,m^{-3}}$
Thermal conductivity	K_{11}	3.972	$\mathrm{W\,m^{-1}\,K}$
	$K_{22} \equiv K_{33}$	0.3363	$\mathrm{W\,m^{-1}\,K}$
Specific heat capacity	C_p	1130	$\mathrm{J\,kg^{-1}\,K}$
Thermal expansion coefficient	α_{11}	-0.2×10^{-6}	$\mathrm{K^{-1}}$
	$\alpha_{22} \equiv \alpha_{33}$	30×10^{-6}	$\mathrm{K^{-1}}$
Reference temperature	T_{ref}	288	K
Longitudinal tensile strength	X_{t}	2950	MPa
Longitudinal compressive strength	X_{c}	1570	MPa
Transverse tensile strength	Y_{t}	79	MPa
Transverse compressive strength	Y_{c}	190	MPa
Longitudinal shear strength	S_{l}	140	MPa
Transverse shear strength	S_{t}	88	MPa

3.1.3 Figures of merit

Gravimetric efficiency

As anticipated, the profound differences existing between hydrogen- and kerosene-powered aviation originate from the physical properties of H_2, which demands peculiar storage conditions in order to achieve practical energy density. Accordingly, the integration of hydrogen storage systems into viable aircraft configurations is typically associated with mass penalties, which are commonly quantified through the *gravimetric efficiency* ($\eta_{\,\mathrm{tank}}$), also referred to as the *gravimetric index*:

$$\eta_{\,\mathrm{tank}} = \frac{W_{\mathrm{H_2}}}{W_{\mathrm{H_2}} + W_{\mathrm{tank}} + W_{\mathrm{subsystems}}}, \tag{3.1}$$

where $W_{\mathrm{H_2}}$ denotes the weight of hydrogen stored at design conditions, W_{tank} is the structural weight of the tank, and $W_{\mathrm{subsystems}}$ represents the weight of the ancillary systems required for tank operation. In the case of purely passive components, the latter contribution is assumed to be negligible and is therefore set to zero.

The gravimetric efficiency provides a direct measure of the penalties associated with specialized hydrogen storage systems when compared to conventional, highly optimized kerosene fuel tanks that are usually characterized by values of gravimetric efficiencies of 100%, being integral with the wing structure and effectively adding minimal mass to the structural elements themselves. In general, increasing $\eta_{\,\mathrm{tank}}$ reduces the overall mass penalty associated with fuel storage and, consequently, lowers the total energy demand of a hydrogen-powered aircraft. This metric therefore has a system-level impact on both aircraft feasibility and competitiveness.

As evidenced by Adler and Martins [5], the impact of the tank gravimetric efficiency on aircraft-level performance is non-linear and coupled to

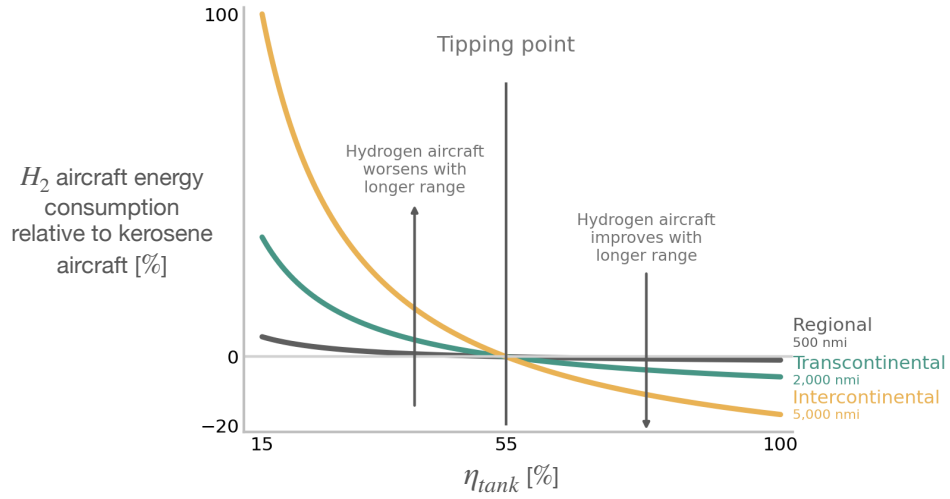

Figure 3.4: Effect of tank gravimetric efficiency on the relative fuel energy consumption of hydrogen- and kerosene-powered aircraft across different mission ranges. A transition occurs at $\eta_{\text{tank}} \approx 55\%$, beyond which hydrogen-powered aircraft become energetically favourable. Adapted from Adler et al. [5].

mission range. This behaviour is illustrated in Fig. 3.4, which compares the total energy required by hydrogen-powered aircraft to that of an equivalent kerosene-fuelled configuration over a range of mission lengths and tank gravimetric efficiencies. Accordingly, for low values of η_{tank} the additional mass associated with hydrogen storage systems offsets the benefit of hydrogen's high specific energy. Consequently, the total energy consumption of hydrogen-powered aircraft increases more rapidly with mission range than that of conventional kerosene aircraft. Critically, as the tank gravimetric efficiency increases, Fig. 3.4 shows a transition in this trend: when η_{tank} exceeds 55%, the reduction in required fuel mass enabled by H_2 energy density outweighs the mass penalty introduced by the specialized storage system. Hence, beyond this threshold, hydrogen-powered aircraft exhibit lower overall energy consumption than their kerosene-powered counterparts, with the relative advantage increas-

ing with mission range. This transition occurs at approximately the same gravimetric efficiency across the investigated range of mission lengths. These results indicate that tank gravimetric efficiency plays a governing role in determining whether hydrogen-powered aircraft yield an energy benefit relative to conventional configurations.

Boil-off rate

In addition to the mass penalties associated with hydrogen storage, cryogenic fuel tanks present a further challenge related to the heat ingress driven by the temperature differential between the inner cavity of the vessel and the external environment. While practical insulation methods significantly reduce heat transfer, in practice they cannot completely avoid it. As a result, a fraction of the cryogenic liquid continuously evaporates. Under *autogenous pressurization*, the gaseous hydrogen generated by this heat input must be vented in order to prevent internal pressures from exceeding the structural limits of the vessel.

To quantify the thermal performance of the tank, the *boil-off rate* (BOR) is adopted and defined as

$$\mathrm{BOR} = \frac{Q}{\rho_{\mathrm{LH_2}} V_{\mathrm{LH_2}} \lambda_{v_{\mathrm{LH_2}}}}, \tag{3.2}$$

where Q denotes the total heat entering the tank cavity from the external environment, $\rho_{\mathrm{LH_2}}$ is the density of liquid hydrogen, $V_{\mathrm{LH_2}}$ is the volume of fuel contained in the tank, and $\lambda_{v_{\mathrm{LH_2}}}$ represents the latent heat of vaporization of $\mathrm{LH_2}$.

For layered tank architectures, such as the configuration illustrated in Fig. (3.3), the overall thermal resistance of the wall (R_{th}) can be approximated

using an electrical analogy as

$$R_{\text{th}} = \sum_i \frac{t_i}{\kappa_i \, S_i} \qquad i \in \{\text{Liner, Insulation, Outer shell}\}, \tag{3.3}$$

where t_i is the thickness of the i^{th} layer, κ_i is the thermal conductivity of the corresponding material, and S_i is the surface area through which heat transfer occurs. Under steady conditions, the total heat flux can therefore be estimated as $Q = \Delta T / R_{\text{th}}$, which allows the boil-off rate to be evaluated through Eq. (3.2). It should be noted that the instantaneous boil-off rate is not constant over the course of a mission. As fuel is consumed and the filling ratio decreases, the BOR increases, following an approximately quadratic trend [50].

Therefore, to enable consistent and meaningful comparisons of thermal performance across different tank designs, the boil-off rate is evaluated assuming a full-tank condition. This assumption is necessary to avoid misleading comparisons between partially filled and fully filled configurations and thus provides a uniform benchmark for design assessment. As discussed in Sec. (5.2.1), future developments of the framework will extend the analysis to account for fuel consumption and transient mission-dependent effects.

A maximum BOR magnitude is identified by Mital et al. [42] as a technologically and commercially viable compromise, enabling practical energy densities for airborne liquid hydrogen storage systems. Therefore, as a design requirement, a maximum allowable daily boil-off rate of $\text{BOR}_{\text{allowable}} = 2.50\%$ of the stored LH_2 mass, corresponding for the reference capacity of $100\,\text{m}^3$, to approximately $8.18\,\text{kg}\,\text{h}^{-1}$, is adopted throughout the study and will represent a major driver in insulation quantity optimization.

3.2 Tank computational model

This section describes the methodology adopted for the thermo-mechanical analysis of the passively-insulated composite LH_2 tanks within the finite-element framework, providing justification for various design and modelling assumptions. As previously stated, the considered tank features a multi-layered architecture specifically designed for the storage of hydrogen at cryogenic temperatures. The tank geometry, material properties, and structural details are implemented in the finite-element model through dedicated parametric scripts.

3.2.1 Thermo-mechanical loads and boundary conditions

In addition to the geometric and material definitions defined in Sec.3.1.2, the thermo-elastic analyses performed in this work require the specification of operational boundary conditions. These include the internal and external temperatures and pressures acting on the tank, which are dictated by the requirement to maintain hydrogen in its liquid phase while preventing the ingress of ambient air into the vessel.

Given that non-integral tanks are assessed, the external surface of the vessel is assumed to be exposed to the temperature of the surrounding fuselage compartment. The fuselage environment is assumed to be pressurized air at a controlled temperature of $T_{\text{fus}} = 283\,\text{K}$, which is consistent with the minimum achievable value provided by environmental control systems in commercial airliners [129]. This temperature is selected to minimize the temperature difference ΔT between the tank exterior and the cryogenic interior.

The temperature of the tank external wall, denoted as T_{ext}, is treated as an unknown in the thermal model, while natural convection is assumed to occur in the surrounding fuselage environment. Under steady-state conditions, the inward convective heat flux at the external wall is driven by the tem-

perature difference between the fuselage air and the tank surface, defined as $\Delta T_{\text{ext}} = T_{\text{fus}} - T_{\text{ext}}$. Accordingly, the convective heat flux at the tank exterior is expressed as

$$q_{\text{ext}} = h_c^{\text{ext}} \left(T_{\text{fus}} - T_{\text{ext}} \right), \tag{3.4}$$

where h_c^{ext} is the external convective heat transfer coefficient. In line with Ref. [6], a value of $h_c^{\text{ext}} = 10\,\text{W/m}^2\text{/K}$ is adopted, representative of natural convection in a pressurized fuselage environment. The steady-state thermo-mechanical coupling employed in the present analysis reflects the quasi-static conditions expected during cruise, where boundary temperatures evolve slowly compared with the characteristic thermal diffusion time of the tank wall.

Conversely, heat transfer through the tank wall is governed by thermal conduction, driven by the temperature difference between the external environment and the cryogenic hydrogen. The temperature field exhibits gradients across the wall thickness, affected by the thermal conductivity coefficients κ_i of the individual material layers. Each layer therefore contributes to shaping the overall temperature distribution within the multi-layered structure and, consequently, to the conductive heat flux from the ambient environment toward the cryogenic fluid.

Although practical tank filling levels do not typically exceed approximately 97%, the entire inner liner is assumed to be at the constant temperature of 20 K in order to simplify the thermal model. Owing to the high thermal conductivity of the metallic liner, the same temperature is assigned to the internal surface of the inner layer.

The presence of localized geometric discontinuities, such as refuelling ports or feed-line cutouts, introduces additional conductive paths that may locally increase the heat flux through the insulation. In the absence of detailed geometric descriptions or experimental data applicable to these regions, a thermal-bridge correction is applied to tank configurations featuring such additions.

Accordingly, following Ref. [130], this correction is implemented by amplifying the insulation-averaged heat flux by 50%, thereby approximating the thermal penalty associated with metallic reinforcements and partial insulation of the feed lines.

From a mechanical standpoint, the tank is subjected to an internal pressurization selected to prevent ambient air ingress and to ensure adequate fuel delivery to the feed lines. Hence, a constant pressure differential of $\Delta p = 1.7\,\mathrm{bar}$ is imposed between the tank interior and the surrounding environment. In addition, the stored LH_2 generates a hydrostatic load acting on the internal tank walls. Under the assumption of a 1 g acceleration field, the resulting hydrostatic pressure varies with depth according to $p_{\mathrm{hyd}}(z) = \rho_{\mathrm{LH_2}}\, g\, z$, where $0 \leq z \leq h_{\mathrm{fuel}}$ represents the depth below the free surface at which the pressure is evaluated.

Regarding mechanical boundary conditions, a constraint layout derived from the recent H2FLY demonstrator [131] is implemented. The vessel, whose longitudinal axis is aligned with that of the fuselage, is supported along three circumferential interfaces on the outer shell. These constrained regions are located at the junctions between the cylindrical section and the two end domes, as well as at the midpoint of the cylindrical body, Fig. (3.5). At these locations, all translational and rotational degrees of freedom are restrained, providing structural support while preventing rigid-body motion of the tank.

3.2.2 Finite-element simulation

The multi-physics tank model is implemented in `ABAQUS/CAE` [132] through fully parametric Python scripts, ensuring robustness, flexibility, and reproducibility needed for the systematic evaluation of numerous design configurations.

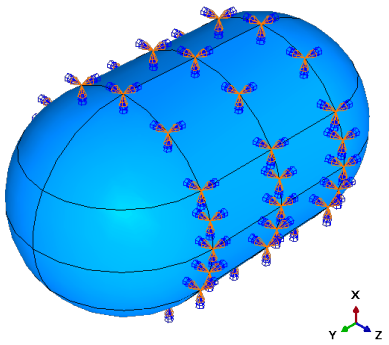

Figure 3.5: Representation of the boundary conditions applied to the H_2 tank model. The schematic illustrates the constraint configuration used to simulate realistic component-airframe anchoring strategies.

The tank inner liner and the outer structural layer are discretized using two three-dimensional shell-of-revolution parts. Their sections are assigned with geometrically consistent offsets to preserve the correct spatial arrangement, while the insulating layer is modelled as an intermediate solid domain whose thickness is approximately two orders of magnitude greater than that of the adjacent shell entities.

The need to prevent erratic fuel motion under acceleration requires the inclusion of anti-sloshing devices. In the numerical model, these are represented by planar shell baffles connected to the inner liner through a merging operation. Dedicated partitions are introduced to ensure node coincidence at the liner–baffle interfaces, thereby resulting in a conformal mesh that enforces nodal displacement continuity. Such bulkheads in the real component are therefore assumed mechanically attached to the inner surface of the liner along their perimeter. The components of the assembly are illustrated in Fig. (3.6).

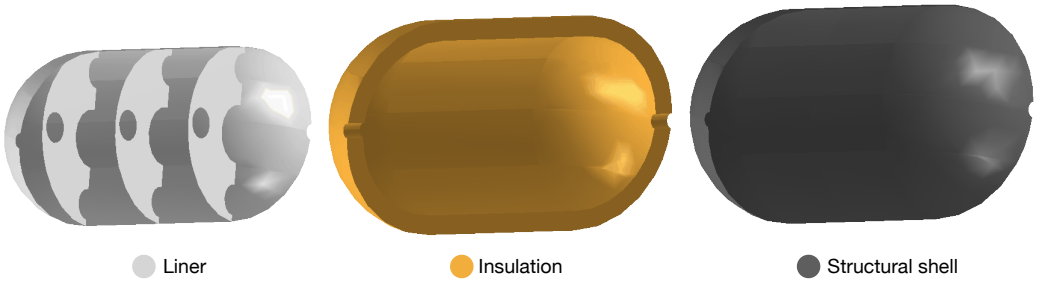

Figure 3.6: Exploded representation of the three finite-element entities constituting the pressure vessel featuring hemi-spherical domes, axial cutouts and three anti-sloshing baffles.

All tank components are discretized using thermally coupled elements with both temperature and displacement degrees of freedom. Specifically, S4RT reduced-integration shell elements are adopted for the inner and outer structural layers to mitigate shear locking and reduce computational cost, while S3RT elements are used to mesh the anti-sloshing baffles. The polyurethane insulation is discretized using fully integrated C3D8T eight-node thermally coupled brick elements. This choice avoids the bending instabilities and hour-glassing phenomena commonly associated with reduced-integration C3D8RT elements when used in thick solid domains [133]. The C3D8T formulation, in fact, provides improved accuracy in stress and displacement fields near interfaces and in regions characterized by strong thermal gradients, making it well suited for coupled thermo-mechanical analyses. Hence, for preliminary design stages and large-scale parametric studies, reduced-integration elements may nevertheless be employed to construct more efficient models with significantly reduced computational cost.

A coupled steady-state thermo-elastic analysis is performed to evaluate the tank response under prolonged operating conditions, during which the structure is subjected to severe temperature gradients induced by cryogenic

storage. The analysis step is defined considering a staggered solution where the thermal field and mechanical equilibrium are solved sequentially within each increment, allowing efficient convergence while maintaining full coupling through temperature-dependent material properties and thermal strains. The step is advanced incrementally, while nonlinear equilibrium within each increment is attained iteratively. A maximum of 100 increments is allowed, with an initial increment size of unity. Geometric non-linearities are neglected, as the expected deformations remain small relative to the characteristic dimension of the vessel. The solution procedure employs the Newton–Raphson method and iterates until equilibrium residuals in forces, moments, and heat fluxes fall below 5.0×10^{-3}, while corrections in displacement, rotation, and temperature remain below 1.0×10^{-2}. Convergence is typically achieved within two equilibrium iterations, with no cutbacks or divergence warnings recorded.

Mesh sensitivity study

Mesh convergence is assessed through progressive refinements, monitoring both scalar outputs and field distributions. Particular attention is given to the through-the-thickness profiles and spatial distributions of temperature, heat flux per unit area, and equivalent stress. Mesh density is considered converged when further refinement produces no appreciable variation in such quantities, indicating grid-independent results.

The outcomes of the mesh convergence study are reported in Fig. (3.7), and a final discretization comprising approximately 3.6×10^5 degrees of freedom (DoF) is selected. For generality, the abscissa of the convergence plots is expressed in non-dimensional form as the ratio between the position across the insulation thickness, χ_{PUR}, and a reference polyurethane thickness, $t_{\mathrm{PUR_{ref}}}$.

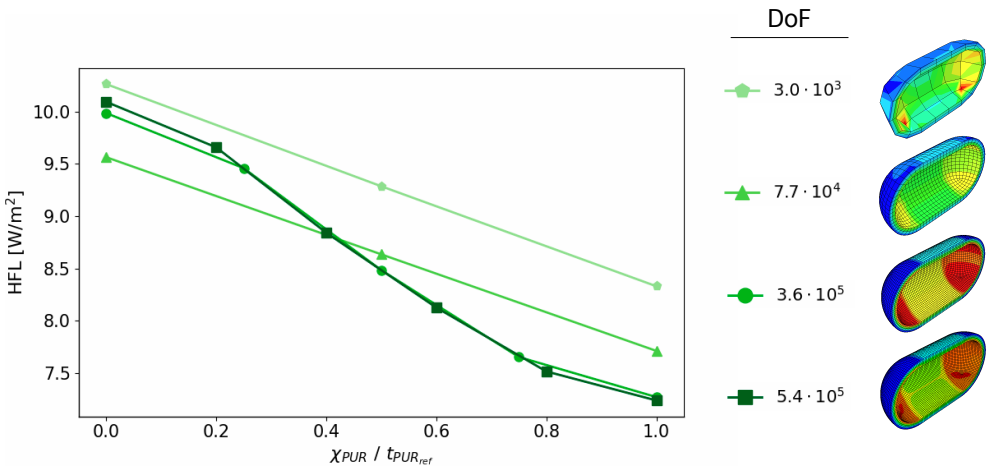

Figure 3.7: Mesh convergence study showing the profiles of heat flux per unit area (HFL) measured at the endcap apex across the normalized insulation thickness ($\chi_{\mathrm{PUR}}/t_{\mathrm{PUR_{ref}}}$) for increasing numbers of DoF. The right column illustrates the corresponding domain discretization and variable distribution at different levels of refinement.

3.2.3 Material failure criteria

Material failure is evaluated using layer-specific criteria consistent with the mechanical behaviour of the constituent materials. Therefore, assuming ε_{kl} as the total strain tensor and α_{kl} as the thermal expansion tensor, the thermo-mechanical stress state within the tank wall is expressed as

$$\sigma_{ij} = C_{ijkl}\left(\varepsilon_{kl} - \Delta T \alpha_{kl}\right), \tag{3.5}$$

where C_{ijkl} denotes the fourth-order elasticity tensor. The tank is sized such that the resulting stresses remain below the allowable limits in each layer of the sandwich structure under combined thermal and mechanical loading.

For isotropic layers, namely the aluminum liner, the polyurethane insulation, and the optional Ti-6Al-4V outer shell, failure is assessed using the von

Mises equivalent stress criterion, written as

$$\sigma_{\text{eq}} = \sqrt{\frac{1}{2}\left[(\sigma_1 - \sigma_2)^2 + (\sigma_2 - \sigma_3)^2 + (\sigma_3 - \sigma_1)^2\right]} < \bar{\sigma}_y^{\text{mat}}, \tag{3.6}$$

where σ_1, σ_2, and σ_3 are the principal stresses and $\bar{\sigma}_y^{\text{mat}}$ is the yield strength of the material. This criterion has been previously adopted for both metallic and polyurethane foam layers in cryogenic tank applications [62, 119, 134].

For the orthotropic outer composite shell, damage initiation is evaluated using the Hashin failure criteria, distinguishing between fibre- and matrix-dominated modes. Fibre failure is assessed as

$$\text{Fibres} \quad \begin{cases} \left(\dfrac{\sigma_{11}}{X_T}\right)^2 \leq 1 & \textit{Tension} \\ \left(\dfrac{\sigma_{11}}{X_C}\right)^2 \leq 1 & \textit{Compression} \end{cases} \tag{3.7}$$

while matrix failure is evaluated through

$$\text{Matrix} \quad \begin{cases} \left(\dfrac{\sigma_{22}}{Y_T}\right)^2 + \left(\dfrac{\sigma_{12}}{S_L}\right)^2 \leq 1 & \textit{Tension} \\ \left(\dfrac{\sigma_{22}}{2S_L}\right)^2 + \left[\left(\dfrac{Y_C}{2S_T}\right)^2 - 1\right]\dfrac{\sigma_{22}}{Y_C} + \left(\dfrac{\sigma_{12}}{S_L}\right)^2 \leq 1 & \textit{Compression} \end{cases} \tag{3.8}$$

In equations (3.7) and (3.8), the terms X_T and X_C denote the tensile and compressive strengths in the fibre direction and Y_T and Y_C the corresponding matrix strengths. The quantities S_L and S_T denote the lamina shear strengths. Specifically, S_L is the in-plane shear strength associated with the local 1–2 ply plane and therefore governs the resistance to the shear stress σ_{12}, whereas S_T is the transverse shear strength parameter appearing in the matrix-compression criterion, accounting for the contribution of transverse shear resistance to matrix-dominated failure. The stresses σ_{11}, σ_{22}, and σ_{12} are evaluated in the local material ply reference frame.

To comply with commercial aviation structural requirements, a uniform safety factor of SF = 1.5 is adopted from FAR §25.303 [135] and explicitly

embedded within the optimization algorithm so that the feasible design space directly reflects the certified structural margins. Accordingly, the resulting safety-factor-adjusted failure thresholds are defined as:

- $\bar{\sigma}_{\mathrm{SF}}^{\mathrm{Al}} = 333\,\mathrm{MPa}$
- $\bar{\sigma}_{\mathrm{SF}}^{\mathrm{PUR}} = 1.5\,\mathrm{MPa}$
- $\bar{\sigma}_{\mathrm{SF}}^{\mathrm{Ti}} = 849\,\mathrm{MPa}$
- $\mathrm{HSNCRT}_{\mathrm{SF}} = 0.667$

All failure criteria defined in Eqs. (3.6)–(3.8) are employed as explicit constraints within the optimization framework, enabling automatic updates of tank geometry and structural properties while enforcing compliance with material strength requirements.

It should be emphasized that the structural constraints adopted in the present framework are formulated with reference to the cryogenic, low-pressure nature of the LH_2 storage system investigated in this thesis. Under nominal conditions, boil-off gas generated by heat ingress is assumed to be managed by a dedicated venting system, which prevents uncontrolled pressure build-up and maintains the tank pressure within the prescribed limit. Accordingly, the von Mises and Hashin criteria introduced above are employed to constrain material yielding and damage initiation under the considered steady-state thermo-mechanical operating condition. They provide information on the onset of local failure mechanisms within the adopted modelling framework, but they do not describe the evolution of damage. A complete burst-pressure assessment would require a separate ultimate-load case, in which the internal pressure is increased up to collapse, together with progressive damage modelling, stiffness degradation, interface failure modelling, and manufacturing-consistent representation of local features such as dome-cylinder transitions, cutouts, attachments, and

possible ply drops. Therefore, satisfying the safety-factor-adjusted stress and Hashin constraints in this work should not be interpreted as equivalent to demonstrating a burst-pressure margin. Rather, the present formulation provides an early-stage thermo-mechanical and damage-initiation-constrained sizing approach for low-pressure cryogenic tanks. Burst-pressure verification is identified as a necessary future extension for certification-oriented pressure-vessel design.

3.2.4 Finite-element model validation

Validation of the numerical tank model is carried out by comparing the temperature distribution predicted by the present finite-element framework with reference data. The assessment is restricted to the thermal field, since the benchmark case provides sufficiently detailed and reliable thermal boundary conditions, which can therefore be reproduced consistently within the present model. A quantitative validation of the stress field is not pursued, as many of the mechanical material properties, constitutive assumptions, and modelling details required are not fully documented in the reference source. In such a case, a direct stress comparison would risk being performed under non-unified conditions. Nevertheless, the stress magnitudes predicted by the present model are consistent in order of magnitude with those reported in the reference study, thereby providing a preliminary qualitative confirmation of the mechanical plausibility of the results. Accordingly, validation is limited to the temperature field, for which the available data are both adequate and robust, thus providing the most reliable basis for assessing the predictive capability of the model. The results exhibit a satisfactory agreement with the reference study by Mantzaroudis et al. [6], both in terms of spatial gradients and overall magnitude. A root mean square error (RMSE) of 9.29 K is ob-

served along selected paths, corresponding to a maximum local deviation of approximately 15%, as illustrated in Fig. (3.8). This discrepancy between the two computational models is attributed to the combined influence of modelling assumptions and uncertainties in the input data. In particular, differences in mesh topology, implementation of thermal boundary conditions, and the inclusion of temperature-dependent thermal properties can considerably affect local heat-flux gradients and wall temperature levels. Furthermore, the current limited availability of open-access experimental data for full-scale cryogenic vessels, largely due to proprietary constraints and the high commercial value of such systems, precludes a precise calibration of numerical parameters against physical tests. Accordingly, the present validation should be interpreted as a numerical cross-comparison rather than an absolute experimental benchmark. Nonetheless, within these limitations, the level of agreement obtained supports the adequacy of the adopted thermal modelling strategy for comparative thermo-mechanical design and optimization studies of liquid-hydrogen storage tanks.

It should also be noted that, while the temperature-field comparison provides an indirect verification of the thermal response and of the resulting heat-transfer trends, the BOR predictions are not independently validated against experimental measurements. Similarly, the mechanical quantities used as optimization constraints, namely the von Mises stresses in the isotropic layers and the Hashin damage-initiation indices in the composite shell, are not benchmarked against dedicated coupon-level or component-level tests. Consequently, the present validation supports the use of the model as a physics-based comparative tool for early-stage design exploration, but it does not constitute a complete experimental verification of the coupled thermo-mechanical response of a cryogenic pressure vessel. The framework should be interpreted as a thermal and damage-initiation-constrained optimization methodology, rather than

as a fully validated structural design procedure for a readily certifiable tank.

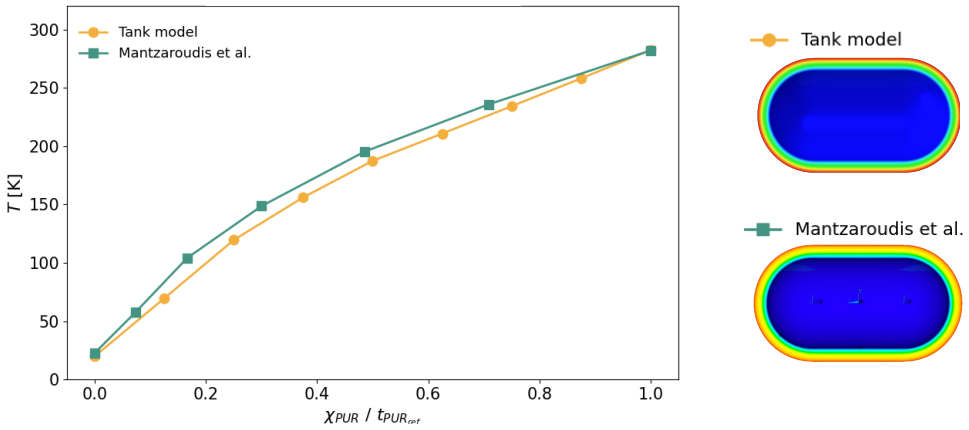

Figure 3.8: Comparison of temperature magnitude (T) and spatial distribution across the normalized insulation thickness ($\chi_{\mathrm{PUR}}/t_{\mathrm{PUR}_{\mathrm{ref}}}$) for the tank model developed in this thesis and the reference simulation from Ref. [6], used for validation of the thermo-mechanical FE framework.

3.3 Thermo-mechanical analysis of a reference tank

To complement the description of the numerical framework with a reference application case, a baseline LH_2 vessel is here analysed. The objective of this section is to: *i*) provide a physical interpretation of the temperature, heat flux, and stress fields generated by the FEM analysis; *ii*) identify the regions and mechanisms that drive the optimization process later detailed.

The reference tank is selected based on configurations considered in previous studies [6, 99, 36] and consists of a cylindrical vessel with hemi-spherical endcaps, whose main geometric and operational characteristics are summarized in Tab. (3.3). A filling ratio of $\phi_f = 0.75$ is adopted in this representative analysis to highlight the local thermo-mechanical effects associated with the

coexistence of liquid hydrogen and ullage gas. Accordingly, the BOR value reported in Tab. (3.3) refers only to this representative operating condition. The full-tank assumption introduced in Sec. (3.1.3) remains the reference condition used for consistent thermal comparison and optimization.

Table 3.3: Geometry, layer thicknesses, operating conditions and figures of merit adopted for the reference tank.

Base geometry	Storage volume	V	$100\,\mathrm{m}^3$
	Cylindrical section length	L	$4.24\,\mathrm{m}$
	Cylinder/spherical caps radius	R	$2.12\,\mathrm{m}$
Wall thickness	Inner layer	t_{Al}	$10\,\mathrm{mm}$
	Middle layer	t_{PUR}	$0.5\,\mathrm{m}$
	Outer layer	t_{CFRP}	$10\,\mathrm{mm}$
Operating condition	Filling ratio	ϕ_f	0.75
Figures of merit	Gravimetric efficiency	η_{tank}	36.7%
	Boil-off rate	BOR	$12.03\,\mathrm{kg\,h^{-1}}$

Two reference locations, denoted as A and B, are introduced for the evaluation of through-the-thickness field quantities. Location A is placed on the dome region and is representative of the endcap behaviour, whereas location B is taken in the cylindrical portion away from geometric discontinuities. A representative geometry discretization, together with the selected reference locations, is shown in Fig. (3.9).

For the reference filling ratio $\phi_f = 0.75$, the inner aluminium liner exhibits two distinct thermal regions, as shown in Fig. (3.10a). The lower portion of the liner, in contact with liquid hydrogen, remains close to the prescribed cryogenic temperature of 20 K, whereas the upper region, in contact with the

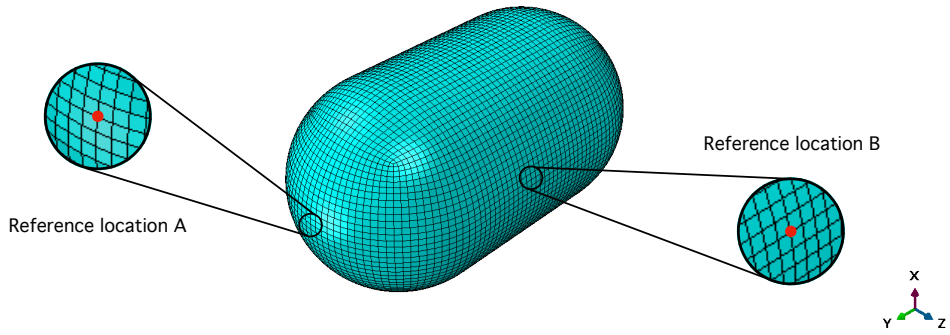

Figure 3.9: Finite-element mesh of the reference LH_2 tank highlighting the two reference locations used for field evaluation.

ullage gas, reaches slightly higher values, with a maximum temperature of approximately 25.3 K farthest away from the LH_2. The corresponding heat-flux distribution in Fig. (3.10*b*) is consistent with the non-uniform thermal boundary condition at the internal wall. Lower values occur where the local temperature difference across the wall is smaller, whereas the highest values are found near the liquid–gas interface region, where the local thermal gradient is more pronounced. From a structural standpoint, in this reference configuration the liner remains far from yielding. In fact, the maximum von Mises stress, reported in Fig. (3.10*c*), is approximately 11.4 MPa and occurs near the junction between the cylindrical region and the hemi-spherical domes, as well as in the central region of the cylindrical portion.

The polyurethane layer is characterized by the strongest thermal gradient across the tank wall and governs the overall thermal resistance of the system. Significant thermal gradients across t_{PUR} are observed, as the temperature varies from the storage temperature of LH_2 on the inner surface to the external temperature $T_{\mathrm{ext}} = 282.2\,\mathrm{K}$ on the outer surface, as shown in Fig. (3.11*a*). The temperature increases almost linearly through the polyurethane thickness without evident distinctions between the cylindrical and hemispherical regions,

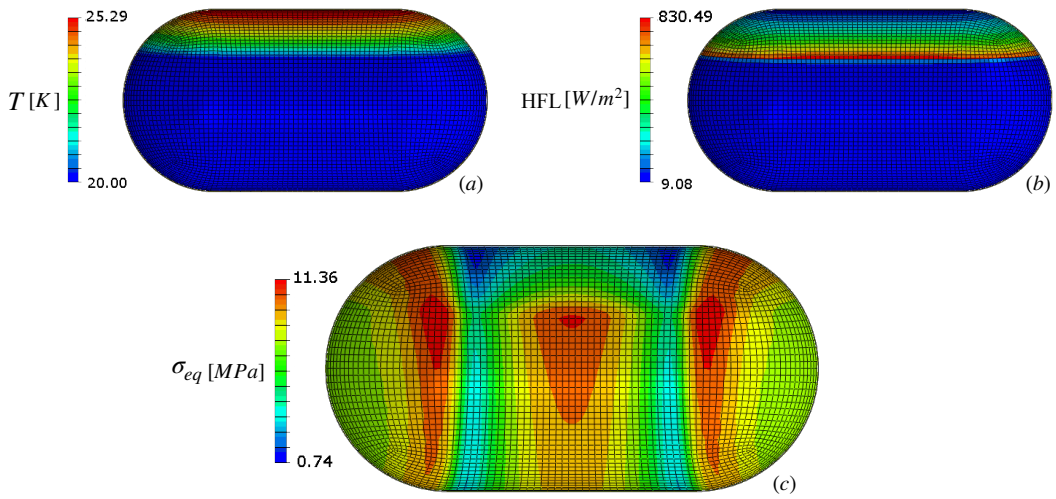

Figure 3.10: Thermo-mechanical fields in the inner aluminium liner of the reference tank: *a*) absolute temperature; *b*) heat flux per unit area; *c*) von Mises stress.

as illustrated in Fig.(3.12a). Heat flux per unit area distribution is shown in Fig.(3.11b), and exhibits a minimum on the outer surface of the part, particularly over the hemispherical regions due to the effects of curvature. In contrast, at the inner surface, which is in contact with the liner, HFL reaches its maximum value. The effect of partial filling results in a slight flux reduction on the inner surface of the foam in the cylindrical region, where the presence of ullage, associated with a higher temperature with respect to the liquid fuel, reduces the temperature differential with respect to the external environment. The equivalent stress in the insulation, reported in Fig. (3.11*c*), remains below the allowable threshold throughout the domain, with a maximum value of approximately 0.90 MPa reached on the outer surface of the cylindrical portion. The corresponding through-the-thickness profiles of heat flux per unit area and equivalent stress at locations A and B are shown in Fig. (3.12*b*–*c*).

Due to its position outside the insulation, the CFRP shell remains close to ambient temperature and is therefore only marginally affected by the cryo-

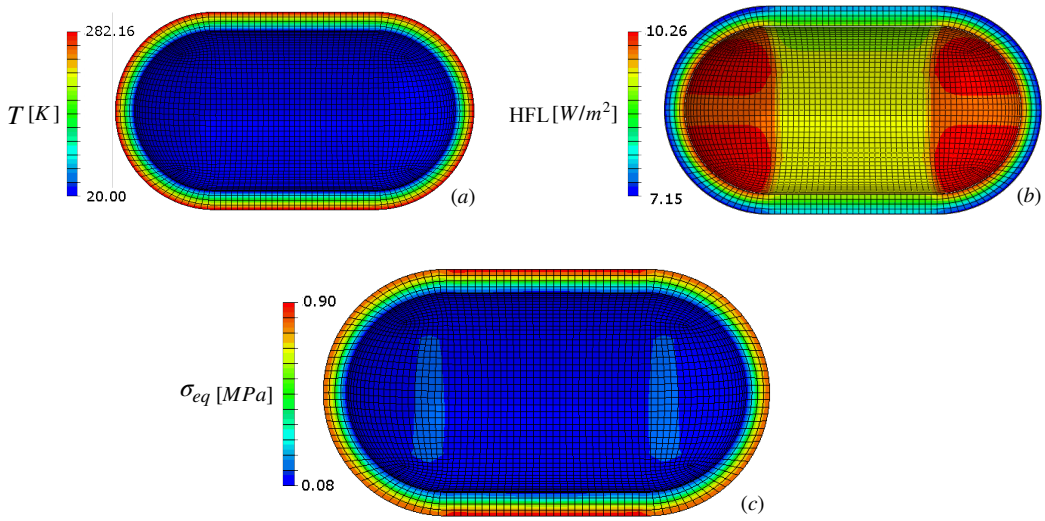

Figure 3.11: Thermo-mechanical fields at the middle polyurethane layer in the reference tank model: *a*) absolute temperature [K]; *b*) heat flux per unit area [W/m^2]; *c*) von Mises stress [MPa].

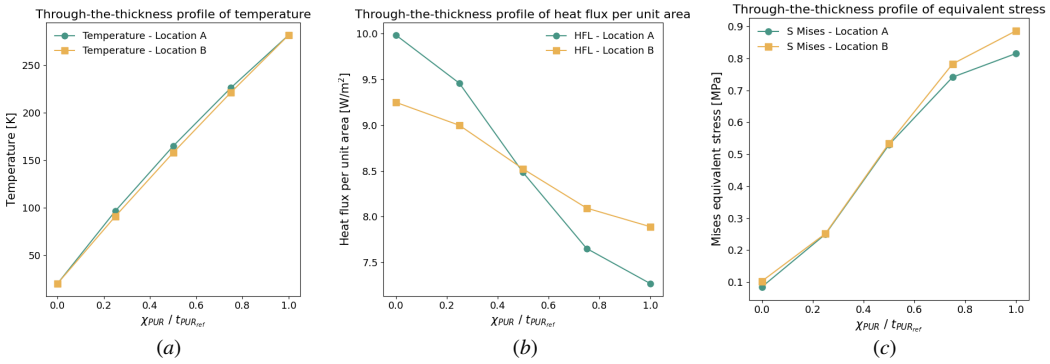

Figure 3.12: Through-the-thickness profiles of *a*) absolute temperature, *b*) heat flux per unit area, and *c*) equivalent stress across the middle layer in the reference tank configuration at the locations A and B.

genic environment. Results for the Hashin failure criterion are reported in Fig.(3.13). Since the lamination sequence adopted is symmetric, results are discussed only for the four outermost, slightly more highly loaded plies of the eight-ply laminate. For each ply in the stacking sequence, the active damage

initiation criteria are fiber tension – HSNFTCRT – and matrix compression – HSNMCCRT, while fiber compression – HSNFCCRT – and matrix tension – HSNMTCRT – damage initiation criteria are not met for the reference tank configuration. For all four composite plies (*Ply-0,* 0°*; Ply-1,* 90°*; Ply-2,* 45°*; Ply-3,* −45°), the fiber tension criterion indicates that the plies are far from damage initiation under the considered conditions. The through-the-thickness profiles of the Hashin fiber tension and matrix compression indices are shown in Fig.(3.14), where χ_{CFRP} represents the location through the composite thickness. The indices are evaluated in both the hemispherical and cylindrical regions of the tank, at the reference locations A and B respectively, at the mid-thickness integration point of each ply. The use of a quasi-isotropic stacking sequence combined with the small laminate thickness compared to the tank geometrical dimensions leads to an almost symmetric stress distribution with respect to the laminate mid-surface, which results in nearly symmetric Hashin indices for both fiber tension and matrix compression.

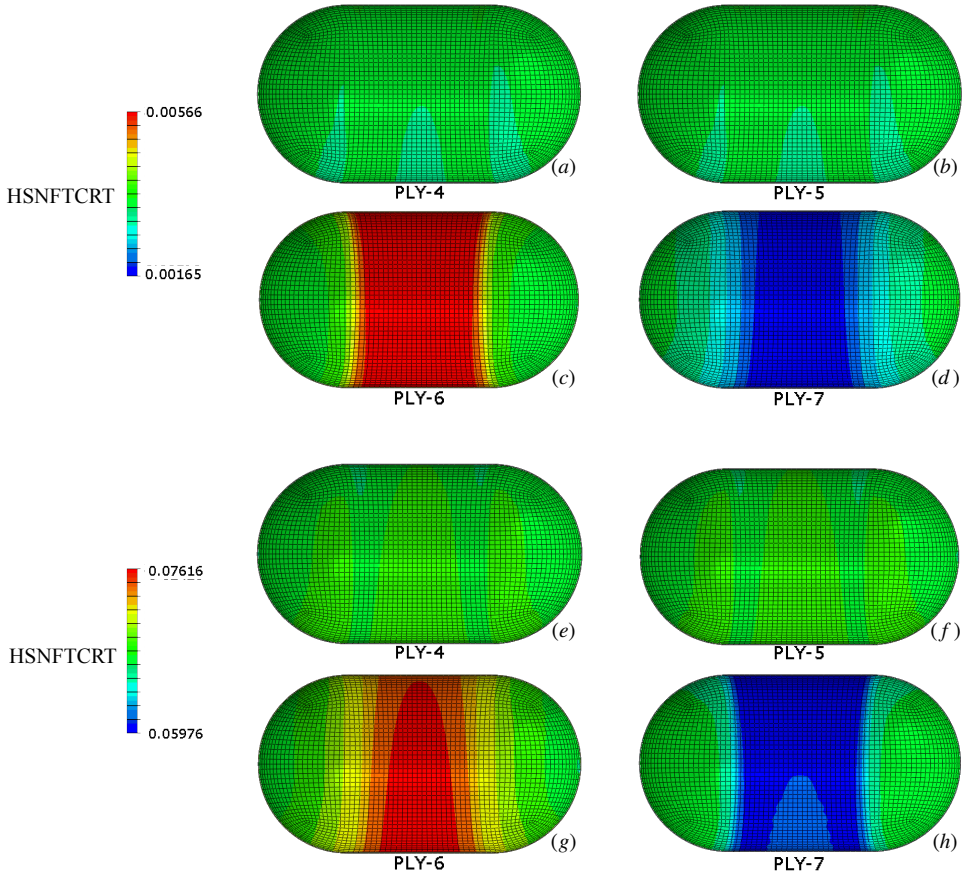

Figure 3.13: Hashin threshold indices for the external composite layer of the reference tank. Only plies 4-7, which exhibit the highest stress levels, are shown (the plies are numbered from 0 to 7). *a*–*d*) Hashin fiber tension criterion; *e*–*h*) Hashin matrix compression criterion.

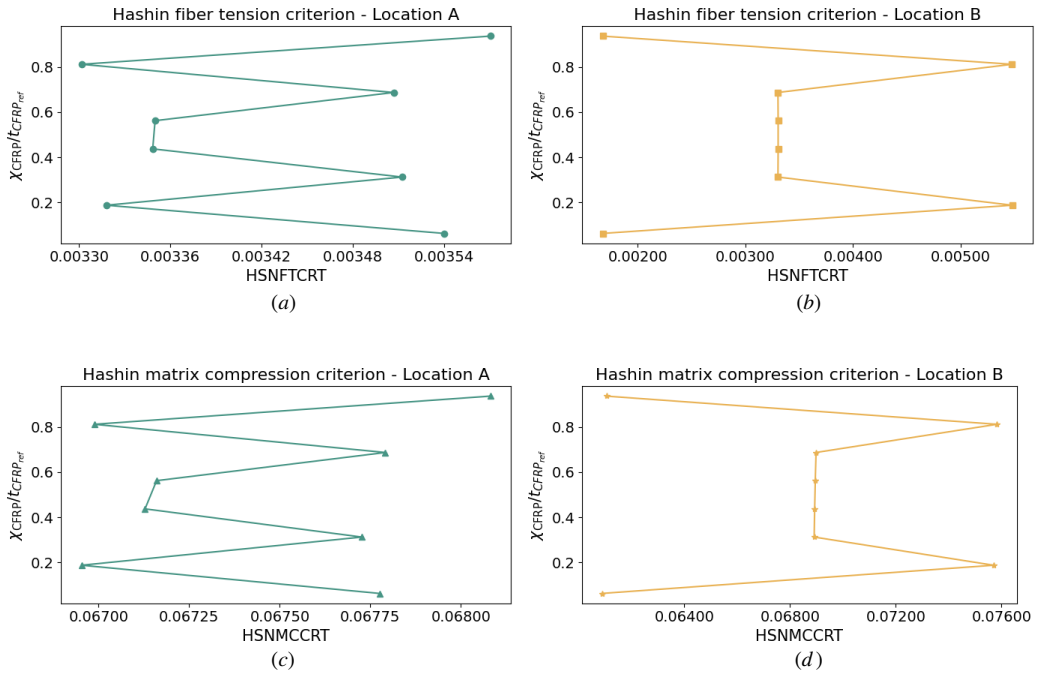

Figure 3.14: Through-the-thickness profiles at the reference locations A and B of the Hashin indices for fiber tension (a–b) and matrix compression (c–d) for the considered layup of the external composite shell in the reference tank configuration.

3.4 Optimization problem formulation and workflow integration

The optimization problem aims at minimizing the total tank mass m_{tank}, by varying a vector of geometrical design variables while enforcing mechanical and thermal performance constraints. The design variables are the thicknesses of the individual layers composing the tank wall

$$t_j = [t_{\text{Al}}, t_{\text{PUR}}, t_{\text{Ti}}, t_{\text{CFRP}}],$$

which are bounded by prescribed lower and upper limits t_j^{lb} and t_j^{ub}, reflecting manufacturability and design feasibility considerations [7].

The optimization problem is therefore stated as

$$\begin{aligned} \texttt{minimize} \quad & m_{\text{tank}}(t_j) \\ \texttt{with respect to} \quad & t_j^{\text{lb}} \leq t_j \leq t_j^{\text{ub}} \\ \texttt{subject to} \quad & g_i(t_j) \leq 0, \end{aligned} \tag{3.9}$$

where the inequality constraints enforce both safety-factor-adjusted structural and thermal performance requirements. Specifically, the constraint set is defined as

$$g_i = \begin{cases} \dfrac{\sigma_{\text{Al}}}{\bar{\sigma}_{\text{SF}}^{\text{Al}}} - 1 \leq 0, \\ \dfrac{\sigma_{\text{PUR}}}{\bar{\sigma}_{\text{SF}}^{\text{PUR}}} - 1 \leq 0, \\ \dfrac{\sigma_{\text{Ti}}}{\bar{\sigma}_{\text{SF}}^{\text{Ti}}} - 1 \leq 0, \\ \text{HSNCRT}_{\text{SF}} - 0.667 \leq 0, \\ \text{BOR} - \text{BOR}_{\text{allowable}} \leq 0. \end{cases} \tag{3.10}$$

The stress-based constraints ensure that the maximum thermo-mechanical stress in each isotropic layer does not exceed the corresponding safety-factor-adjusted allowable strength, while the Hashin criterion constraint limits damage initiation indices in the composite shell. The BOR constraint enforces compliance with the prescribed thermal performance requirement introduced in Sec. (3.1.3).

It must be noted that only one of the two outer-layer constraints–either titanium yielding or composite damage initiation–is active at a time. This reflects the mutually exclusive nature of the design evaluation, in which the outer structural layer is realized either in titanium alloy or in CFRP.

3.4.1 Numerical implementation

The constrained optimization problem is solved using the *Interior-Point* algorithm implemented in MATLAB's `fmincon` solver [136]. This approach reformulates the constrained problem into a sequence of unconstrained problems by introducing a logarithmic barrier function, which penalizes constraint violations, while ensuring that all iterations remain strictly within the feasible region.

Thus, the modified objective function takes the form

$$F(t_j) = f(t_j) - \mu \sum_i \log(-g_i(t_j)) \,, \tag{3.11}$$

where μ is a positive barrier parameter that is progressively reduced during the optimization process. As any constraint $g_i(t_j)$ approaches zero from below, the corresponding logarithmic term tends to infinity, thereby preventing violation of the constraint. In the limit $\mu \to 0$, the solution converges to that of the original constrained problem. Upper and lower bounds on the design variables, which will be discussed in Sec. (3.4.6), are enforced in an analogous manner by augmenting the objective function with additional barrier terms,

$$\min \; f(t_j) + \mu \sum_i \log(-g_i(t_j)) - \sum_j \left[\log(t_j - t_j^{\text{lb}}) + \log(t_j^{\text{ub}} - t_j)\right] , \tag{3.12}$$

which ensure that the design variables remain strictly within their admissible ranges.

3.4.2 Gradient evaluation and search direction

Gradients of the objective function with respect to the design variables are approximated using forward finite differences,

$$\frac{\partial f}{\partial t_j} \approx \frac{f(t_j + h) - f(t_j)}{h}, \tag{3.13}$$

where h is a suitably small perturbation.

The search direction Δt at each iteration is obtained by solving the Newton system

$$H(t)\,\Delta t = -\nabla F(t), \tag{3.14}$$

with $H(t)$ denoting the Hessian matrix of the barrier-augmented objective function and $\nabla F(t)$ its gradient.

Given that the exact computation of the Hessian matrix is computationally expensive, `fmincon` employs a quasi-Newton approach based on the BFGS update scheme

$$H_{k+1} = H_k + \frac{y_k y_k^\top}{y_k^\top s_k} - \frac{H_k s_k s_k^\top H_k}{s_k^\top H_k s_k}, \tag{3.15}$$

where $s_k = t_{k+1} - t_k$ represents the change in the design variables between successive iterations and $y_k = \nabla f_{k+1} - \nabla f_k$ is the corresponding change in the objective function gradient.

3.4.3 Convergence criteria

The optimization process is considered converged when all of the following conditions are satisfied:

- the first-order optimality measure is below a prescribed tolerance, indicating proximity to a stationary point;
- the norm of the design-variable update satisfies $\|\Delta t\| < \varepsilon$, implying negligible further improvement;
- all inequality constraints satisfy $g_i(t_j) \leq 0$ within the specified feasibility tolerance.

3.4.4 Constraint aggregation

As is common in structural optimization problems characterized by a large number of constraints, an aggregation technique is employed to limit computational cost and improve numerical robustness. Evaluating and enforcing each individual constraint independently would significantly increase the dimensionality of the optimization problem and negatively affect the convergence behaviour.

Accordingly, the Kreisselmeier–Steinhauser (KS) aggregation function [137, 138] is adopted to provide a smooth and conservative approximation of the maximum constraint violation over the entire structure. The aggregated constraint is defined as

$$\mathrm{KS}(t) = \frac{1}{\rho_{\mathrm{ag}}} \ln \left(\sum_{i}^{N} e^{\rho_{\mathrm{ag}} g_i(t)} \right), \tag{3.16}$$

where $g_i(t)$ are the individual constraint functions and ρ_{ag} is the aggregation parameter controlling the sharpness of the approximation. In the limit $\rho_{\mathrm{ag}} \to \infty$, the KS function converges to the exact maximum constraint. In the present study, a value of $\rho_{\mathrm{ag}} = 100$ is selected after several tests, providing a smooth representation of the critical constraint while maintaining stable convergence.

3.4.5 Step-size sensitivity

The use of finite-difference schemes for gradient evaluation introduces the classical step-size dilemma, which requires balancing truncation errors and round-off errors. A sensitivity study on the perturbation size is therefore conducted to identify a suitable finite-difference step length.

The step-size analysis considers representative output quantities driving the optimization, namely:

- the equivalent von Mises stress in the aluminum liner and insulating layer;
- the heat flux per unit area within the insulation;
- the Hashin damage index in the outer composite shell.

Accordingly, a perturbation step of $\Delta t = 1.0 \times 10^{-5}\,\mathrm{m}$ is selected.

3.4.6 Design-variable bounds and technological constraints

Since the optimization focuses on the thicknesses of the individual tank layers, practical lower and upper bounds must be defined for each design variable. These bounds, denoted as t^{lb} and t^{ub}, are derived primarily from technological and manufacturing considerations and are summarized in Tab. (3.4).

Table 3.4: Lower and upper thickness bounds for each material considered in the LH_2 vessel architecture.

	Al 2219-T8	**PUR-96**	**Ti-6Al-4V**	**CFRP$_{\mathrm{ply}}$**	**Unit**
t^{lb}	0.5	25	3	0.125	mm
t^{ub}	10	950	50	10	mm

Although the aluminum liner contributes to the global structural response, its primary functions are to provide fuel containment, prevent H_2 permeation, and protect the outer layers from HE. Consequently, optimized configurations are expected to drive the liner thickness toward its lower bound. As it will be shown later, optimal values of t_{Al} are indeed typically close to $t_{\mathrm{Al}}^{\mathrm{lb}} \approx 0.5\,\mathrm{mm}$. Such thin-gauge components can be reliably manufactured using hydroforming processes [139], which are well suited for producing water-tight geometries such as the considered vessel, with an upper practical thickness limit of approximately 10 mm [140].

By contrast, the polyurethane insulation layer is expected to be two orders of magnitude thicker than the liner. The lower bound $t_{\mathrm{PUR}}^{\mathrm{lb}}$ is based on the experimental work of Fesmire et al. [120], while the upper bound reflects previous studies on foam-insulated cryogenic hydrogen tanks, which identify values beyond $\sim 950\,\mathrm{mm}$ as impractical due to excessive volume and mass, and are therefore incompatible with aircraft integration requirements [50].

The thickness of the titanium outer shell, denoted as t_{Ti}, is bounded by manufacturing limitations associated with conventional forming, joining processes, and metal additive manufacturing techniques, all leading to a practical minimum thickness of approximately 3 mm [141].

For composite configurations, the lower bound for individual CFRP plies is set to 0.125 mm, in accordance with Ref. [142]. Thinner plies may introduce manufacturability and process-compatibility issues, particularly with automated fibre placement technologies [66]. The composite outer shell is modelled as an eight-ply laminate with fixed ply count, while the thickness of each ply is treated as a design variable. As a result, the total laminate thickness varies with the optimized ply thickness, allowing for consistent exploration of composite sizing.

3.4.7 Optimization performance and computational cost

Optimization convergence is achieved when the first-order optimality measure falls below 1.0×10^{-3} and all constraint violations are smaller than 1.0×10^{-3}. Step updates with magnitude below 1.0×10^{-5} are considered numerically insignificant and trigger termination when the remaining criteria are satisfied. Gradient evaluations employ finite differences with perturbations bounded between 1.0×10^{-4} and 1.0×10^{-3}.

For a representative case involving a hemi-ellipsoidal-domed composite tank

equipped with refuelling cutouts and anti-sloshing bulkheads, the optimization converges in 16 iterations and 195 function evaluations, achieving a first-order optimality of 6.0×10^{-4} with zero constraint violation.

Each function evaluation triggers a full FEM analysis. On a 32-core workstation, a single evaluation requires approximately 40 s of wall time, corresponding to a total serial computational cost of roughly 2 h. Nonetheless, the framework is conceived to be inherently parallelizable, allowing further reductions in turnaround time when additional computational resources are available.

3.4.8 Integrated optimization workflow

The optimization problem is fully coupled with the finite-element analysis stage, forming the integrated computational framework schematized in Fig. (3.15).

Material properties, geometric parameters, and thermal and mechanical boundary conditions are defined at a high level and passed to a Python-based `ABAQUS` interface, which generates the finite-element model using the current set of layer thicknesses and thus launching the simulation. Following completion of the analysis, a post-processing routine extracts the relevant quantities from the output file and transfers them to the MATLAB environment. The optimization algorithm then updates the vector of design variables and supplies it to the FEM model for the next iteration. This loop continues until all convergence criteria are satisfied, at which point the optimal tank configuration and the associated finite-element results are obtained.

The framework allows further spatial discretization of the tank wall into independent patches, with each patch thickness treated as a separate design variable. This capability has been implemented to enable refined thickness tailoring, particularly between cylindrical sections and dome regions, in accor-

dance with thin-walled pressure vessel theory, which predicts lower tangential stresses in spherical shells compared to cylindrical ones. As will be outlined later in Sec. (5.2.2) when discussing future developments of the framework, increasing the number of patches expands the design space dimensionality and enables more advanced structural optimization strategies.

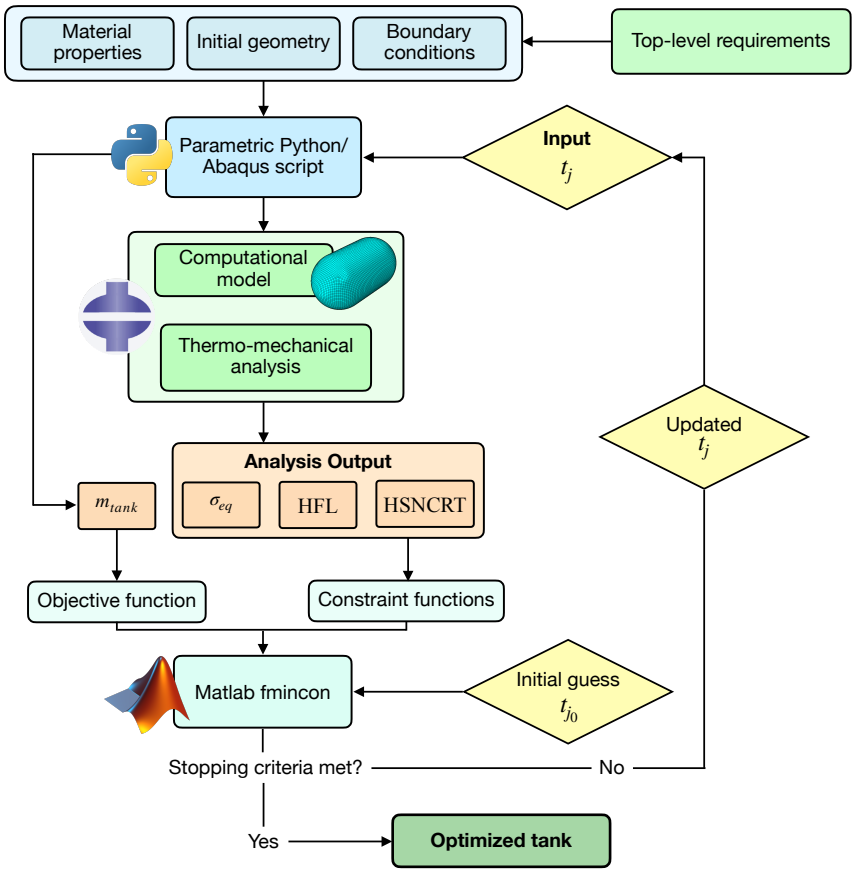

Figure 3.15: Block diagram representing the optimization logic. Design variables are fed into the FE model and solver and, based on resulting metrics and residuals, the optimization algorithm iteratively updates the design variable vector until convergence criteria are satisfied [7].

3.4.9 Optimization loop validation

The optimization methodology is validated through a dedicated study in which the tank geometry—specifically the aspect ratio $\phi = L/R$, where L denotes the length of the cylindrical section and R the radius of the hemi-spherical endcaps—is treated as an additional design variable. For a fixed internal volume and prescribed thermo-mechanical boundary conditions, the optimization algorithm is therefore allowed to modify the vessel shape.

To ensure a consistent compromise between numerical accuracy and computational cost as the tank dimensions vary during the optimization process, a constant ratio between the characteristic mesh seed size and the reference tank dimension is enforced. This strategy maintains a comparable level of spatial resolution across all geometrical configurations and avoids spurious numerical effects associated with mesh coarsening or refinement induced solely by shape changes.

As discussed in Sec. 3.1.1, in the absence of constraints related to vehicle integration, the thermally optimal configuration always corresponds to a spherical tank. This geometry minimizes the surface-to-volume ratio, thereby reducing heat ingress and the required insulation mass. Therefore, the optimization is initialized from an arbitrary cylindrical-based configuration with aspect ratio $\phi = 3.5$. The algorithm converges toward an optimal aspect ratio $\phi_{\text{opt}} = 0$, representing the spherical limit. The progressive evolution of the tank geometry from the initial configuration to the optimized shape is schematically illustrated in Fig. (3.16). It is noted that this result is strictly valid under the assumption of constant internal volume and in the absence of additional constraints.

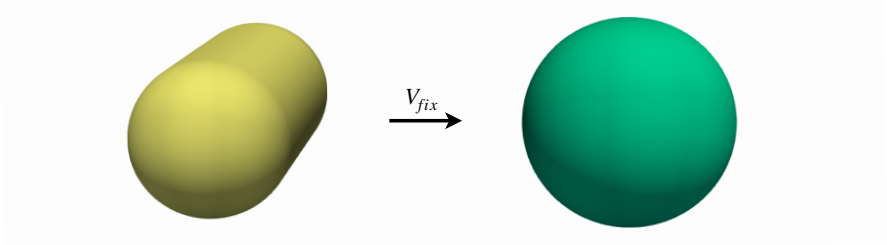

Figure 3.16: Initial (yellow) and optimized (green) vessel shapes resulting from the optimization process where ϕ is treated as a design variable. Thermo-mechanical boundary conditions, material properties, and tank capacity are held constant throughout the analysis.

Chapter 4

Optimized layouts and aircraft integration

This section details the liquid hydrogen vessel configurations investigated in the present study. For each configuration, the optimized mass distribution and the resulting fuel mass fraction are discussed and compared. Based on this assessment, a representative tank layout is selected and subsequently integrated into an advanced sustainable airframe evaluating the associated thermo-mechanical fields.

Each tank architecture is characterized by a specific combination of geometric and design features, including dome shape, the presence of refuelling cutouts, and internal anti-sloshing baffles. As outlined in Section (3.1.1), all configurations are evaluated under identical conditions in terms of theoretical fuel capacity and allowable boil-off rate, ensuring a consistent basis for comparison.

The geometric parameters defining each vessel—indexed using ascending Roman numerals (I–VI)—are summarized in Table (4.1). The associated geometric variables are defined with reference to the schematics shown in

Fig. (4.1). In particular, L denotes the length of the cylindrical section of the tank, while R represents the radius of the hemispherical endcaps. For tanks featuring hemi-ellipsoidal domes, R corresponds to the semi-major axis a, whereas the semi-minor axis is denoted by b. The diameter of the circular refuelling cut-out is indicated by D_{co}. Anti-sloshing baffles are modelled as circular disks of diameter R, perforated by five openings. These openings are defined by the diameters D_{BHc} for the central hole and D_{BHr} for the four radially distributed holes. In addition to the geometric parameters, Table (4.1) also summarizes the material composition of each structural layer and highlights the main design features adopted in each tank configuration.

Table 4.1: Summary of geometric parameters, layer composition and structural features for each tank configuration. Dimensions defining the internal cavity are reported for all vessels, while cutout and bulkhead openings diameters are specified only for configurations that incorporate such features.

	Parameter	**I**	**II**	**III**	**IV**	**V**	**VI**
Internal cavity [m]	L	4.24	4.24	5.32	4.24	4.24	5.32
	$R = a$	2.12	2.12	2.12	2.12	2.12	2.12
	b	-	-	1.32	-	-	1.32
Cutout [m]	D_{co}	-	-	-	0.15	0.15	0.15
Bulkhead [m]	D_{BHc}	-	-	-	-	1.40	1.40
	D_{BHr}	-	-	-	-	0.37	0.37
Material	Inner	Al2219-T8					
	Middle	PUR-96					
	Outer	Ti-6Al-4V	CFRP	CFRP	CFRP	CFRP	CFRP
Feature	Domes	Hem.-sph.	Hem.-sph.	Hem.-ellip.	Hem.-sph.	Hem.-sph.	Hem.-ellip.
	Cutouts	-	-	-	Yes	Yes	Yes
	Bulkheads	-	-	-	-	Yes	Yes

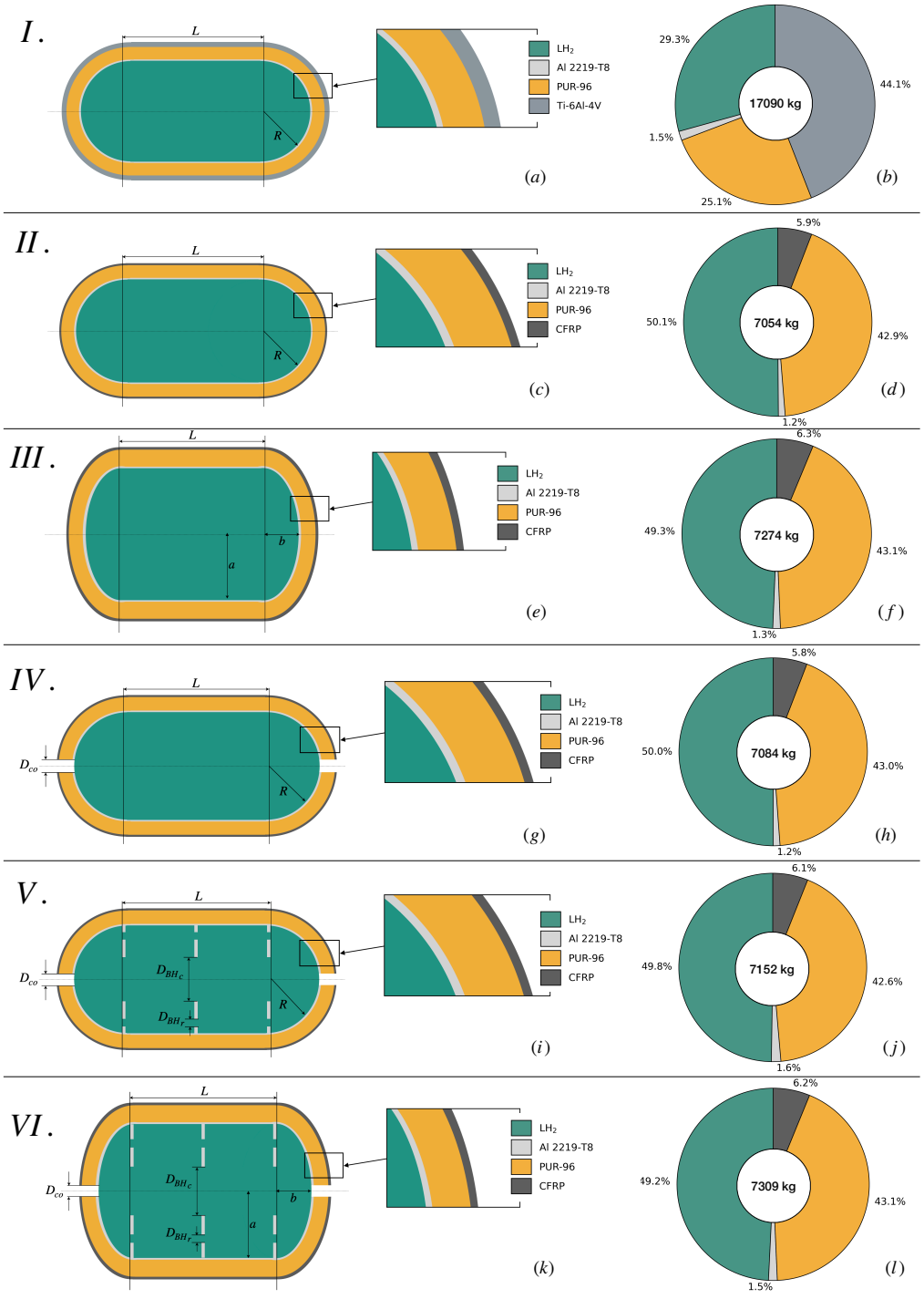

Figure 4.1: Schematic representation of each vessel materials and geometry (*a, c, e, g, i, k*); optimized mass breakdown between fuel and constituent layers (*b, d, f, h, j, l*).

4.1 *I* - Metallic reference tank

As a baseline for comparison, a relatively straightforward tank configuration featuring a titanium-alloy outer structural layer and hemispherical endcaps is first analysed. The corresponding vessel architecture, schematically shown in Fig. (4.1a), employs Ti-6Al-4V as the load-bearing outer shell, while the inner liner and the insulation layer adopt the same materials used in all other configurations, namely aluminium and polyurethane foam respectively.

The feasibility of employing the same aluminium Al 2219-T8 alloy used for fuel containment also for the outer structural layer is investigated. However, this configuration fails to satisfy the mechanical constraints across the entire range of design variables defined in Tab. (3.4), yielding insufficient safety margins even at the upper bound of admissible thicknesses. This limitation reflects an intrinsic physical constraint rather than a numerical artefact: the optimizer is indeed unable to identify any feasible solution within the prescribed bounds and safety-factor-adjusted limits. The combination of moderate elastic stiffness and relatively high coefficient of thermal expansion of Al 2219-T8 leads to significant thermally-induced stresses in the outer shell, particularly under the steep temperature gradients experienced across the tank wall. Although this alloy indeed exhibits excellent strength at cryogenic temperatures, its mechanical properties degrade sharply as temperature increases [118], as occurs at the external surface of the vessel where ΔT-induced stresses are highest. Even as the outer shell thickness is increased, the safety-factor-adjusted yielding criterion remains violated, indicating that an all-aluminium configuration would require impractically thick and heavy sections or additional specific reinforcements to achieve acceptable structural margins.

Consequently, the use of a titanium alloy outer shell represents a feasible, albeit more costly, compromise. The specific market price of Ti-6Al-4V is ap-

proximately seventeen times higher than that of aluminium alloys [143, 144], but its superior mechanical performance under the relevant thermo-mechanical loading conditions enables compliance with the imposed constraints. Having defined the baseline architecture, the corresponding optimization results are now summarized: the mass breakdown of the all-metal vessel is reported in Fig. (4.1*b*), where the relatively thick and dense titanium structural layer accounts for the majority of the total tank mass. As a result, the gravimetric efficiency of this configuration is limited to approximately 30%, and is therefore considerably lower than the threshold considered in Fig. 3.4. The aluminium liner constitutes only about 1.5% of the total tank mass, while the amount of insulation is primarily dictated by thermal performance requirements, a trend that is also observed in the other tank configurations considered in this thesis.

4.2 *II* - Composite-based reference tank

While retaining Al 2219-T8 and PUR-96 for the inner liner and insulation layers respectively, the tank configuration schematized in Fig. (4.1*c*) replaces the Ti-6Al-4V outer shell with a fibre-reinforced composite material.

The composite layer is assigned with a quasi-isotropic stacking sequence, consistent with Ref. [6], namely the $[0°/90°/45°/-45°]_S$, which effectively decouples in-plane shear and extensional deformations. As later demonstrated in Sec. 4.6, this stacking sequence is found to outperform other commonly adopted configurations, consistently yielding the lowest overall component mass. Accordingly, it is selected as the reference laminate architecture for all analyses presented in this chapter, unless otherwise stated.

The optimized tank, which, at this stage, does not incorporate practical features such as cutouts or anti-sloshing baffles, exhibits a profoundly different mass distribution compared to the all-metal construction previously assessed,

as shown in Fig. (4.1*d*). The introduction of a composite outer shell indeed proves highly effective: the mass of the structural external layer is reduced by a factor of 13 compared to the metallic design of Sec. (4.1). In addition, the mass of the aluminium liner, although primarily intended as a containment and protective layer, still contributes to the overall mechanical response, is also reduced by approximately a factor of 2. As observed in the all-metal case, the thickness of the insulating layer is predominantly governed by thermal performance requirements and therefore remains mostly unchanged.

Overall, the adoption of a composite outer shell leads to a reduction in total tank mass of 59% relative to the all-metal counterpart, corresponding to an absolute increase in gravimetric efficiency of 20.8%.

4.3 *III* - Composite-based tank with hemi-ellipsoidal endcaps

Given their favourable compromise between manufacturability, volumetric efficiency, and integration capability, hemi-ellipsoidal domed pressure vessels are widely adopted in the aerospace sector [131, 145, 146]. Compared with spherical-based dome geometries, such endcap shape may indeed facilitate integration with surrounding elements, especially within fuselage-constrained environments.

Accordingly, to assess the influence of dome geometry on tank performance, hemi-ellipsoidal endcaps are implemented in the vessel configuration schematized in Fig. (4.1*e*). Following the findings of Gomez and Smith [61], optimal structural efficiency for such domes is achieved when the ratio of the ellipsoidal semi-axes satisfies $a/b = 1.6$; such a value is therefore adopted throughout the present analysis when sizing hemi-ellipsoidal endcaps. For consistency with

the previously analysed hemi-spherical configurations, no refuelling cutouts or internal anti-sloshing baffles are introduced at this stage. Relative to hemi-spherical domes, the hemi-ellipsoidal geometry exhibits a larger surface area for an equivalent internal volume. This increase leads to higher heat inflow and a less favourable stress distribution, which together result in a modest mass penalty, as shown in Fig. (4.1*f*).

Specifically, compared to Tank *II*, the liner mass increases by 12% to accommodate both the increased surface area and the reduced load-bearing efficiency of the dome geometry, while the mass of the structural outer layer increases by about 8.5%. In addition, the higher global surface-to-volume ratio necessitates a slightly thicker insulation layer to maintain the prescribed boil-off rate. Consequently, these effects yield an overall increase in total tank mass of 3.1% relative to Tank *II*, attributable solely to the change in endcap geometry.

4.4 *IV* - Composite-based tank with refuelling cutouts

Cutouts required to interface the tank inner cavity with fuel lines, sensors, and gaseous hydrogen extraction pipes, along with other necessary elements, are now introduced in the vessel layout.

Considering that the tank is intended to be integrated within the aircraft fuselage, with its longitudinal axis aligned with that of the airframe, a practical and commonly adopted placement for such openings is on the tank endcaps [147]. The cut-out diameter, highlighted in Fig. (4.1*g*), is selected in accordance with the dimensions of commercially available cryogenic liquid hydrogen feed lines [148]. The introduction of such openings locally disrupts the continuity of the insulation layer and may lead to increased heat ingress at the

interface between the tank and external components. To account for this effect, a thermal penalty is applied following an approach similar to that proposed in Ref. [130]. Specifically, the thermal model is updated by imposing an additional heat flux on the internal surface of the insulation exposed by the cutout. The magnitude of this flux is set equal to 50% of the average heat flux per unit area computed for the corresponding insulation layer in the absence of cutouts. This correction is intended to approximate the local degradation of insulation performance due to metallic reinforcements, partial insulation of feed lines, and thermal bridging effects.

As a consequence of the increased local heat ingress, a slight increase in the required insulation thickness is necessary to satisfy the prescribed boil-off rate constraint. This adjustment results in a 0.6% increase in polyurethane mass relative to the reference composite tank discussed in Sec. 4.2. The resulting mass distribution among the tank layers and the stored LH_2 is reported in Fig. (4.1*h*).

4.5 *V* - Composite-based tank with refuelling cutouts and anti-sloshing baffles

To further expand the design space of onboard LH_2 pressure vessels, a configuration incorporating internal anti-sloshing baffles is investigated in addition to the refuelling cutouts introduced in the previous section. The resulting tank layout is schematized in Fig. (4.1*i*).

The design of the anti-sloshing bulkheads is adapted from the works of Lei et al. [149] and Owens et al. [150], with the corresponding geometric parameters reported in Tab. (4.1). The baffles are assumed to be manufactured from the same aluminium alloy as the inner liner, into which they are structurally

integrated. Their thickness is treated as an additional design variable and is therefore determined by the optimization process.

As evidenced by the optimized weight distribution in Fig. (4.1j), the inclusion of anti-sloshing devices leads to a substantial increase in the mass of the inner metallic layer relative to the configuration without baffles. In particular, the presence of the bulkheads results in an approximately 40% increase in m_{Al}. Despite this localized mass increase, the thicknesses of the insulation and composite outer shell remain largely unaffected, as they are primarily governed by thermal and global structural requirements. Consequently, the impact on the overall tank mass is limited, with an increase of approximately 1% relative to the corresponding baffle-less configuration.

4.6 *VI* - Composite-based tank with hemi-ellipsoidal endcaps, refuelling cutouts, and anti-sloshing baffles

The vessel layout described in the previous section is further refined through the adoption of hemi-ellipsoidal endcaps. This final configuration, illustrated in Fig. (4.1k), incorporates all the pragmatic design features considered throughout this study, including refuelling cutouts and internal anti-sloshing baffles, and is therefore regarded as the most representative tank architecture among those investigated.

As already observed in Section 4.3, the introduction of ellipsoidal domes reduces the thermal efficiency of the vessel as a consequence of the increased surface-to-volume ratio. Accordingly, for the configuration analysed in this section, satisfying the prescribed boil-off rate constraint requires an increase in insulation mass of 2.5%. This adjustment results in a corresponding increase

in total tank mass of 2.2% when compared with the analogous configuration employing hemi-spherical endcaps. The optimized mass distribution among the tank layers and the stored fuel for this final layout is reported in Fig. (4.1l).

4.6.1 Influence of alternative composite material lay-ups

The influence of alternative composite lay-ups is assessed using the more pragmatic, thus, higher-fidelity tank model introduced in this section.

In addition to the quasi-isotropic stacking sequence adopted in the preceding analyses, several alternative laminates have been investigated, each consisting of the same number of plies to ensure a consistent basis for comparison. The set of examined configurations includes balanced angle-ply laminates, such as the so-called *magic-angle* lay-up [151], which is specifically designed to optimally distribute hoop and longitudinal stresses in cylindrical pressure vessels, as well as progressive and tailored symmetric stacking sequences. Furthermore, the lay-ups $[11°/90°_2/\pm 25°/18°/90°/21°]$ and $[-87°/36°/47°/33°/-57°/-36°/-50°/-44°]$, derived from Refs. [152] and [153] respectively, are also assessed. These laminates originate from optimization frameworks specifically developed to enhance the structural efficiency of composite pressure vessels operating under high pressure differentials, although the corresponding studies considered monolithic composite vessels rather than the multilayer tank architecture adopted in the present work.

The use of the quasi-isotropic $[0°/90°/45°/-45°]_S$ laminate as the reference configuration is motivated by the specific loading regime of the multilayer cryogenic tank considered in this work. Unlike monolithic high-pressure composite vessels, whose laminate architecture is primarily driven by the hoop-to-longitudinal stress ratio generated by internal pressure, the present LH_2 tank operates at relatively low pressure and includes a thick insulating layer between

the metallic liner and the external composite shell. As a result, the outer CFRP layer is not exposed directly to the cryogenic fuel and remains close to the external environmental temperature during nominal operation. Its stress state is governed by pressure-induced membrane loads, thermal-expansion compatibility, airframe-support constraints, geometric discontinuities, and load transfer through the multilayer wall. A symmetric quasi-isotropic laminate exhibits nearly direction-independent in-plane elastic stiffness, thereby reducing the sensitivity of the structural response to the orientation of the principal stress directions arising from the combined loading conditions [154, 155]. Furthermore, the symmetric stacking sequence eliminates extension-bending coupling, since the corresponding coupling matrix vanishes in Classical Laminate Theory [156].

The corresponding optimization outcomes, summarized in Tab. (4.2), are reported in terms of relative mass penalties affecting both the composite outer shell and the overall tank mass. Among all the considered configurations, the quasi-isotropic $[0°/90°/45°/-45°]_S$ laminate yields the lowest total mass and satisfies all imposed thermo-mechanical constraints. In contrast, the alternative stacking sequences either lead to increased structural mass or fail to satisfy the mechanical constraints within the technological thickness bounds reported in Tab. (3.4). As a result, these configurations are classified as unfeasible for the application under consideration. Achieving feasibility for such lay-ups would require a relaxation of the prescribed technological bounds, resulting in heavier and less practical tank designs.

Table 4.2: Assessment of alternative composite stacking sequences evaluated for the optimization of Tank *VI*. Feasibility is indicated along with the relative increase in CFRP outer layer mass (Δm_{CFRP}) and overall tank mass (Δm_{tank}) with respect to the baseline quasi-isotropic configuration.

Stacking sequence	**Feasibility**	$\Delta m_{\mathbf{CFRP}}$	$\Delta m_{\mathbf{tank}}$
$[0°/90°/45°/-45°]_S$	Yes	/	/
$[11°/90°_2/\pm 25°/18°/90°/21°]$	Yes	+5.1%	+0.8%
$[\pm 54.7°]_8$	Yes	+23.0%	+2.9%
$[\pm 45°]_8$	Yes	+23.6%	+3.0%
$[-87°/36°/47°/33°/-57°/-36°/-50°/-44°]$	Yes	+44.1%	+5.5%
$[90°/45°/30°/0°]_S$	Yes	+61.5%	+7.6%
$[\pm 30°]_8$	No	-	-
$[0°/15°/30°/45°]_S$	No	-	-

It should be emphasized that the quasi-isotropic sequence is not claimed here as a universal or manufacturing-optimal laminate for composite pressure vessels. Rather, under the adopted assumptions, fixed ply count, technological thickness bounds, and damage-initiation constraints, this laminate provides the lowest tank mass among the configurations examined.

4.7 Optimized tank architectures comparative assessment

This section provides an overview of each of the optimized vessels defined and analyzed in the study, comparing their respective configurations and assessing the general influence of design choices on storage-system performance, as summarized in Table (4.3).

Table 4.3: Thermal and gravimetric performance indices of the optimized tank configurations.

		I	**II**	**III**	**IV**	**V**	**VI**
Performance	BOR	2.50% daily					
	$\eta_{\,\mathrm{tank}}$	29.31%	50.11%	49.34%	50.00%	49.76%	49.22%

The total mass, m_{tank}, of each LH_2 tank configuration, decomposed by constituent layers, is reported in Fig. (4.2). The comparison highlights the substantial performance advantage of composite-based architectures over fully metallic designs. In particular, the titanium outer shell of Tank *I* alone results in a mass that is 34% greater than the total mass of the corresponding composite-based Tank *II*. Notably, even when all realistic integration features are included, as in Tank *VI*, the metallic construction still incurs an additional mass penalty of approximately 3.3×10^3 kg relative to the composite solution. This corresponds to a 57% difference in total tank mass between the simple all-metal Tank *I* and the most pragmatic configuration, Tank *VI*. The mass of the foam insulation layer, being primarily dictated by thermal constraints, remains largely unaffected by whether the outer shell is constructed by metallic

or composite materials. By contrast, the aluminium liner of Tank *I*, which, despite its nominal role, indeed contributes to the global load-bearing capability of the vessel, yields nearly twice the mass of the average liner mass observed in tanks equipped with a composite outer shell.

The inclusion of features required for operational viability generally has an adverse impact on the gravimetric efficiency. Accordingly, the adoption of end-caps deviating from a hemi-spherical geometry has considerable detrimental effects. For a fixed internal volume, the use of hemi-ellipsoidal domes increases the surface-to-volume ratio, thus requiring thicker insulation to satisfy the thermal constraints. This mass penalty is further amplified by the external placement of the structural shell: since the structural layer conforms to the outer surface of the insulation, any increase in insulation thickness directly leads to a larger and, therefore, heavier external shell. Similarly, the introduction of refuelling cutouts introduces localized geometric discontinuities that act as stress concentrators, requiring additional material to satisfy structural constraints. Simultaneously, these openings introduce thermal bridges that locally facilitate heat ingress, further affecting the vessel thermal performance. The integration of anti-sloshing bulkheads results in a significant increase in m_{Al}. However, since this layer represents only a small fraction of the total tank mass, the impact on m_{tank} remains relatively limited.

Despite these penalizing yet necessary additions, the gravimetric efficiency achieved by the optimized tank configurations remains attractive, reaching values of approximately 50%, only about 5% short of the theoretical threshold identified by Adler and Martins [5].

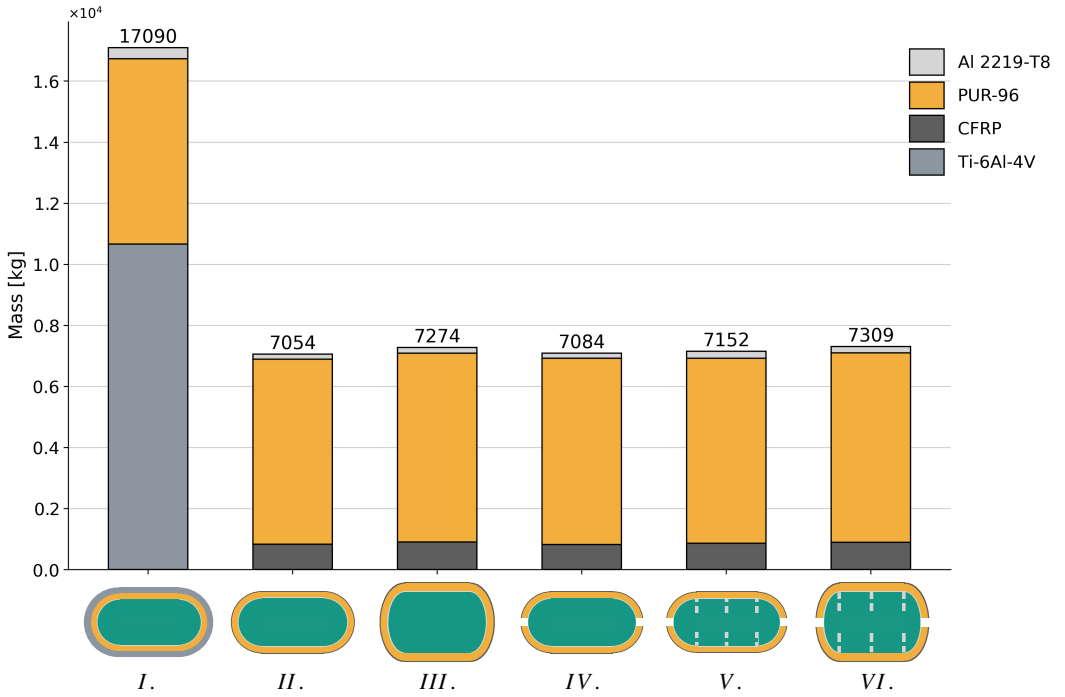

Figure 4.2: Comparison of minimum achievable mass for each tank configuration, with breakdown by layer. The all-metal design (*I*) results in substantially higher total mass compared to composite architectures (*II* to *VI*). The improved mass efficiency enables the integration of realistic design features while pushing $\eta_{\text{tank}} \approx 50\%$.

4.8 Integration of the optimized storage solution into an advanced sustainable airframe

The pressure vessel of configuration *VI*, being the most realistic among those considered by the present study, is tailored for integration into a state-of-the-art LH_2-powered aircraft concept, namely the ultra-high aspect ratio strut-braced wing (UHARW) configuration proposed by Wahler et al. [8]. This aircraft concept targets performance levels comparable to those of current single-aisle commercial transports. To meet the specified design range of 3400 NM,

the total onboard liquid hydrogen requirement is estimated to be 6534 kg. Fuel storage is distributed between two cryogenic tanks located within the forward and aft fuselage sections, as illustrated in Fig. (4.3*a*). This arrangement enables effective volumetric utilization while satisfying aircraft balance and integration constraints.

The aft tank is designed to conform to the full internal fuselage diameter (D_f), thereby maximizing volumetric efficiency. In contrast, the forward tank is constrained by certification requirements. Specifically, Certification Specification §25.772 mandates a continuous access path between the flight deck and the passenger cabin [157]. To satisfy this requirement, the forward tank is designed with a reduced external diameter ($D_{t\text{ext}}$) allowing the integration of a catwalk alongside the tank. A catwalk width of $W_{cw} = 58$ cm is adopted, consistent with standard aisle dimensions in certified commercial aircraft [9], as schematized in Fig. (4.3*b*). Additionally, to maintain the aircraft longitudinal centre-of-gravity within the prescribed design envelope, 60% of the total liquid hydrogen mass is allocated to the aft tank, with the remaining 40% stored in the forward tank.

The two vessels are therefore optimized independently under their respective geometric and operational constraints. For the forward tank, the optimization yields a required polyurethane insulation thickness of approximately 0.33 m, resulting in an internal cavity diameter ($D_{t\text{int}}$) equal to approximately 70% of the fuselage internal diameter (D_f), while the aft tank is set to conform to the entire available internal fuselage diameter.

The proposed component integration highlights how the performance of the storage system cannot be interpreted solely at tank level. As discussed by Cipolla et al. [59], aircraft-level assessment of H_2 storage requires the simultaneous consideration of tank geometry, fuel volume, available fuselage space, passenger and payload accommodation, and mission requirements. In

the present configuration, these couplings are partly evident in the different roles played by the forward and aft tanks. For example, the forward vessel is limited by the need to preserve a continuous access path between the cockpit and the passenger cabin, which constrains the admissible external diameter and therefore reduces the internal volume available for fuel once the insulation thickness is accounted for. Conversely, the aft vessel can exploit the full fuselage diameter, leading to a more favourable surface-to-volume ratio and, therefore, to improved thermal and gravimetric performance. Accordingly, the resulting aircraft-level feasibility is governed by the interaction between several quantities that are optimized or constrained at tank level. Increasing the insulation thickness reduces heat ingress and helps satisfy the boil-off constraint, but also increases tank mass and external dimensions, thereby affecting volumetric efficiency and fuselage-space allocation. Increasing the stored fuel volume improves mission capability, but requires larger vessels and may penalize cabin or payload arrangement. Finally, the distribution of fuel between forward and aft locations is not only a storage-sizing choice, but also an aircraft-integration requirement, since it affects longitudinal balance and centre-of-gravity management.

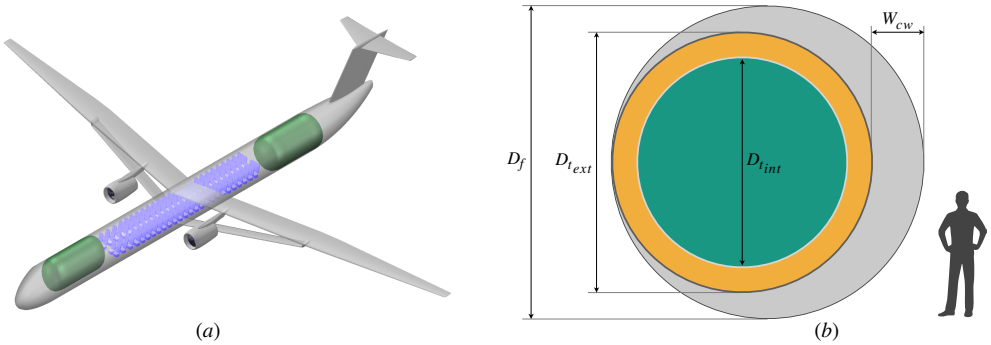

Figure 4.3: Integration of the optimized vessels in the sustainable aircraft concept from Ref.[8]: *a*) isometric view of the LH_2-powered strut-braced wing aircraft complete with fuel tanks and passenger seats; *b*) sectional view of the forward fuselage highlighting the vessel integration into the available volume, along with the standard-height civilian male for reference according to Ref.[9].

The thermo-mechanical behaviour of the optimized LH_2 storage units is evaluated through the analysis of representative field distributions for each tank layer, as reported in Fig. 4.4. For conciseness, only the plots corresponding to the highest magnitude fields are reported, without distinction between the forward and aft tanks due to the similarity of the resulting contour distributions.

The equivalent von Mises stress distribution in the inner metallic liner, including the integrated anti-sloshing baffles, is shown in Fig. (4.4*a*). The normalized peak stress reaches approximately 61% of the allowable limit ($\bar{\sigma}_{\mathrm{SF}}^{\mathrm{Al}}$). This margin indicates that, subject to manufacturing feasibility, a moderate reduction in the Al 2219-T8 liner thickness could potentially yield additional mass savings without compromising structural integrity.

The tank layer that appears to limit global resistance is the low-density insulating PUR. Specifically, as Fig. (4.4*b*) highlights, the safety-factor-adjusted yielding threshold is reached along the central restrained edge on the outer

foam surface. This behaviour suggests that improved structural performance could be achieved either through the adoption of advanced insulation materials combining low density with enhanced stiffness, or by re-evaluating the mechanical boundary conditions. In particular, less restrictive supports that allow for controlled dimensional variations, or mounting strategies that distribute reaction forces over a wider contact area, may reduce stress concentrations and improve the structural response. The localized stress peaks observed on the foam surface indeed primarily arise from the combined effects of the anti-sloshing baffles and the tank–airframe integration constraints, which locally inhibit the natural thermal contraction of the insulation layer. Given the relatively low internal and hydrostatic pressures, the mechanical response of the tank is predominantly driven by thermally induced loads. While relaxing the mechanical constraints would indeed reduce stress levels [50], practical integration and safety considerations generally necessitate a certain degree of over-constraining, thereby resulting in a hyperstatic structural configuration. The heat-flux-per-unit-area distribution within the insulation layer is shown in Fig. (4.4c). Localized increases in heat flux are observed in correspondence of the refuelling cutouts, reflecting the thermal penalty associated with insulation discontinuities and thermal bridging effects.

The structural performance of the composite outer shell is assessed using the Hashin damage initiation criteria, considering fibre tension (HSNFTCRT) and matrix compression (HSNMCCRT) failure modes. Owing to the symmetric stacking sequence, the inner four plies yield analogous but lower-magnitude indices and are therefore omitted for conciseness. The discussion is thus focused on the outermost composite plies. Figure (4.4d) presents the contour distribution of the Hashin fibre tension index, which reaches its maximum value in proximity to the cutout-induced geometric discontinuities. Similarly, Fig. (4.4e) shows that the maximum matrix compression index is again

strongly influenced by the tank–airframe integration strategy, with peak values occurring near the three restrained circular support edges. In both cases, the maximum values of the fibre tension and matrix compression indices are consistently observed within the 90°-oriented plies.

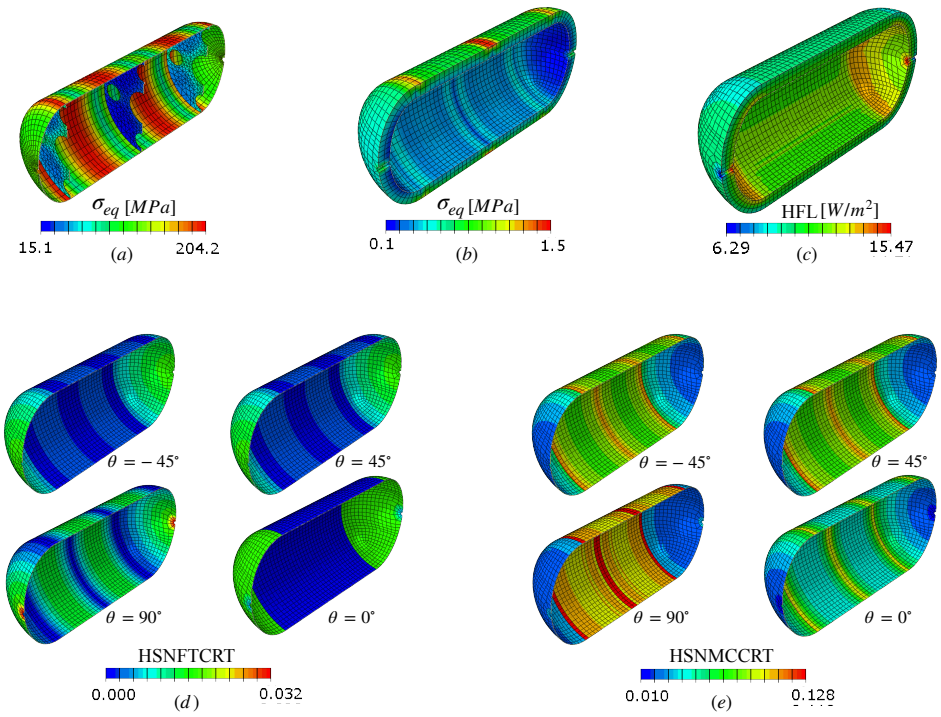

Figure 4.4: Optimized UHARW vessels thermo-mechanical fields. Equivalent stress in the inner (a) and middle (b) layers; heat flux per unit area in the middle layer (c); Hashin fibre tension (d) and matrix compression (e) indices distribution for the four more loaded plies of the composite outer shell.

Beyond the layer-wise thermo-mechanical response, consideration of the global tank performance reveals an additional effect associated with fuel capacity scaling. The forward and aft tanks, designed to store 37% and 55% of the reference tank volume V_{tank} respectively, provide insight into the scaling behaviour characteristic of cryogenic storage systems. Accordingly, a reduction in tank dimensions leads to an increased surface-to-volume ratio, which in turn

increases thermal ingress, negatively affecting the insulation mass required to satisfy a given boil-off rate constraint [5]. As a consequence, optimization of the smaller UHARW storage tanks, while enforcing the daily boil-off rate limit of 2.50%, results in a reduction of approximately 1% in η_{tank} relative to Tank *VI*, which serves as the reference configuration for the storage system.

Chapter 5

Discussion, conclusions and future work

This thesis presents the conceptual design and optimization of a passively insulated sandwich-composite cryogenic pressure vessel for onboard LH_2 aircraft storage, together with a dedicated FEM-based optimization framework tailored to this layered tank architecture. By coupling multiphysics finite-element modelling with nonlinear constraint-based optimization, the proposed methodology enables systematic exploration of the tank design space under realistic thermal, structural, and integration constraints, with the objective of minimizing tank mass while preserving thermo-mechanical feasibility. In this sense, the work provides quantitative insight into the trade-offs governing the performance of aviation-oriented hydrogen storage systems and supports the identification of pragmatic storage architectures for future sustainable aircraft.

The results consistently show that composite-based tank architectures outperform metallic alternatives in terms of storage performance. While Al 2219-T8 proves well suited for the inner liner, owing to its favourable cryogenic strength and corrosion resistance, a structurally more efficient material is re-

quired for the outer load-bearing shell. For such role, the use of high-strength metallic alloys leads to significant penalties in mass, cost, manufacturability, and material availability. Although Ti-6Al-4V is mechanically viable as an external shell material, the resulting optimized all-metal configuration achieves a gravimetric efficiency below 30%, with the metallic outer layer alone accounting for more than 44% of the total tank mass.

By contrast, the adoption of composite materials for the external shell emerges as a necessary condition for achieving competitive aviation storage performance. Relative to metallic designs, CFRP-based configurations reduce total tank mass by up to 59%, corresponding to an improvement in η_{tank} of 21.8%. Among the laminate solutions examined, the quasi-isotropic stacking sequence consistently yields the minimum tank mass while satisfying all imposed constraints, and should therefore be regarded as a primary candidate for the manufacture of the outer structural layer of composite cryogenic vessels. Overall, these results indicate that the use of composite materials is a prerequisite for high-performance LH_2 storage systems in aviation applications.

From a geometric perspective, apart from purely spherical vessels, which entail substantial aircraft integration penalties, configurations featuring a cylindrical section with hemi-spherical endcaps provide the most favourable thermomechanical response. Nevertheless, practical aircraft integration may require alternative dome geometries, such as hemi-ellipsoidal endcaps. For equal internal volume, these geometries induce a mass increase of 3.1% relative to hemi-spherical counterparts, primarily because of their less favourable surface-to-volume ratio. The resulting increase in heat ingress requires thicker insulation to satisfy the prescribed boil-off rate constraint, thereby increasing overall tank mass. The analyses further underline the importance of geometric scaling and aircraft-level integration strategy in shaping the achievable performance of liquid-hydrogen storage systems.

The results also show that pragmatic features required for aircraft integration systematically introduce stress concentrations and mass penalties, highlighting the need to account for such effects already at the conceptual design stage. For instance, the inclusion of refuelling cutouts, thermally represented through localized penalties to reflect reduced insulation effectiveness, causes a small but non-negligible increase in insulation thickness in order to preserve the target thermal performance. Similarly, the incorporation of anti-sloshing baffles, required to mitigate uncontrolled fuel motion during aircraft acceleration, leads to a substantial increase in liner mass. For the configurations analysed, the liner mass increases by approximately 40% relative to the corresponding baffle-less solution. However, since this layer represents only about 1.6% of the total tank mass, the impact on overall gravimetric efficiency remains limited, on the order of 1%.

Ultimately, although the optimized composite-based designs presented in this thesis do not reach the gravimetric efficiency threshold $\eta_{\text{tank}} > 55\%$, identified by Adler et al. in Fig. (3.4) as critical for surpassing kerosene-fuelled aircraft in range and energy efficiency, they consistently achieve values around 50%, even when realistic integration features are explicitly included. Accordingly, the exploration of the optimized tank design space indicates that passively insulated composite-based architectures can approach the performance levels required for viable H_2-powered aviation, thereby confirming the effectiveness of targeted optimization approaches for enabling high-performance cryogenic storage. Such performance, however, has not yet been fully attained. The thermo-mechanical analyses suggest that further progress may depend on more refined tank-airframe integration strategies and on advanced insulating materials capable of combining low thermal conductivity, low thermal diffusivity, and high specific strength. These aspects may prove decisive in further enhancing the performance of the proposed foam-based layered architecture.

Accordingly, building upon these results, the following sections discuss the methodological limitations of the present work and outline key directions for future research aimed at extending the framework toward increased fidelity and operational applicability.

5.1 Methodological limitations and scope of validity

The results presented in this thesis are subject to a number of methodological limitations arising from a combination of modelling assumptions, uncertainties in material behaviour under extreme conditions, and the necessity to adopt simplified boundary conditions and operating scenarios to ensure computational feasibility.

Material properties at cryogenic temperatures represent a primary source of uncertainty. While the numerical model adopted employs property values drawn from the available literature, parameters such as elastic moduli, thermal conductivities, and failure strengths may exhibit variability due to manufacturing processes, material heterogeneity, and temperature-dependent effects that are not fully captured by nominal data. In composite materials, additional sources of variability may stem from fibre misalignment and local defects, which may influence the stress state and damage initiation at the local scale [158]. Similarly, uncertainties in external heat-transfer coefficients, surface emissivity, and environmental conditions may lead to localized variations in predicted heat-flux distributions. Furthermore, all model parameters are treated as deterministic inputs within the optimization framework, and the propagation of parametric uncertainty is not explicitly addressed. Another limitation lies in the scarcity of high-quality experimental data for validation.

These uncertainties may affect the results at different extents. Variations in thermal conductivity, external convection coefficients, or imposed boundary temperatures directly modify the heat-flux distribution through the insulation and, consequently, the predicted boil-off rate and required insulation thickness. Likewise, uncertainties in elastic moduli, coefficients of thermal expansion, allowable strengths, and idealized contact or constraint representations may influence the local stress peaks predicted near restrained edges, dome-cylinder transitions, cutouts, baffle attachments, tank-airframe interfaces, and geometric discontinuities in general. Thus, the optimization results reported in this thesis should be interpreted as deterministic outputs of the adopted modelling assumptions. They are indeed suitable for comparing architectures, identifying dominant design drivers, and quantifying achievable performance trends within a consistent computational framework. They should not, however, be interpreted as absolute design margins.

In this context, although the present study is computational in nature and intended to support early-stage design decisions, experimental validation of cryogenic hydrogen tanks for aviation remains challenging due to the limited technology readiness level and the associated commercial sensitivity of these systems. Despite these constraints, deviations in thermal or mechanical parameters may affect local stress or heat-flux levels, but are not expected to alter the fundamental conclusions regarding the performance of the different materials and structural architectures identified in this work. Therefore, while the adopted assumptions reduce the ability of the framework to capture stochastic effects or time-dependent phenomena, they allow consistent comparison across a large number of design configurations and enable the identification of robust global design trends. Hence, future extensions of the methodology may be directed toward the incorporation of uncertainty quantification and reliability-based design principles. In particular, the integration of probabilis-

tic material models, stochastic boundary conditions, and experimental data for model calibration would enable systematic evaluation of design robustness and the inclusion of confidence bounds on optimal solutions.

Finally, it must be noted that the optimized values of η_{tank} should be interpreted in light of the adopted mechanical constraints. The optimization indeed enforces material yielding and damage-initiation limits under representative thermo-mechanical operating conditions, but does not include burst-pressure assessment, progressive damage evolution, or ultimate structural collapse. Consequently, the optimized mass values quantify the attainable performance of the proposed architectures within an early-stage damage-initiation-constrained design framework. They should not be interpreted as burst-verified or certification-ready design targets. Future burst-pressure-constrained optimization may modify the optimum thickness distribution and could reduce the attainable gravimetric efficiency if ultimate pressure loading or local reinforcement requirements become sizing drivers.

5.2 Future developments in tank design and optimization

5.2.1 Transient mission-dependent thermal behaviour

As stated, the analyses presented in this thesis focus exclusively on steady-state thermal conditions, which provide a consistent and computationally efficient basis for comparative assessment and optimization of cryogenic storage tanks.

While this approach is well suited for the identification of design trends and performance envelopes, it does not capture the inherently transient thermal evolution experienced by cryogenic tanks throughout an aircraft mission. In operational scenarios, the thermal state of a LH_2 pressure vessel evolves

continuously as a function of time, fuel consumption, and external boundary conditions [60]. Extended pre-departure holds, as well as ground operations in general, may subject the tank to considerable additional heat exposure, while climb, cruise, and descent may be characterized by varying ambient temperatures, convective heat-transfer coefficients, and cabin internal pressures.

In this context, a relevant operational constraint is represented by the allowable dormancy time of the storage system. For aircraft applications, dormancy is not limited to long-term storage, but also includes ground waiting periods, refuelling-to-take-off intervals, taxi, turnaround operations, extended pre-departure holds, and other non-propulsive phases of the mission. During these intervals, heat ingress continues to promote liquid evaporation and ullage pressurization, while propulsive fuel consumption is absent or strongly reduced. Consequently, these phases affect tank performance through the accumulated thermal load imposed before or between propulsive mission segments. For a given tank architecture, longer non-propulsive periods increase the amount of hydrogen that may evaporate, reduce the usable fuel available for the mission if venting occurs, and increase the demand on pressure-control systems. Therefore, the relevant performance quantity is not only the instantaneous boil-off rate, but also the integrated heat input over the complete operational timeline. The practical consequence is that dormancy requirements may directly affect tank sizing, insulation design, pressure management, and safety procedures. Longer allowable ground or pre-departure times require either lower heat leak, larger pressure margins, active pressure-control strategies, or acceptance of additional hydrogen losses. Increasing insulation thickness can reduce heat ingress and extend dormancy, but it also increases tank mass and external dimensions, thereby penalizing gravimetric and volumetric efficiency [159]. Conversely, relaxing the insulation requirement may reduce tank mass, but increases the likelihood of excessive boil-off, pressure rise, or vent-

ing during non-propulsive mission phases. Accordingly, future extensions of the present framework should treat dormancy as a mission-dependent operational constraint, linking integrated heat input, allowable pressure rise, venting strategy, hydrogen losses, and ground-safety procedures within a unified tank–aircraft design assessment. Previous aircraft-level LH_2 integration and transient-operation studies support this perspective, showing that tank sizing and storage-system performance should be evaluated together with the time-dependent fuel demand and thermodynamic evolution of the storage system [59].

Extending the present framework to account for transient thermal behaviour would therefore enable prediction of mission-dependent boil-off rates and cumulative hydrogen losses, thus providing a more realistic assessment of operational performance. Such transient analyses could support the development of tank management strategies, including pressure control [160], venting schedules, and integration within the aircraft environmental control systems. From a modelling perspective, transient simulations introduce additional challenges related to computational cost and model complexity. Hence, specific reduced-order thermal models or surrogate representations derived from high-fidelity FE analyses may be required to maintain compatibility with multidisciplinary optimization workflows.

5.2.2 Local thickness tailoring

The optimization framework developed in this thesis primarily employs global or shape-specific thicknesses to balance structural integrity and mass efficiency. While this approach enables efficient exploration of the design space and yields physically consistent solutions, it limits the ability to exploit localized stress patterns emerging from the FE analyses. Regions such as dome-cylinder in-

terfaces, cutouts, and geometric discontinuities in general may experience considerable stress concentrations, while large portions of the structure operate well below critical limits. Globally parameterized thickness distributions may therefore remain conservative.

To address this limitation and pursue additional performance improvement, a natural extension of the present methodology is the introduction of patch-wise thickness tailoring [161], in which the tank structure is subdivided into a finite number of surface patches, each associated with an independent thickness variable. This approach would increase the number of design variables and, consequently, the computational cost, but may lead to more competitive storage system performance. However, abrupt thickness variations between adjacent patches may introduce artificial stiffness discontinuities, mesh-dependent stress peaks, or non-manufacturable local features. Accordingly, patch-wise tailoring should be complemented by suitable regularization, smoothing, or blending constraints, as commonly adopted in structural and topology optimization to mitigate spurious numerical patterns and mesh-dependent solutions [162]. Additionally, further topology refinement may be achieved through the addition of supporting structures, such as stiffening ribs, load-spreading elements, or localized thickening [163].

The composite outer shell is modelled in the present work through an equivalent laminate description with a prescribed stacking sequence. This modelling choice is intended to support comparison between material architectures and tank layouts, rather than to define an absolute manufacturing-ready tank standard. The composite shell is assumed to be manufactured using filament winding. However, no specific manufacturing assessment is carried out, as the present work is intended as a conceptual design study focused on identifying the governing thermo-structural aspects of the multilayer cryogenic tank rather than establishing a complete pressure vessel design methodology. If filament

winding were adopted, the laminate architecture would indeed have to be formulated in terms of admissible hoop and helical winding paths, with particular attention to the dome regions, where geodesic constraints, fibre-angle variation, tow steering limitations, and thickness build-up may prevent the direct realization of an idealized lay-up. Conversely, automated fibre placement could offer greater freedom in reproducing locally tailored or quasi-isotropic laminates, but at the expense of increased process complexity, possible steering-induced defects, and additional inspection requirements. Moreover, the present laminate model does not explicitly represent local ply terminations or manufacturing-induced thickness transitions. Consequently, three-dimensional effects associated with ply drops, such as interlaminar stress concentrations, stiffness discontinuities, delamination initiation, and local load redistribution, are not captured [164]. This limitation may be relevant near dome-cylinder transitions or cutouts where real composite tanks may exhibit failure mechanisms that are not predicted by a homogenized model.

5.2.3 Extension to conformal tank architectures and alternative insulation concepts

A further extension of the proposed framework concerns its application to conformal tank architectures, which represent a mitigation strategy to the spatial integration challenges associated with cryogenic hydrogen storage in aircraft [165]. Unlike cylindrical or spherical vessels, conformal tanks are shaped to follow the available airframe volume, enabling improved volumetric efficiency. For example, the tail-cone section of the fuselage offers a potential location for conformal vessels, as such a component can be placed between the rear of the passenger cabin and the auxiliary power unit, thereby minimizing interference with payload and primary structural members.

While extending the present modelling and optimization framework to conformal tanks introduces additional challenges related to geometric complexity, the multiphysics and optimization capabilities developed in this thesis provide a suitable foundation for such investigations. Moreover, the assessment of conformal H_2 tanks would allow direct comparison between cylinder-based vessels and airframe-adapted architectures, supporting trade-offs between mass and volumetric efficiency at the aircraft integration level.

A further line of development concerns the adoption of advanced insulation concepts. Beyond the foam-based solutions considered in the present work, future investigations may address alternative insulation systems capable of further reducing heat ingress. In this respect, high-performance vacuum-based insulation concepts may represent a promising option, provided that adequate levels of reliability, gravimetric efficiency, and durability can be ensured under realistic operating conditions.

5.2.4 Structural health monitoring and non-destructive testing

The use of mandated safety factors in H_2 tank design, typically ranging between 1.4 and 2.0, is further augmented by uncertainties associated with material characterization, manufacturing-related variability, and the mechanical and thermal behaviour of materials under severe operating conditions, particularly when advanced or non-traditional materials are employed [42]. This results in design conservatism, which, however, significantly constrains the achievable mass efficiency of hydrogen storage systems, making the development of lightweight tank architectures particularly challenging.

A potential pathway to alleviating this conservatism lies in the systematic integration of structural health monitoring (SHM) and non-destructive test-

ing (NDT) technologies, which can enable continuous or periodic assessment of structural integrity and provide quantitative information on local damage states and operating conditions, thereby supporting the adoption of less conservative $\bar{\sigma}_{\mathrm{SF}}$ design values [93]. Nevertheless, the implementation of SHM in cryogenic pressure vessels remains non-trivial, as low temperatures and repeated thermal cycling may adversely affect sensor durability, measurement quality, and long-term signal reliability [94]. Recent experimental investigations indicate that embedded sensing solutions, such as Lead Zirconate Titanate (PZT)-based transducers and optical fibre systems, can retain functionality under cryogenic environments while enabling effective damage detection and hydrogen leakage monitoring [95, 96].

For reusable liquid hydrogen tanks, future research should therefore focus on the development of integrated monitoring architectures that combine real-time in-flight sensing with advanced ground-based NDI methods. Such frameworks require optimized sensor placement, robust data-processing strategies, and experimentally validated failure-mode identification approaches, with particular attention to composite tank configurations operating under extreme conditions [97].

5.3 Component interface with aircraft systems and crashworthiness assessment

The interface between the highly specialized cryogenic tank and the aircraft structure represents a design challenge extending beyond the vessel itself, as it directly affects overall system safety and crashworthiness, in addition to the structural integrity and thermal performance discussed previously. While the present work models the tank as a non-integral self-supporting component

with simplified, yet prototype-inspired, boundary conditions, future developments may explicitly address the design of tank–airframe interfaces capable of meeting safety requirements without compromising thermal efficiency.

From a structural perspective, tank mounts must ensure reliable load transfer under normal operating conditions, while accommodating both thermal and pressure-induced deformations. Concurrently, structural attachments may constitute a substantial source of parasitic heat ingress. Mounts that mechanically bypass the insulating layer may act as thermal bridges, thereby degrading insulation performance and increasing boil-off rates [166]. Conventional metallic attachment solutions may therefore be challenging in cryogenic applications, as they combine high structural stiffness with high thermal conductivity. Hence, tank supports in LH_2-powered aircraft must reconcile competing requirements through thermally decoupled load paths or hybrid solutions that minimize conductive heat flow while maintaining adequate crash-load capacity.

Additionally, crashworthiness considerations impose further and potentially dominant constraints on the design of the tank–airframe interface [167]. In the event of a crash, attachment systems must absorb and dissipate kinetic energy while preventing catastrophic tank rupture or penetration of the pressure vessel by surrounding elements [168]. Crash-compliant mounting concepts may therefore incorporate sacrificial elements or controlled failure paths that limit peak loads transmitted to the tank during impact. In this context, the integration of self-sealing technologies represents an interesting prospect for enhancing crash safety. Self-sealing liners could limit hydrogen leakage in the event of localized damage or penetration [169]. When combined with crash-compliant mounting systems, such approaches could significantly improve the overall survivability of the H_2 system.

Beyond structural attachments, the tank–airframe interface also involves multiple interactions with aircraft subsystems, including but not limited to

fuel feed and venting lines, gas extraction devices, leak detection systems, the environmental control system, and multiple sensors. The integration of such subsystems may introduce additional geometric discontinuities and potential thermal bridges.

5.4 Safety, risk, and certification aspects

5.4.1 Risk assessment and mitigation

The introduction of LH_2 as an onboard energy carrier alters the aircraft risk landscape relative to mature kerosene-based systems, thus requiring systematic safety assessment methodologies from the earliest design stages. In contrast to conventional fuel systems, cryogenic H_2 storage introduces hazards associated with extremely low temperatures, rapid phase change, and high flammability, all of which must be addressed within an integrated risk management framework.

A necessary step in the safety-driven development of hydrogen-powered aircraft is the application of formal hazard identification and analysis techniques [170]. Hazard Identification (HAZID) is a qualitative, high-level process aimed at identifying hazard scenarios, together with their potential causes and consequences. HAZID studies can be used to systematically identify hazards related to tank rupture, leakage, venting malfunctions, thermal insulation failure, and unintended interactions with surrounding aircraft systems. As the technology matures, Hazard and Operability Analysis (HAZOP) will provide a complementary and more detailed methodology, focusing on deviations from intended system behaviour and their potential impact on safety and operability. By collecting and monitoring parameters such as pressure, temperature, flow rate, and structural integrity, HAZOP studies will enable structured exploration of

abnormal conditions that may arise during flight operation, refuelling, ground handling, or emergency scenarios.

Risk mitigation strategies emerging from both HAZID and HAZOP studies will likely include measures such as multiple system redundancy, physical isolation of hydrogen systems, controlled venting paths, and crash-compliant mounting concepts.

5.4.2 Regulatory framework and certification pathways

The current airworthiness framework for large transport aircraft has been developed around conventional kerosene-based fuel systems and does not explicitly address the distinctive features associated with cryogenic hydrogen storage and distribution [171]. As a result, while many CS-25 requirements remain applicable at a high level, substantial gaps persist with respect to H_2-specific aspects [172]. Under the existing regulatory structure, hydrogen-powered aircraft would likely be certified through a combination of compliance with applicable CS-25 paragraphs and the definition of Special Conditions, Equivalent Level of Safety (ELOS) findings, or Issue Papers to address aspects not covered by current rules. In particular, key areas in which CS-25 [116] currently lacks explicit guidance include the treatment of cryogenic temperatures, management of boil-off and vented fuel, crash behaviour of cryogenic pressure vessels, and the consequences of H_2 leakage and dispersion within the aircraft. Hence, the current absence of specific certification standards introduces uncertainty and should motivate, in the near future, the implementation of dedicated Acceptable Means of Compliance (AMC), or, in the longer term, hydrogen-specific airworthiness requirements explicitly addressing the unique aspects of sustainable aviation.

As the regulatory framework evolves to include H_2 aircraft operations, com-

putational modelling tools such as those developed in this thesis may play an important role in enabling the safe introduction of alternative storage systems into commercial aviation. In this sense, the work presented here may contribute to the technical foundation required to support future certification processes. The proposed thermo-mechanical modelling framework, in fact, provides insight into structural margins, thermal behaviour, and failure-sensitive regions of cryogenic aircraft tanks. These results can be used to inform safety objectives, support the definition of certification assumptions, and contribute to the technical formulation of future regulatory requirements for H_2 operations.

Bibliography

[1] Climate Action Tracker. International aviation. https://climateactiontracker.org/sectors/aviation/, 2025. Accessed: 29 December 2025.

[2] Tiwari, S., Pekris, M. J., and Doherty, J. J. A review of liquid hydrogen aircraft and propulsion technologies. *International Journal of Hydrogen Energy*, 57:1174–1196, 2024. ISSN 0360-3199. doi: https://doi.org/10.1016/j.ijhydene.2023.12.263. URL https://www.sciencedirect.com/science/article/pii/S0360319923065631.

[3] NASA. Sts-133 repair work external tank closeup. https://images.nasa.gov/details/KSC-2011-1003, 2011. Photo ID: KSC-2011-1003, photograph by Jack Pfaller, accessed 10 April 2026.

[4] Mass Timber Connections (MTC) Solutions. A comprehensive overview of environmental hydrogen embrittlement, 2024. URL https://mtcsolutions.com/resources/tech-blogs/a-comprehensive-overview-of-environmental-hydrogen-embrittlement/. Available online, accessed on 20/01/2026.

[5] Adler, E. J. and Martins, J. R. Hydrogen-powered aircraft: Fundamental concepts, key technologies, and environmental impacts. *Progress in Aerospace Sciences*, 141:100922, 2023. ISSN 0376-0421. doi: https:

//doi.org/10.1016/j.paerosci.2023.100922. Special Issue on Green Aviation.

[6] Mantzaroudis, V. K. and Theotokoglou, E. E. Computational analysis of liquid hydrogen storage tanks for aircraft applications. *Materials*, 16 (6), 2023. ISSN 1996-1944. doi: 10.3390/ma16062245.

[7] Bagarello, S., Elham, A., and Benedetti, I. Design, optimization, and integration of passively-insulated liquid hydrogen tanks for sustainable aviation. *International Journal of Hydrogen Energy*, 202:153042, 2026. ISSN 0360-3199. doi: https://doi.org/10.1016/j.ijhydene.2025.153042. URL `https://www.sciencedirect.com/science/article/pii/S0360319925060458`.

[8] Wahler, N. F. M., Ma, Y., and Elham, A. Conceptual design and aerostructural trade-offs in hydrogen- powered strut-braced wing aircraft: Insights into dry and wet ultra-high aspect ratio wings. *Aerospace*, 12(2), 2025. ISSN 2226-4310. doi: 10.3390/aerospace12020077.

[9] Raymer, D. P. *Aircraft design: A conceptual approach*. AIAA education series. American Institute of Aeronautics and Astronautics, Reston, Va., 4. ed. edition, 2006. ISBN 1563478293. URL `http://www.loc.gov/catdir/toc/ecip068/2006004706.html`.

[10] Kousoulidou, M. and Lonza, L. European aviation environmental report 2016. easa, eea, eurocontrol. *JRC99523*, 2016.

[11] Dahal, K., Brynolf, S., Xisto, C., Hansson, J., Grahn, M., Gronstedt, T., and Lehtveer, M. Techno-economic review of alternative fuels and propulsion systems for the aviation sector. *Renewable and Sustainable*

Energy Reviews, 151:111564, 2021. ISSN 1364-0321. doi: https://doi.org/10.1016/j.rser.2021.111564.

[12] European Commision, Mobility Transport Directorate General, Research and Innovation Directorate General. Flightpath 2050: Europe's vision for aviation : maintaining global leadership and serving society's needs, 2011. URL `https://data.europa.eu/doi/10.2777/50266`. Available online.

[13] Hammad, A. W., Rey, D., Bu-Qammaz, A., Grzybowska, H., and Akbarnezhad, A. Mathematical optimization in enhancing the sustainability of aircraft trajectory: A review. *International Journal of Sustainable Transportation*, 14(6):413–436, 2020.

[14] Ozturk, F., Cobanoglu, M., and Ece, R. E. Recent advancements in thermoplastic composite materials in aerospace industry. *Journal of Thermoplastic Composite Materials*, 37(9):3084–3116, 2024.

[15] Adler, E. J. and Martins, J. R. Blended wing body configuration for hydrogen-powered aviation. *Journal of Aircraft*, 61(3):887–901, 2024.

[16] Benad, J. and Vos, R. Design of a flying v subsonic transport. In *33rd Congress of the International Council of the Aeronautical Sciences*, 2022.

[17] Ansell, P. J. Review of sustainable energy carriers for aviation: Benefits, challenges, and future viability. *Progress in Aerospace Sciences*, 141: 100919, 2023. ISSN 0376-0421. doi: https://doi.org/10.1016/j.paerosci.2023.100919. Special Issue on Green Aviation.

[18] Wang, B., Ting, Z. J., and Zhao, M. Sustainable aviation fuels: Key opportunities and challenges in lowering carbon emissions for aviation

industry. *Carbon Capture Science & Technology*, 13:100263, 2024. ISSN 2772-6568. doi: https://doi.org/10.1016/j.ccst.2024.100263.

[19] Degirmenci, H., Uludag, A., Ekici, S., and Karakoc, T. H. Challenges, prospects and potential future orientation of hydrogen aviation and the airport hydrogen supply network: A state-of-art review. *Progress in Aerospace Sciences*, 141:100923, 2023. ISSN 0376-0421. doi: https://doi.org/10.1016/j.paerosci.2023.100923. Special Issue on Green Aviation.

[20] Tarhan, C. and Çil, M. A. A study on hydrogen, the clean energy of the future: Hydrogen storage methods. *Journal of Energy Storage*, 40: 102676, 2021. ISSN 2352-152X. doi: https://doi.org/10.1016/j.est.2021.102676.

[21] Ratnakar, R. R., Gupta, N., Zhang, K., van Doorne, C., Fesmire, J., Dindoruk, B., and Balakotaiah, V. Hydrogen supply chain and challenges in largescale lh2 storage and transportation. *International Journal of Hydrogen Energy*, 46(47):24149–24168, 2021.

[22] Muhammed, N. S., Gbadamosi, A. O., Epelle, E. I., Abdulrasheed, A. A., Haq, B., Patil, S., Al-Shehri, D., and Kamal, M. S. Hydrogen production, transportation, utilization, and storage: Recent advances towards sustainable energy. *Journal of Energy Storage*, 73:109207, 2023. ISSN 2352-152X. doi: https://doi.org/10.1016/j.est.2023.109207.

[23] Smith, J. R. and Mastorakos, E. An energy systems model of large commercial liquid hydrogen aircraft in a low-carbon future. *International Journal of Hydrogen Energy*, 52:633–654, 2024. ISSN 0360-3199. doi: https://doi.org/10.1016/j.ijhydene.2023.04.039.

[24] Moliner, R., Lázaro, M., and Suelves, I. Analysis of the strategies for

bridging the gap towards the hydrogen economy. *International Journal of Hydrogen Energy*, 41(43):19500–19508, 2016. ISSN 0360-3199. doi: https://doi.org/10.1016/j.ijhydene.2016.06.202. URL `https://www.sciencedirect.com/science/article/pii/S0360319916303287`. The 5th Iberian Symposium on Hydrogen, Fuel Cells and Advanced Batteries (HYCELTEC 2015), 5-8 July 2015, Tenerife, Spain.

[25] Kastell, D. Hydrogen storage technology for aerial vehicles. In Colpan, C. O. and Kovač, A., editors, *Fuel Cell and Hydrogen Technologies in Aviation*, pages 1–22. Springer International Publishing, Cham, 2022.

[26] Yusaf, T., Mahamude, A. S. F., Kadirgama, K., Ramasamy, D., Farhana, K., Dhahad, H. A., and Talib, A. R. A. Sustainable hydrogen energy in aviation - a narrative review. *International Journal of Hydrogen Energy*, 52:1026–1045, 2024. ISSN 0360-3199. doi: https://doi.org/10.1016/j.ijhydene.2023.02.086.

[27] Rao, A. G., Yin, F., and Werij, H. G. Energy transition in aviation: The role of cryogenic fuels. *Aerospace*, 7(12):181, 2020.

[28] Khandelwal, B., Karakurt, A., Sekaran, P. R., Sethi, V., and Singh, R. Hydrogen powered aircraft: The future of air transport. *Progress in Aerospace Sciences*, 60:45–59, 2013.

[29] Teoh, Y. H., How, H. G., Le, T. D., Nguyen, H. T., Loo, D. L., Rashid, T., and Sher, F. A review on production and implementation of hydrogen as a green fuel in internal combustion engines. *Fuel*, 333:126525, 2023. ISSN 0016-2361. doi: https://doi.org/10.1016/j.fuel.2022.126525.

[30] Afonso, F., Sohst, M., Diogo, C. M., Rodrigues, S. S., Ferreira, A., Ribeiro, I., Marques, R., Rego, F. F., Sohouli, A., Portugal-Pereira,

J., Policarpo, H., Soares, B., Ferreira, B., Fernandes, E. C., Lau, F., and Suleman, A. Strategies towards a more sustainable aviation: A systematic review. *Progress in Aerospace Sciences*, 137:100878, 2023. ISSN 0376-0421. doi: https://doi.org/10.1016/j.paerosci.2022.100878.

[31] Brelje, B. J. and Martins, J. R. R. A. Aerostructural wing optimization for a hydrogen fuel cell aircraft. *AIAA SCITECH*, 2021.

[32] Verstraete, D. An assessment of the potential of hydrogen fuelled large long-range transport aircraft. *26th International Congress of the Aeronautical Sciences*, 2008.

[33] Nash, D., Aklil, D., Johnson, E., Gazey, R., and Ortisi, V. Hydrogen storage: Compressed gas. *Comprehensive Renewable Energy*, 4, 2012.

[34] Hua, T. Q., Roh, H.-S., and Ahluwalia, R. K. Performance assessment of 700-bar compressed hydrogen storage for light duty fuel cell vehicles. *International Journal of Hydrogen Energy*, 42(40):25121–25129, 2017. ISSN 0360-3199. doi: https://doi.org/10.1016/j.ijhydene.2017.08.123.

[35] Xu, P., Zheng, J., and Liu, P. Finite element analysis of burst pressure of composite hydrogen storage vessels. *Materials & Design*, 30(7):2295–2301, 2009. ISSN 0261-3069.

[36] Regassa, Y., Gari, J., and Lemu, H. G. Composite overwrapped pressure vessel design optimization using numerical method. *Journal of Composites Science*, 6(8):229, 2022.

[37] Bagarello, S., Campagna, D., and Benedetti, I. A survey on hydrogen tanks for sustainable aviation. *Green Energy and Intelligent Transportation*, page 100224, 2024. ISSN 2773-1537. doi: https://doi.org/10.1016/

j.geits.2024.100224. URL https://www.sciencedirect.com/science/article/pii/S2773153724000768.

[38] Fuel Cells and Hydrogen 2 Joint Undertaking. *Hydrogen-powered aviation – A fact-based study of hydrogen technology, economics, and climate impact by 2050.* Publications Office, 2020. URL https://op.europa.eu/en/publication-detail/-/publication/55fe3eb1-cc8a-11ea-adf7-01aa75ed71a1. Available online.

[39] National Aeronautics and Space Administration. Hydrogen-powered aircraft overview. nasa technical reports, 2023. URL https://ntrs.nasa.gov/api/citations/20230009800/downloads/CEC%20NASA%20aircraft%20overview_v2-c.pdf. Available online, accessed on 19/01/2026.

[40] Jiang, W., Sun, P., Li, P., Zuo, Z., and Huang, Y. Transient thermal behavior of multi-layer insulation coupled with vapor cooled shield used for liquid hydrogen storage tank. *Energy*, 231:120859, 2021. ISSN 0360-5442. doi: https://doi.org/10.1016/j.energy.2021.120859.

[41] Yu, Y., Xie, F., Zhu, M., Yu, S., and Li, Y. Design and optimization of the insulation performance of a 4000 m3 liquid hydrogen spherical tank. *Processes*, 11(6):1778, 2023.

[42] Mital, S., Gyekenyesi, J., Arnold, S., Sullivan, R., Manderscheid, J., and Murthy, P. Review of current state of the art and key design issues with potential solutions for liquid hydrogen cryogenic storage tank structures for aircraft applications. *NASA-TM 2006-214346*, 2006.

[43] Millis, M. G., Tornabene, R. T., Jurns, J. M., Guynn, M. D., Tom-

sik, T. M., and Overbeke, T. J. V. Hydrogen fuel system design trades for high-altitude long-endurance remotely-operated aircraft. *NASA/TM—2009-215521*, 2009.

[44] Jennifer A. Harbaugh. Nasa tests new insulation for sls rocket. `https://www.nasa.gov/humans-in-space/nasa-tests-new-insulation-for-sls-rocket/l`, 2016. Accessed: 2026-02-02.

[45] National Aeronautics and Space Administration. Comprehensive shuttle foam debris reduction strategies, 2009. URL `https://ntrs.nasa.gov/api/citations/20070013736/downloads/20070013736.pdf`. Available online, Accessed on 23/01/2026.

[46] Lee, J. A., , and Woods, S. Hydrogen embrittlement. *National Aeronautics and Space Administration Scientific and Technical Information (STI) Program Office*, 2016.

[47] Benedetti, I., Gulizzi, V., and Milazzo, A. Grain-boundary modelling of hydrogen assisted intergranular stress corrosion cracking. *Mechanics of Materials*, 117:137–151, 2018. ISSN 0167-6636. doi: https://doi.org/10.1016/j.mechmat.2017.11.001. URL `https://www.sciencedirect.com/science/article/pii/S0167663617305276`.

[48] Lynch, S. Hydrogen embrittlement phenomena and mechanisms. *Corrosion reviews*, 30(3-4):105–123, 2012.

[49] Dwivedi, S. K. and Vishwakarma, M. Hydrogen embrittlement in different materials: A review. *International Journal of Hydrogen Energy*, 43 (46):21603–21616, 2018. ISSN 0360-3199. doi: https://doi.org/10.1016/j.ijhydene.2018.09.201.

[50] Bagarello, S., Campagna, D., and Benedetti, I. Computational thermo-mechanical modelling and design-space exploration of cryogenic hydrogen tanks for aviation. *Aerospace Science and Technology*, 168: 110755, 2026. ISSN 1270-9638. doi: https://doi.org/10.1016/j.ast.2025.110755. URL `https://www.sciencedirect.com/science/article/pii/S1270963825008260`.

[51] Bagarello, S., Campagna, D., and Benedetti, I. A short overview of hydrogen storage for sustainable aviation. *Materials Research Proceedings*, 42, 2024.

[52] Bagarello, S., Campagna, D., and Benedetti, I. Conceptual design and thermo-mechanical modelling of liquid hydrogen storage vessels for aircraft integration. *Sumbitted to: Materials Research Proceedings*, 2025.

[53] Bagarello, S., Campagna, D., Milazzo, A., and Benedetti, I. An overview of hydrogen storage for airborne applications. In *RESEARCH & EDUCATION IN AIRCRAFT DESIGN*, 2026. Extended abstract, indexed in Scopus.

[54] Bagarello, S., Campagna, D., Elham, A., and Benedetti, I. Multidisciplinary optimization of passively-insulated liquid hydrogen tanks for aircraft applications. In *Fifth International Conference on Mechanics of Advanced Materials and Structures*, 2026.

[55] Brewer, G. D. *Hydrogen aircraft technology*. Routledge, 1991.

[56] Winnefeld, C., Kadyk, T., Bensmann, B., Krewer, U., and Hanke-Rauschenbach, R. Modelling and designing cryogenic hydrogen tanks for future aircraft applications. *Energies*, 11:105, 2018.

[57] Verstraete, D., Hendrick, P., Pilidis, P., and Ramsden, K. Hydrogen fuel tanks for subsonic transport aircraft. *International Journal of Hydrogen Energy*, 35(20):11085–11098, 2010. ISSN 0360-3199. doi: https://doi.org/10.1016/j.ijhydene.2010.06.060. URL `https://www.sciencedirect.com/science/article/pii/S036031991001236X`. Hyceltec 2009 Conference.

[58] Huete, J. and Pilidis, P. Parametric study on tank integration for hydrogen civil aviation propulsion. *International Journal of Hydrogen Energy*, 46(74):37049–37062, 2021. ISSN 0360-3199. doi: https://doi.org/10.1016/j.ijhydene.2021.08.194. URL `https://www.sciencedirect.com/science/article/pii/S0360319921034418`.

[59] Cipolla, V., Zanetti, D., Abu Salem, K., Binante, V., and Palaia, G. A parametric approach for conceptual integration and performance studies of liquid hydrogen short–medium range aircraft. *Applied Sciences*, 12 (14), 2022. ISSN 2076-3417. doi: 10.3390/app12146857. URL `https://www.mdpi.com/2076-3417/12/14/6857`.

[60] Adler, E. and Martins, J. Liquid hydrogen tank boil-off model for design and optimization. *Journal of Thermophysics and Heat Transfer*, 11 2024. doi: 10.2514/1.T7005.

[61] Gomez, A. and Smith, H. Liquid hydrogen fuel tanks for commercial aviation: Structural sizing and stress analysis. *Aerospace Science and Technology*, 95:105438, 2019. ISSN 1270-9638. doi: https://doi.org/10.1016/j.ast.2019.105438.

[62] Tzoumakis, G., Fotopoulos, K., and Lampeas, G. Multi-physics digital model of an aluminum 2219 liquid hydrogen aircraft tank. *Aerospace*, 11 (2), 2024. ISSN 2226-4310. doi: 10.3390/aerospace11020161.

[63] Murray, C., Newhouse, N., Schimenti, J., and Tiller, D. Development of composite pressure vessels with nonmetallic liners. In *28th Joint Propulsion Conference and Exhibit*, page 3853, 1992.

[64] Cohen, D., Mantell, S. C., and Zhao, L. The effect of fiber volume fraction on filament wound composite pressure vessel strength. *Composites Part B: Engineering*, 32(5):413–429, 2001.

[65] Cohen, D. Influence of filament winding parameters on composite vessel quality and strength. *Composites Part A: Applied Science and Manufacturing*, 28(12):1035–1047, 1997.

[66] Wang, B., Wen, L., Xiao, J., Wang, S., Ren, P., Wang, L., Zu, L., and Hou, X. Automated fiber placement path planning and analysis of pressure vessels. *Materials*, 16(18), 2023. ISSN 1996-1944. doi: 10.3390/ma16186187. URL `https://www.mdpi.com/1996-1944/16/18/6187`.

[67] Daghighi, S., Zucco, G., Rouhi, M., and Weaver, P. M. Bend-free design of super ellipsoids of revolution composite pressure vessels. *Composite Structures*, 245:112283, 2020.

[68] Daghighi, S., Zucco, G., and Weaver, P. M. Design methods for variable-stiffness super-ellipsoidal pressure vessels under thermomechanical loading. *AIAA Journal*, 61(1):475–488, 2023. doi: 10.2514/1.J062168.

[69] Liu, P., Chu, J., Hou, S., Xu, P., and Zheng, J. Numerical simulation and optimal design for composite high-pressure hydrogen storage vessel: A review. *Renewable and Sustainable Energy Reviews*, 16(4):1817–1827, 2012.

[70] Wang, L., Zheng, C., Luo, H., Wei, S., and Wei, Z. Continuum damage modeling and progressive failure analysis of carbon fiber/epoxy com-

posite pressure vessel. *Composite Structures*, 134:475–482, 2015. ISSN 0263-8223.

[71] Wang, L., Zheng, C., Wei, S., and Wei, Z. Micromechanics-based progressive failure analysis of carbon fiber/epoxy composite vessel under combined internal pressure and thermomechanical loading. *Composites Part B: Engineering*, 89:77–84, 2016. ISSN 1359-8368.

[72] Rafiee, R. and Torabi, M. A. Stochastic prediction of burst pressure in composite pressure vessels. *Composite Structures*, 185:573–583, 2018.

[73] Lin, S., Yang, L., Xu, H., Jia, X., Yang, X., and Zu, L. Progressive damage analysis for multiscale modelling of composite pressure vessels based on puck failure criterion. *Composite Structures*, 255:113046, 2021.

[74] Xu, P., Zheng, J., Chen, H., and Liu, P. Optimal design of high pressure hydrogen storage vessel using an adaptive genetic algorithm. *International Journal of Hydrogen Energy*, 35(7):2840–2846, 2010. ISSN 0360-3199. 2008 International Hydrogen Forum (HyForum2008).

[75] Leh, D., Saffré, P., Francescato, P., Arrieux, R., and Villalonga, S. A progressive failure analysis of a 700-bar type iv hydrogen composite pressure vessel. *International Journal of Hydrogen Energy*, 40(38):13206–13214, 2015. ISSN 0360-3199.

[76] Liu, P., Xing, L., and Zheng, J. Failure analysis of carbon fiber/epoxy composite cylindrical laminates using explicit finite element method. *Composites Part B: Engineering*, 56:54–61, 2014. ISSN 1359-8368.

[77] Wang, L., Zheng, C., Luo, H., Wei, S., and Wei, Z. Continuum damage modeling and progressive failure analysis of carbon fiber/epoxy com-

posite pressure vessel. *Composite Structures*, 134:475–482, 2015. ISSN 0263-8223.

[78] Nguyen, B. N., Roh, H. S., Merkel, D. R., and Simmons, K. L. A predictive modeling tool for damage analysis and design of hydrogen storage composite pressure vessels. *International Journal of Hydrogen Energy*, 46(39):20573–20585, 2021.

[79] Ma, P.-S. and Zhang, L.-W. High pressure and long-term gas diffusion coupled damage of composites through a multi-physical phase field framework. *Computer Methods in Applied Mechanics and Engineering*, 410:116006, 2023.

[80] Bui, T. Q. and Hu, X. A review of phase-field models, fundamentals and their applications to composite laminates. *Engineering Fracture Mechanics*, 248:107705, 2021. ISSN 0013-7944.

[81] Maimí, P., Camanho, P., Mayugo, J., and Dávila, C. A continuum damage model for composite laminates: Part i – constitutive model. *Mechanics of Materials*, 39(10):897–908, 2007. ISSN 0167-6636.

[82] THOR Project. Thermoplastic hydrogen tanks optimised and recyclable, 2022. URL `https://thor-fch2.eu/`. Available on line, accessed on 22/11/2023.

[83] Dwivedi, S. K. and Vishwakarma, M. Hydrogen embrittlement in different materials: A review. *International Journal of Hydrogen Energy*, 43 (46):21603–21616, 2018. ISSN 0360-3199. doi: https://doi.org/10.1016/j.ijhydene.2018.09.201.

[84] National Aeronautics and Space Administration. X-33 lh2 tank failure in-

vestigation findings, 2013. URL `https://ntrs.nasa.gov/citations/20030067586`. Available online, Accessed on 08/09/2025.

[85] Islam, M. S., Benninger, L. F., Pearce, G., and Wang, C.-H. Toughening carbon fibre composites at cryogenic temperatures using low-thermal expansion nanoparticles. *Composites Part A: Applied Science and Manufacturing*, 150:106613, 2021.

[86] European Commission. Cryogenic hypersonic advanced tank technologies, 2015. URL `https://cordis.europa.eu/project/id/285117`. Available on line, accessed on 29/12/2023.

[87] Klopčič, N., Grimmer, I., Winkler, F., Sartory, M., and Trattner, A. A review on metal hydride materials for hydrogen storage. *Journal of Energy Storage*, 72:108456, 2023. ISSN 2352-152X. doi: https://doi.org/10.1016/j.est.2023.108456.

[88] Zhao, H., Zhang, H., Wang, J., Li, B., Zhu, Y., and Liu, H. Theoretical calculation and tests of hydrogen storage properties of nano mos2 doped ce-mof-808. *Journal of Energy Storage*, 88:111526, 2024. ISSN 2352-152X. doi: https://doi.org/10.1016/j.est.2024.111526.

[89] Rezaie, S., Smeulders, D. M., and Luna-Triguero, A. Enhanced hydrogen storage in gold-doped carbon nanotubes: A first-principles study. *Chemical Engineering Journal*, 476:146525, 2023. ISSN 1385-8947. doi: https://doi.org/10.1016/j.cej.2023.146525.

[90] Elemike, E. E., Osafile, O. E., and Omugbe, E. New perspectives 2ds to 3ds mxenes and graphene functionalized systems as high performance energy storage materials. *Journal of Energy Storage*, 42:102993, 2021. ISSN 2352-152X. doi: https://doi.org/10.1016/j.est.2021.102993.

[91] Mishra, S. and Kundalwal, S. Hydrogen sorption kinetics and mobility on li-functionalized polycrystalline carbon nanotube bundles: A molecular dynamics study. *Journal of Energy Storage*, 86:111129, 2024. ISSN 2352-152X. doi: https://doi.org/10.1016/j.est.2024.111129.

[92] Shelby, J. and Hall, M. Glass microspheres for hydrogen storage. *DOE Hydrogen Program*, 2008.

[93] Hassani, S. and Dackermann, U. A systematic review of advanced sensor technologies for non-destructive testing and structural health monitoring. *Sensors*, 23(2204), 2023.

[94] Gao, D., Wu, Z., Yang, L., Zheng, Y., and Yin, W. Structural health monitoring for long-term aircraft storage tanks under cryogenic temperature. *Aerospace Science and Technology*, 92:881–891, 2019. ISSN 1270-9638. doi: https://doi.org/10.1016/j.ast.2019.02.045.

[95] Kosiel, K. and Śmietana, M. *Detection in Harsh Environments*, chapter 13, pages 441–476. John Wiley & Sons, Ltd, 2020. ISBN 9781119534730. doi: https://doi.org/10.1002/9781119534730.ch13.

[96] Santoni-Bottai, G. and Giurgiutiu, V. Damage detection at cryogenic temperatures in composites using piezoelectric wafer active sensors. *Struct. Health Monit. 11*, 2012.

[97] Liang, Z., Liu, D., Wang, X., Zhang, J., Wu, H., Qing, X., and Wang, Y. Fbg-based strain monitoring and temperature compensation for composite tank. *Aerospace Science and Technology*, 127:107724, 2022. ISSN 1270-9638. doi: https://doi.org/10.1016/j.ast.2022.107724.

[98] Klug, H. G. and Faass, R. Cryoplane: hydrogen fuelled aircraft – status

and challenges. *Air & Space Europe*, 3(3):252–254, 2001. ISSN 1290-0958. doi: https://doi.org/10.1016/S1290-0958(01)90110-8.

[99] Sippel, M., Kopp, A., Mattsson, D., Freund, J., Tapeinos, I., and Koussios, S. Final results of advanced cryo-tanks research project chatt. *6th European Conference for Aeronautics and Space Sciences (EUCASS)*, 2015.

[100] ENABLEH2. Enableh2, 2022. URL `https://cordis.europa.eu/project/id/769241`. Available on line, accessed on 11/05/2026.

[101] National Aeronautics and Space Administration. NASA-STD-6016C w/Change 1: Standard Materials and Processes Requirements for Spacecraft. NASA Technical Standard NASA-STD-6016C w/Change 1, National Aeronautics and Space Administration, Washington, DC, USA, 2023. Baseline issued 30 September 2021; Change 1 issued 15 November 2023.

[102] European Union Aviation Safety Agency. Special Condition SC E-19: Electric / Hybrid Propulsion System. Special Condition SC E-19, Issue 01, European Union Aviation Safety Agency, Cologne, Germany, Apr. 2021.

[103] Airbus. Zeroe - towards the world's first hydrogen-powered commercial aircraft, 2023. URL `https://www.airbus.com/en/innovation/energy-transition/hydrogen/zeroe-our-hydrogen-powered-aircraft`. Available on line, accessed on 11/05/2026.

[104] Hepher, T. Airbus postpones development of new hydrogen aircraft. Reuters, Feb. 2025. URL `https:`

//www.reuters.com/business/aerospace-defense/airbus-postpones-development-new-hydrogen-aircraft-2025-02-07/. Available online, accessed on 11/05/2026.

[105] Harrington, T. Hydrogen aviation pioneer universal hydrogen fails, citing lack of funding. GreenAir News, July 2024. URL https://www.greenairnews.com/?p=5860. Available online, accessed on 11/05/2026.

[106] H2FLY GmbH. Breaking the hydrogen barrier, 2026. URL https://www.h2fly.de/. Available on line, accessed on 11/05/2026.

[107] ZeroAvia. Hydrogen-electric propulsion and power systems. ZeroAvia, 2026. URL https://zeroavia.com/. Available online, accessed on 11/05/2026.

[108] European Commission. HYDEA – HYdrogen DEmonstrator for Aviation. CORDIS – EU research results, 2026. URL https://cordis.europa.eu/project/id/101102019. Available online, accessed on 11/05/2026.

[109] Wikipedia contributors. Project Fresson. Wikipedia, The Free Encyclopedia, 2026. URL https://en.wikipedia.org/wiki/Project_Fresson. Available online, accessed on 11/05/2026.

[110] European Commission. H2ELIOS – HydrogEn Lightweight & Innovative tank for zerO-emisSion aircraft. CORDIS – EU research results, 2026. URL https://cordis.europa.eu/project/id/101102003. Available online, accessed on 11/05/2026.

[111] European Commission. CAVENDISH – Consortium for the AdVent of aero-Engine Demonstration and aircraft Integration Strategy with Hydrogen. CORDIS – EU research results, 2026. URL https://

cordis.europa.eu/project/id/101102000. Available online, accessed on 11/05/2026.

[112] Clean Hydrogen Partnership. COCOLIH2T – COmposite COnformal LIquid H2 Tank. Clean Hydrogen Partnership – Projects repository, 2026. URL https://www.clean-hydrogen.europa.eu/projects-dashboard/projects-repository/cocolih2t_en. Available online, accessed on 11/05/2026.

[113] SHZ Advanced Technologies. LH2 storage solutions. SHZ Advanced Technologies, 2026. URL https://shz-advancedtechnologies.com/en/storage-solutions/. Available online, accessed on 11/05/2026.

[114] Beyond Aero. Aviation will be electric. Beyond Aero, 2026. URL https://www.beyond-aero.com/. Available online, accessed on 11/05/2026.

[115] Licheva, G. and Liscouet-Hanke, S. Cryogenic tank sizing model for the conceptual design of hydrogen-powered aircraft. In *34th Congress of the International Council of the Aeronautical Sciences, 09-13/09/2024, Florence, Italy*. ICAS, 2024.

[116] European Aviation Safety Agency. Certification specifications and acceptable means of compliance for large aeroplanes cs-25, 2016.

[117] John M. (Tim) Holt, Technical Ed; C. Y. Ho, E. Structural alloys handbook. In *1996 edition*. CINDAS/Purdue University, 1996.

[118] Simon, N., Drexler, E., and Reed, R. Review of cryogenic mechanical and thermal properties of Al-Li alloys and alloy 2219. *United States Department of Commerce - National Institute of Standards and Technology*, page 196, 09 1990.

[119] Li, K. C., Wu, Z. J., Liu, M. J., Xu, X. S., and Xu, W. An application of reinforced polyurethane foam in design of the common bulkhead for cryogenic tanks. In *Materials Science Forum*, volume 975, pages 182–187. Trans Tech Publ, 2020.

[120] l. E. Fesmire, Coffman, B., Menghelli, B., and Heckle, K. Spray-on foam insulations for launch vehicle cryogenic tanks. NASA Technical Paper NASA/TP–2011–20110014400, NASA Space Cryogenics Workshop, Idaho, July 2011, 2011. https://ntrs.nasa.gov/citations/20110014400.

[121] Sparks, L. L. and Arvidson, J. *Thermal and mechanical properties of polyurethane foams and a survey of insulating concretes at cryogenic temperatures*. National Bureau of Standards Boulder, CO., 1984.

[122] Songhan Plastic Technology Co., Ltd. Overview of materials for thermoset polyurethane foam, unreinforced. https://www.lookpolymers.com/pdf/Overview-of-materials-for-Thermoset-Polyurethane-Foam-Unreinforced.pdf, 2025. Available online.

[123] Bartolomeu, F., Gasik, M., Silva, F. S., and Miranda, G. Mechanical properties of Ti-6Al-4V fabricated by laser powder bed fusion: A review focused on the processing and microstructural parameters influence on the final properties. *Metals*, 12(6), 2022. ISSN 2075-4701. doi: 10.3390/met12060986.

[124] Vandenbroucke, B. and Kruth, J. Selective laser melting of biocompatible metals for rapid manufacturing of medical parts. *Rapid Prototyping Journal*, 13(4), 2007. ISSN 196-203. doi: https://doi.org/10.1108/13552540710776142.

[125] Wysocki, B., Maj, P., Sitek, R., Buhagiar, J., Kurzydłowski, K. J., and Święszkowski, W. Laser and electron beam additive manufacturing methods of fabricating titanium bone implants. *Applied Sciences*, 7(7), 2017. ISSN 2076-3417. doi: 10.3390/app7070657.

[126] Horiuchi, T. and Ooi, T. Cryogenic properties of composite materials. *Cryogenics*, 35(11):677–679, 1995.

[127] Gates, T. S., Su, X., Abdi, F., Odegard, G. M., and Herring, H. M. Facesheet delamination of composite sandwich materials at cryogenic temperatures. *Composites science and technology*, 66(14):2423–2435, 2006.

[128] Xue, J., Wang, W., Zhang, J.-Z., and Wu, S.-J. Progressive failure analysis of the fiber metal laminates based on chopped carbon fiber strands. *Journal of Reinforced Plastics and Composites*, 34:364–376, 03 2015. doi: 10.1177/0731684415571659.

[129] National Research Council Committee on Air Quality in Passenger Cabins of Commercial Aircraft. The airliner cabin environment and the health of passengers and crew. *Washington (DC)*, PMID: 25032286., 2002.

[130] Curto, D., Franzitta, V., Guercio, A., and Martorana, P. Fem analysis: A review of the most common thermal bridges and their mitigation. *Energies*, 15(7), 2022. ISSN 1996-1073. doi: 10.3390/en15072318. URL `https://www.mdpi.com/1996-1073/15/7/2318`.

[131] H2FLY. H2fly accelerates progress towards zero-emission commercial flight. https://www.h2fly.de/2023/04/05/h2fly-accelerates-progress-

towards-zero-emission-commercial-flight-3/, 2023. Accessed: Jan. 5, 2026.

[132] Smith, M. *ABAQUS/Standard User's Manual, Version 6.9*. Dassault Systèmes Simulia Corp, United States, 2009.

[133] Belytschko, T., Ong, J. S.-J., Liu, W. K., and Kennedy, J. M. Hourglass control in linear and nonlinear problems. *Computer methods in applied mechanics and engineering*, 43(3):251–276, 1984.

[134] Lampeas, G. and Tzoumakis, G. Thermo-mechanical simulation of a small-scale liquid hydrogen fuel tank for aviation applications. In *9th EUROPEAN CONFERENCE FOR AERONAUTICS AND SPACE SCIENCES*. EUCASS, 2022. doi: 10.13009/EUCASS2022-7281.

[135] Federal Aviation Administration. § 25.303 Factor of Safety. U.S. Government Publishing Office, 2023. URL `https://www.ecfr.gov/current/title-14/part-25`. Title 14 Code of Federal Regulations (CFR), Part 25.

[136] Inc., T. M. Matlab version: 9.13.0 (r2022b), 2022. URL `https://www.mathworks.com`.

[137] Kreisselmeier, G. and Steinhauser, R. Systematic control design by optimizing a vector performance index. In *Computer aided design of control systems*, pages 113–117. Elsevier, 1980.

[138] Poon, N. and Martins, J. An adaptive approach to constraint aggregation using adjoint sensitivity analysis. *Structural and Multidisciplinary Optimization*, 34:61–73, 07 2007. doi: 10.1007/s00158-006-0061-7.

[139] AircraftMaterialsUK Ltd Reg Co. Aluminium alloy 2219 - technical data sheet. https://www.aircraftmaterials.com/data/aluminium/2219.html, 2025. Accessed: 07-Jan-2026.

[140] Mo, C., Xu, Y., and Yuan, S. Analysis of thickness variation in 2219 aluminum alloy ellipsoid shell with differential thickness by hydroforming. *Metals*, 14(10), 2024. ISSN 2075-4701. doi: 10.3390/met14101140. URL `https://www.mdpi.com/2075-4701/14/10/1140`.

[141] Nguyen, H. D., Pramanik, A., Basak, A., Dong, Y., Prakash, C., Debnath, S., Shankar, S., Jawahir, I., Dixit, S., and Buddhi, D. A critical review on additive manufacturing of Ti-6Al-4V alloy: Microstructure and mechanical properties. *Journal of Materials Research and Technology*, 18:4641–4661, 2022.

[142] Malekinejad, H., Ramezani, F., Carbas, R. J. C., Marques, E. A. S., and da Silva, L. F. M. Study of cfrp laminate gradually modified throughout the thickness using thin ply under transvers tensile loading. *Materials*, 17(10), 2024. ISSN 1996-1944. doi: 10.3390/ma17102388. URL `https://www.mdpi.com/1996-1944/17/10/2388`.

[143] Triton Alloys Inc. Aluminum 2219 plate supplier exporter stockist dealer. `https://www.tritonalloysinc.com/2219-aluminum-plate.html`, 2024. Accessed: 2026-12-01.

[144] AM-Material. Introduction to Ti-6Al-4V titanium alloy. https://am-material.com/news/introduction-to-ti-6al-4v-titanium-alloy/, Sept. 13 2023. Accessed: 2026-12-01.

[145] Airbus. How to store liquid hydrogen for zero-emission flight.

https://www.airbus.com/en/newsroom/news/2021-12-how-to-store-liquid-hydrogen-for-zero-emission-flight, 2021. Accessed: 2026-12-01.

[146] ZeroAvia. Zeroavia awarded uk government grant for development and flight test of liquid hydrogen fuel system. https://zeroavia.com/zeroavia-awarded-uk-government-grant-for-development-and-flight-test-of-liquid-hydrogen-fuel-system/, 2023. Accessed: 2026-12-01.

[147] Krishna, R., Titus, E., Salimian, M., Okhay, O., Rajendran, S., Rajkumar, A., Sousa, J. M. G., Ferreira, A. L. C., Gil, J. C., and Gracio, J. Hydrogen storage for energy application. In Liu, J., editor, *Hydrogen Storage*, chapter 10. IntechOpen, London, 2012. doi: 10.5772/51238. URL `https://doi.org/10.5772/51238`.

[148] Demaco Cryogenics. Vacuum insulated transfer lines for LH_2, 2024. URL `https://demaco-cryogenics.com/products/vacuum-insulated-transfer-lines-lh2-vip/`. Accessed: Jan 12, 2026.

[149] Lei, Y., Zhang, L., Zhong, S., and Huang, B. Multi-objective optimization of a t-shaped anti-sloshing baffle based on nsga-ii. *Frontiers in Energy Research*, 10, 2022. ISSN 2296-598X. doi: 10.3389/fenrg.2022.810937.

[150] Owens, C. A.-H., Park, H., Flores, R. J., Wentlent, L., Brouwer, J., and Lee, J. Thermal analysis of baffle effects in cryogenic hydrogen tanks. *International Journal of Heat and Mass Transfer*, 255:127863, 2026. ISSN 0017-9310. doi: https://doi.org/10.1016/j.ijheatmasstransfer.2025.127863. URL `https://www.sciencedirect.com/science/article/pii/S0017931025011986`.

[151] Demirkoparan, H. and Pence, T. J. Magic angles for fiber reinforcement in rubber-elastic tubes subject to pressure and swelling. *International Journal of Non-Linear Mechanics*, 68:87–95, 2015. ISSN 0020-7462. doi: https://doi.org/10.1016/j.ijnonlinmec.2014.05.008. URL `https://www.sciencedirect.com/science/article/pii/S0020746214001103`. Mechanics of Rubber - in Memory of Alan Gent.

[152] Liang, J., Ning, Z., Li, Y., Gao, H., Liu, J., Tian, W., Zhao, X., Jia, Z., Xue, Y., and Miao, C. An efficient optimization method for stacking sequence of composite pressure vessels based on artificial neural network and genetic algorithm. *Applied Composite Materials*, 31:1–24, 02 2024. doi: 10.1007/s10443-024-10201-8.

[153] Almeida, J. H. S., Ribeiro, M. L., Tita, V., and Amico, S. C. Stacking sequence optimization in composite tubes under internal pressure based on genetic algorithm accounting for progressive damage. *Composite Structures*, 178:20–26, 2017. ISSN 0263-8223. doi: https://doi.org/10.1016/j.compstruct.2017.07.054. URL `https://www.sciencedirect.com/science/article/pii/S0263822317320317`.

[154] Akkerman, R. On the properties of quasi-isotropic laminates. *Composites Part B: Engineering*, 33(2):133–140, 2002. ISSN 1359-8368. doi: https://doi.org/10.1016/S1359-8368(02)00002-1. URL `https://www.sciencedirect.com/science/article/pii/S1359836802000021`.

[155] Van Otterloo, D. L. and Dayal, V. How isotropic are quasi-isotropic laminates. *Composites Part A: Applied Science and Manufacturing*, 34(1):93–103, 2003. ISSN 1359-835X. doi: https://doi.org/10.1016/S1359-835X(02)00180-X. URL `https://www.sciencedirect.com/science/article/pii/S1359835X0200180X`.

[156] Nettles, A. T. Basic mechanics of laminated composite plates. NASA Reference Publication RP-1351, NASA Marshall Space Flight Center, 1994.

[157] European Union Aviation Safety Agency - Easy Access Rules for Large Aeroplanes (CS-25). § 25.772 Pilot compartment doors. https://www.easa.europa.eu/en/document-library/easy-access-rules/online-publications/easy-access-rules-large-aeroplanes-cs-25?page=26, 2023. Accessed: June 2025.

[158] Warkina, R. and Regassa, Y. Optimizing performance of hybrid fiber reinforced overwrapped pressure vessel. *Journal of Composite Materials*, 59(2):187–206, 2025.

[159] Sielemann, M., Huete, J., Andersson, D., Nguyen, A., and Coïc, C. Case study in design and transient analysis of hydrogen-propelled aircraft using direct combustion. In *AIAA Aviation 2023 Forum*, page 3230, 2023.

[160] Onorato, G., Proesmans, P., and Hoogreef, M. Assessment of hydrogen transport aircraft: Effects of fuel tank integration. *CEAS Aeronautical Journal*, 13(4):813–845, 2022.

[161] Lee, C., Greenhalgh, E. S., and Panesar, A. Optimization of patch-wise laminated composite panels for enhanced dynamic characteristics. *Composite Structures*, 269:114017, 2021. ISSN 0263-8223. doi: https://doi.org/10.1016/j.compstruct.2021.114017. URL `https://www.sciencedirect.com/science/article/pii/S0263822321004773`.

[162] Sigmund, O. and Petersson, J. Numerical instabilities in topology optimization: a survey on procedures dealing with checkerboards, mesh-

dependencies and local minima. *Structural optimization*, 16(1):68–75, 1998.

[163] Tuswan, T., Andrian, M., Amiruddin, W., Muttaqie, T., Sari, D. P., Bisri, A., Yuniati, Y., Soetarjo, M., Utina, M. R., and Harmadi, R. Design improvement using topology optimization for the structural frame design of a 40 ft lng iso container tank. *Designs*, 8(2), 2024. ISSN 2411-9660. doi: 10.3390/designs8020021. URL `https://www.mdpi.com/2411-9660/8/2/21`.

[164] Nebe, M., Johman, A., Braun, C., and Van Campen, J. The effect of stacking sequence and circumferential ply drop locations on the mechanical response of type iv composite pressure vessels subjected to internal pressure: A numerical and experimental study. *Composite Structures*, 294:115585, 2022.

[165] Malfroy, J., Steelant, J., and Vandepitte, D. A design guide to tapered conformable pressure tanks for liquid hydrogen storage. *Aerospace*, 12(3), 2025. ISSN 2226-4310. doi: 10.3390/aerospace12030190. URL `https://www.mdpi.com/2226-4310/12/3/190`.

[166] Eko, A. J., Zeng, X., Peerzada, M., Shelley, T., Epaarachchi, J., and Tien, C. M. T. Thermodynamic effects and boil-off management in cryogenic propellant tanks: a systematic review. *Journal of Physics: Energy*, 8:012002, 2026. ISSN 0017-9310. doi: 10.1088/2515-7655/ae3643.

[167] Waimer, M., Schatrow, P., Wegener, E., Toso, N., and Voggenreiter, H. Crashworthiness considerations for liquid hydrogen tank integration in transport airplanes. *CEAS Aeronautical Journal*, 2025. ISSN 1869-5590. doi: 10.1007/s13272-025-00933-z.

[168] Zhang, Y., Wang, H., Zhou, Q., Cui, B., Wang, M., and Shi, J. Crashworthiness design of hydrogen-powered regional aircraft with liquid hydrogen tanks. *Journal of Energy Storage*, 147:119987, 2026. ISSN 2352-152X. doi: https://doi.org/10.1016/j.est.2025.119987. URL `https://www.sciencedirect.com/science/article/pii/S2352152X25047012`.

[169] Kumar, N., Sekhar Bag, D., Pratap Singh, K., Dixit, A., Mishra, S., Nath Tripathi, D., and Eswara Prasad, N. Self-sealing polymeric materials: Mechanism and applications. *Advanced Materials Letters*, 11(6): 1–11, 2020. ISSN 0976-3961. doi: 10.5185/amlett.2020.061521. URL `https://aml.iaamonline.org/article_13994.html`.

[170] Dang, X., Shao, Y., Liu, H., Yang, Z., Zhong, M., Zhao, H., and Deng, W. Risk assessment of hydrogen-powered aircraft: An integrated hazop and fuzzy dynamic bayesian network framework. *Sensors*, 25(10), 2025. ISSN 1424-8220. doi: 10.3390/s25103075. URL `https://www.mdpi.com/1424-8220/25/10/3075`.

[171] O'Sullivan, G., Horvat, A. B., Jézégou, J., Carrasco, B. J., and André, R. Hydrogen aircraft, technologies and operations towards certification readiness level 1. *Aerospace*, 12(6), 2025. ISSN 2226-4310. doi: 10.3390/aerospace12060490. URL `https://www.mdpi.com/2226-4310/12/6/490`.

[172] Jézégou, J., Almeida-Marino, A. M., O'Sullivan, G., Carrasco, B. J., André, R., and Gourinat, Y. Certification gap analysis for normal-category and large hydrogen-powered airplanes. *Aerospace*, 12(3), 2025. ISSN 2226-4310. doi: 10.3390/aerospace12030239. URL `https://www.mdpi.com/2226-4310/12/3/239`.

Acknowledgements

The author acknowledges support from the European Union - NextGenerationEU - National Sustainable Mobility Center CN00000023, Italian Ministry of University and Research Decree n. 1033— 17/06/2022, Spoke 12, CUP B73C22000760001.